This is to certify that the

dissertation entitled

Structures of the Heme Chromophores
in Cytochrome Oxidase

presented by

Patricia Mary Callahan

has been accepted towards fulfillment
of the requirements for

Ph.D. degree in Chemistry

Gerald T. Babcock
Major professor

Date June 10, 1983

STRUCTURES OF THE HEME CHROMOPHORES IN CHROCHROME OXIDASE

By

Patricia Mary Callahan

A DISSERTATION

Submitted to
Michigan State University
in partial fulfillment of the requirements
for the degree of

DOCTOR OF PHILOSOPHY

Department of Chemistry

1983

ABSTRACT

STRUCTURES OF THE HEME CHROMOPHORES
IN CYTOCHROME OXIDASE

By

Patricia Mary Callahan

Heme structures important for electron transfer and proton transfer in the enzyme cytochrome oxidase are discussed. The application of resonance Raman spectroscopy, in conjunction with optical absorption, magnetic circular dichroism and electron paramagnetic resonance spectroscopies, to cytochrome oxidase and appropriate heme a model complexes, have enabled us to identify the individual heme electronic and vibrational properties. The pattern of vibrational frequencies, in particular the frequency of a polarized mode in the 1560-1600 cm^{-1} Soret region resonance Raman spectrum, is correlated to the heme iron spin and coordination geometry. After taking into account the porphyrin pyrrole ring β-carbon substituent dependence of this vibration, structural information can be obtained. It is found that cytochrome a_3 is six coordinate and high-spin in the resting enzyme but five coordinate and high-spin in the reduced enzyme;

cytochrome *a* is six coordinate and low-spin in both redox states of the enzyme. Cytochrome a_3 is observed to be in a hydrophobic environment based on the frequency position of its aldehyde substituent. The previously unassigned cytochrome *a* formyl stretching frequency is observed at 1650 cm^{-1} and 1610 cm^{-1} in the ferric and ferrous species, respectively. The formyl frequency down-shift and absorption red-shift of cytochrome *a* relative to low-spin heme *a* model compounds are interpreted to result from a hydrogen-bonding interaction between its position 8 formyl group and a nearby amino acid residue, possibly tyrosine. This hydrogen bond strength depends on the cytochrome *a* iron valence state and is estimated to differ by 2.0 - 2.5 kcal/mole between ferrous and ferric cytochrome *a*. This strengthening of the hydrogen bond upon reduction of the enzyme can be used to drive redox-linked events. Thus, the linkage between cytochrome *a* redox state and chromophore/protein interaction energy provides a mechanism by which electron transfer events and protein structure are coupled. Two models that incorporate this linkage into a redox driven proton pump centered at cytochrome *a* in cytochrome oxidase are presented.

To My Parents

ACKNOWLEDGMENTS

I gratefully acknowledge Professor Gerald T. Babcock for his contributions to all aspects of this research.

I wish to thank Bob Ingle for the preparation of beef heart cytochrome oxidase, and Debra Thompson and Professor Shelagh Ferguson-Miller for the gift of rat liver cytochrome oxidase and Tatsuro Yoshida and Professor James A. Fee for the gift of HB 8 cytochrome oxidase from T. Thermophilus. I wish to acknowledge Brian Ward for his assistance in preparing the model compounds. Ron Haas is acknowledged for the predominant presence of a trouble-free laser system and the following people are acknowledged for the maintenance of my mental health: Jerry, Charlie, Tony, Deb, Chris, Mark, Tom, Margy, Bob, Bob, Jimbo and Ron.

TABLE OF CONTENTS

LIST OF TABLES

Table Page

LIST OF FIGURES

CHAPTER 1

INTRODUCTION

I. Respiration

Cellular respiration is the process whereby reducing equivalents generated from foodstuffs pass through a series of membrane bound electron carriers to a terminal electron acceptor such as oxygen. The synthesis of adenosine triphosphate (ATP) which provides the major energy source for the cell, is coupled to this electron transfer process. A transmembrane pH gradient generated at several locations in the respiratory chain is essential for ATP synthesis but the detailed mechanism of oxidative phosphorylation is not known.

In eukaryotes the respiratory components are found in the inner mitochondrial membrane. These components, labelled complexes I-IV, contain flavoproteins (FP), iron-sulfur centers (Fe-S), quinones (Q) and heme and copper containing proteins. (For a historical perspective of the heme proteins (cytochromes) and comprehensive reviews see (Keilin, 1966; Lemberg and Barrett, 1973 and Tzagoloff, 1982)). The sequence of electron transfer reactions was determined largely after the introduction of dual wavelength spectrophotometry by Chance and Williams (1955, 1956). This

technique enabled the observation of the absorption spectra of individual components of mitochondria while in turbid suspensions. This new spectroscopic method along with specific inhibitors of the electron transport chain and artificial electron acceptors identified the sequence of carriers shown in Scheme 1.

Succinate dehydrogenase

Complex II

$$NADH \rightarrow FP_1(4Fe\text{-}S) \rightarrow \overset{\overset{FP_2}{\downarrow}}{Q} \rightarrow 2(Fe\text{-}S) \rightarrow cyt\underline{b}(Fe\text{-}S)cyt\underline{c}_1 \rightarrow cyt\underline{c} \rightarrow Cu, cyt\underline{aa}_3 \rightarrow O_2$$

NADH dehydrogenase	Cyt $\underline{bc}_1$ complex	Cytochrome oxidase
Complex I	Complex III	Complex IV
Site 1	Site 2	Site 3

Scheme 1

Complex I, called NADH dehydrogenase, accepts electrons from reduced nicotinamide adenine dinucleotide (NADH) and reduces ubiquinone (Q). The active redox components of this complex are flavin and iron-sulfur centers. Complex II or succinate dehydrogenase comprises flavin and iron-sulfur redox components also, and feeds reducing equivalents into the mitochondrial electron transport chain at ubiquinone. Ubiquinone, an electron and proton carrier, is present in approximately a six fold excess relative to the 1:1

stoichiometry of complexes I-IV. Complex III is composed of two b cytochromes, the Rieske iron-sulfur center, associated quinone molecules and cytochrome c_1. After oxidizing Q, this complex transfers electrons to the water soluble redox protein cytochrome c. As the penultimate carrier, cytochrome c reduces the copper and heme a containing protein, cytochrome oxidase, which then carries out the reduction of dioxygen to water.

The redox potential spanned from NADH to O_2 is 1.14 volts. The large decrease in free energy from the passage of two electrons through this series (53 kcal/mole) is liberated as heat in hibernating and hairless newborn animals and some flowering plants (Nicholls and Locke, 1981). In coupled mitochondria, however, this free energy is utilized to translocate protons against a pH gradient. Sites 1, 2, and 3 in Scheme 1 contribute to the transmembrane pH gradient and therefore ATP synthesis with a stoichiometry of approximately three ATP molecules formed per two electrons passed through the respiratory chain.

The soluble and membrane bound components have been isolated and studied in great detail. This thesis is concerned with a spectroscopic study of Complex IV.

II. Cytochrome Oxidase

A. Components and Function

Complex IV or cytochrome oxidase (ferrocytochrome *c*: O_2 oxidoreductase; E C 1.9.3.1) enjoys a central role in the field of membrane bioenergetics because it is responsible for more than 90% of the oxygen consumed by living organisms. Cytochrome oxidase catalyzes the oxidation of ferrocytochrome *c* and the four electron reduction of dioxygen to water. In addition, it contributes to the transmembrane pH gradient by the translocation of two protons per electron (Wikström and Krab, 1979). The overall reaction can be written as:

$$4\text{cyt } \underline{c}^{2+} + O_2 + 8H^+_{in} \rightarrow 4\text{cyt}\underline{c}^{3+} + 2H_2O + 4H^+_{out}$$

where H^+_{in} refers to protons in the internal mitochondrial matrix phase and H^+_{out} refers to protons in the cytoplasmic phase.

This multisubunit enzyme is composed of four metal centers; two heme *a* chromophores, designated cytochrome *a* and cytochrome $\underline{a}_3$ and two protein bound copper ions, designated Cu *a* and $Cu_{\underline{a}_3}$. These four metal centers seem to function in pairs. Cytochrome *a* and $Cu_{\underline{a}}$ are responsible for the oxidation of ferrocytochrome *c* and further intramolecular electron transfer. Cytochrome *a* has recently been implicated

in the proton pumping action of the enzyme (Wikström, 1977). The second pair of metal centers make up the oxygen reducing site, and cytochrome $\underline{a}_3$ is the site of ligand binding such as substrate O_2 or inhibitors (HCN, HN_3, CO, NO).

The structure of the heme a macrocycle is shown in Figure 1. The distinguishing features of this structure relative to the more common protoheme containing proteins (hemoglobin, myoglobin, cyt b) are the hydrophobic hydroxyfarnesylethyl tail at position 2 and the formyl substituent at position 8. The pyrrole nitrogens of the porphyrin ligand fulfill four of the central metal iron coordination positions and fifth and sixth axial ligands can bind to the iron from above and below the plane of the ring. The heme a chromophores in this protein are amenable to a variety of spectroscopic probes. These chromophores and the two copper centers have been studied by absorption, electron paramagnetic resonance (EPR), electron-nuclear double resonance (ENDOR), circular dichroism (CD), magnetic circular dichroism (MCD), infrared (IR), resonance Raman (RR), magnetic susceptibility, Mössbauer and extended x-ray absorption fine structure (EXAFS) spectroscopies. Because of its complexity, cytochrome oxidase has also been the subject of many biochemical investigations. The following discussion focusses on information obtained by biochemical methods and chromophore structure and reactivity as determined by spectroscopic investigations. (For reviews see Malmström, 1979; Wikström et al., 1981 and Wikström et al., 1983).

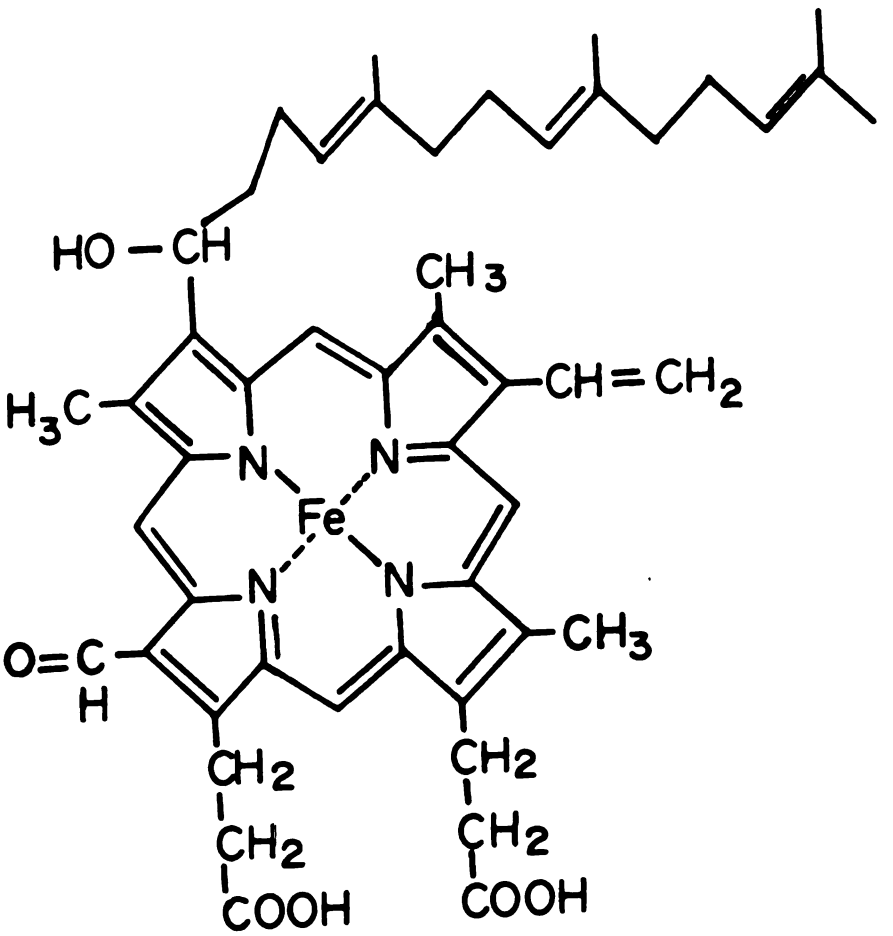

heme a

Figure 1. The structure of heme a.

B. Biochemical Aspects

Cytochrome oxidase from eukaryotic organisms has a molecular weight of approximately 160 kD and is composed of at least seven subunits. Of these, the three largest are coded for by mitochondrial DNA (Subunits I, II and III) and the remainder are of cytoplasmic origin. In contrast, bacterial cytochrome oxidases consist of only two or three polypeptides. The properties of these subunits resemble those of the largest eukaryotic subunits (Ludwig, 1980). With the use of labelling techniques, it is found that several subunits (I, II and III) are accessible from both sides of the membrane (Azzi, 1980; Wikström et al., 1981; Capaldi, 1982). Electron microscopy and image reconstruction data show that the monomeric enzyme spans the membrane in the shape of an inverted Y and it is found to protrude ∿50-60 Å into the cytoplasmic (C) phase and about 10-15 Å into the M or matrix phase (Henderson et al., 1977; Frey et al., 1978) (See Figure 2).

The aggregation state of solubilized cytochrome oxidase is dependent on detergent. In most detergents it is oligomeric, however, in lauryl maltoside, the enzyme seems to be dispersed as a monomer (Ferguson-Miller, 1983). The effect of aggregation on catalytic function or the aggregation state of cytochrome oxidase in vivo is not known. Subunit III has been implicated in the enzyme's ability to form dimers (Georgevich et al., 1983) and removal of this subunit

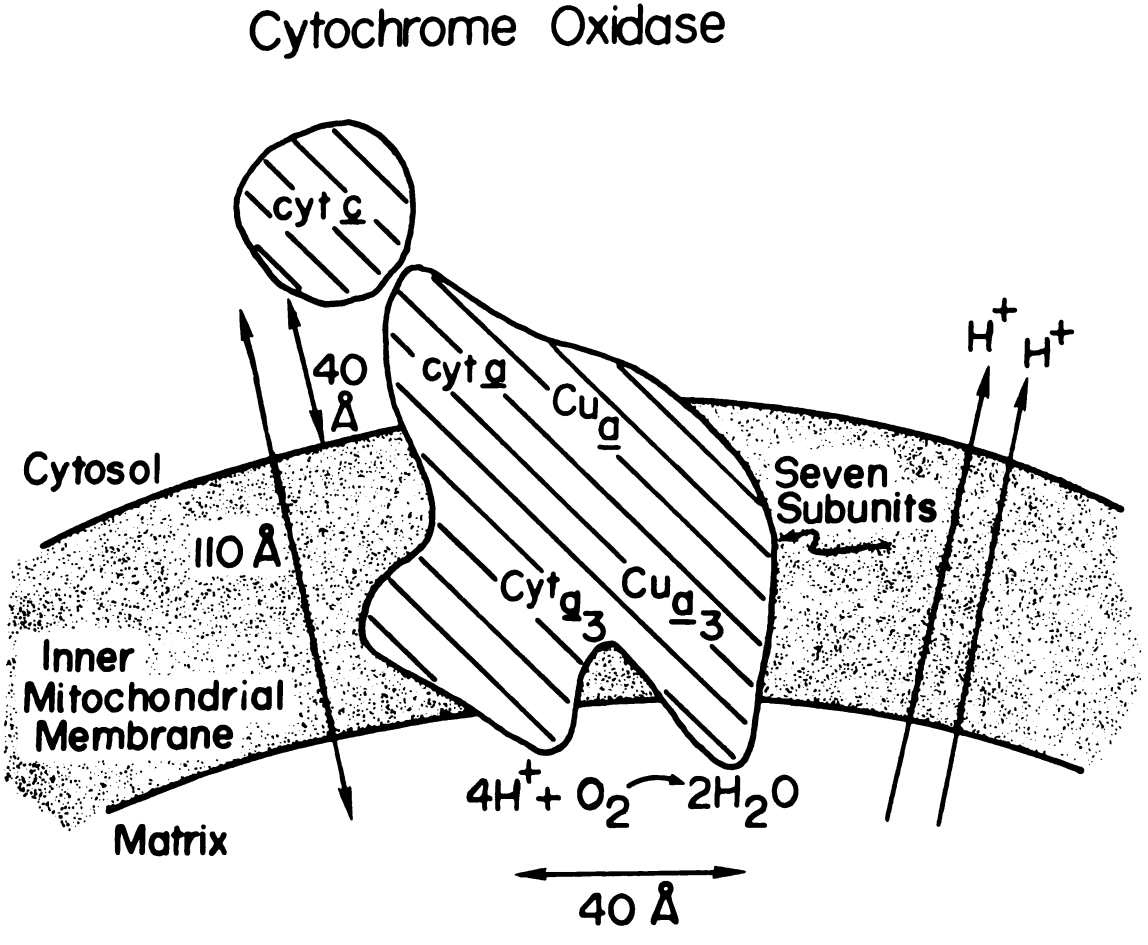

Figure 2. Schematic of membraneous cytochrome oxidase.

has little or no effect on the spectral or electron transfer properties although some evidence suggests that it does eliminate the proton pumping function of the enzyme (Wikström et al., 1981, Penttila, 1983). Wikström et al. (1981) have also implicated the dimeric state in proton pumping by the oxidase.

By monitoring a controlled denaturation of cytochrome oxidase Winter et al. (1980) concluded that the four metal centers are located in subunits I and II. This is supported by the fact that the two subunit bacterial oxidases have the same spectral and catalytic properties as the mammalian enzyme (Ludwig, 1980; Fee et al.,1980; Yamanaka et al., 1981; Powers et al., 1981; Gennis et al., 1982; Sone and Yanagita, 1982).

C. Chromophore Structure

Cytochrome c, the physiological electron donor to cytochrome oxidase, binds in its high affinity site to subunit II of the enzyme (Bisson et al., 1982). Resonance energy transfer measurements of the distance between fluorescence cytochrome c derivatives and the nearest heme a chromophore result in approximately 25-35 Å heme c - heme a distance (Vanderkooi et al., 1977, Dockter et al., 1978). Since cytochrome a is the first electron acceptor from cytochrome c (Halaka, et al., 1982, Antalis and Palmer, 1982), it is postulated that cytochrome a and its functionally

associated Cu, (Cu_a) are located on subunit II (Wikström et al., 1983). Cytochrome a has been shown to be ligated by two histidine residues by comparison of the EPR, MCD and resonance Raman spectra of the in vivo chromophore with heme a model compounds (Blumberg and Peisach, 1979; Babcock et al., 1979). Examination of the invariant histidine residues of subunit II, and the possible folding pattern of this polypeptide locates the cytochrome a binding site close to the cytoplasmic membrane (Wikström et al., 1983). This location is consistent with the EPR defined location of cytochrome a and Cu_a. With the use of water soluble paramagnetic probes it was concluded that these metal centers are close to the cytoplasmic membrane (Ohnishi, et al., 1979).

The EPR signal of Cu_a occurs about g2 but it is atypical of known cupric copper signals; its hyperfine splitting constant can be understood if the unpaired electron spin density is delocalized onto the copper ligand(s). One and possibly two cysteines have been suggested as ligands of Cu_a on the basis of EPR data (Peisach, 1978; Blumberg and Peisach, 1979; Chan et al., 1978, 1979). Two invariant cysteines found in the primary structure of subunit II lie in an area of the polypeptide that has sequence homology with blue copper proteins (Steffens and Buse, 1979). The invariant cysteines and histidine found in this region agree with the recent EPR and ENDOR data of ^{15}N-histidine and ^{2}H-cysteine in which Stevens et al. (1982) conclude that

at least one histidine and one cysteine are ligands to $Cu_{\underline{a}}$. See Figure 3 for a summary of the ligation properties of cyt $\underline{a}$ and $Cu_{\underline{a}}$.

The other two metal centers are most likely located in subunit I. Cytochrome $\underline{a}_3^{3+}$ and $Cu_{\underline{a}_3}^{2+}$ are not detectable by EPR in the resting enzyme. However, EPR signals arising from cyt $\underline{a}_3$ and $Cu_{\underline{a}_3}$ can be induced by addition of ligands and/or reduction of the other metal center (Stevens et al., 1979; Brudvig et al., 1980 and Reinhammar et al., 1980). Magnetic susceptibility measurements suggest that this pair of metals is antiferromagnetically coupled in an S=2 ground state with $|2J|>200$ cm^{-1} (Tweedle et al., 1978). This indicates that the metals are in close proximity to each other. This distance has been measured by EXAFS to be 3.75 ± 0.05 Å (Powers et al., 1981). In the resting enzyme, Powers et al. (1981) suggest the presence of a bridging sulfur ligand between the iron of cyt $\underline{a}_3^{3+}$ and $Cu_{\underline{a}_3}^{2+}$. However, the amount of enzyme with this bridging sulfur ligand varies with the type of isolation procedure used. Heterogeneity in the spectra and properties of cyt $\underline{a}_3$ in the resting enzyme has been observed previously (Kumar et al., 1983, Brudvig et al., 1981).

MCD spectra of ferrous cytochrome $\underline{a}_3$ indicate a five coordinate high-spin iron geometry (Babcock et al., 1976). The identity of the fifth, axial ligand as histidine has been obtained from EPR studies of nitrosyl ferrous cyt $\underline{a}_3$ ($\underline{a}_3^{2+} \cdot NO$) (Blokzijl-Homan and Van Gelder, 1971). Since

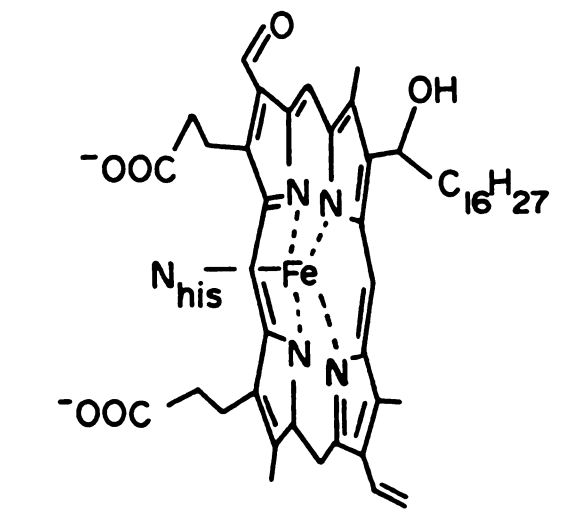

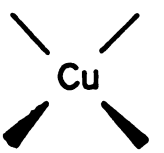

cyt $\underline{a}_3^{2+}$

$Cu_{\underline{a}_3}^{1+}$

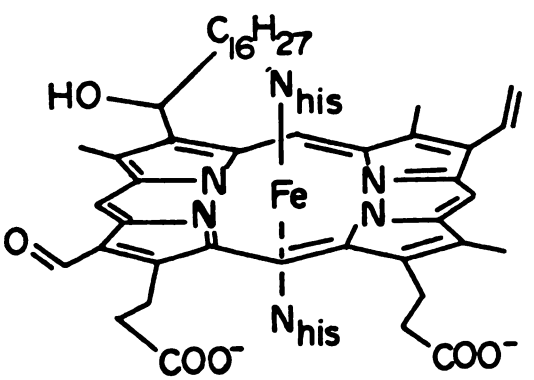

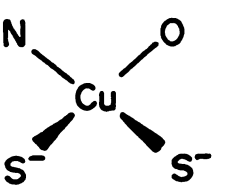

cyt $\underline{a}$

$Cu_{\underline{a}}$

Figure 3. Summary of the structure and ligation spheres of the cytochrome oxidase metal centers.

no EPR signal from $Cu^{2+}_{a_3}$ is observed under most conditions, the nature of its ligands remains obscure.

The currently accepted model for the arrangement of cytochrome a_3 and Cu_{a_3} is described as the "front-side" model and is shown in Figure 3. The close proximity (∿4 Å) of these metal ions as determined by magnetic susceptibility and EXAFS data is satisfied by this model. Further evidence for this structure is supplied by carbonmonoxide flash photolysis studies. After photolyzing the inhibitor from cyt a_3^{2+}, the carbon monoxide is observed to rebind to the Cu_{a_3} site (Alben *et al.*, 1981); therefore a model in which the two metal centers are capable of binuclear ligand binding is suggested.

D. Absorption Spectra

The focus of this thesis is the determination of structure by analysis of the spectral properties of the heme *a* chromophores of cytochrome oxidase. Although optical absorption spectroscopy is the most commonly used spectroscopic probe, a complete understanding of the enzyme's absorption spectrum has not been reached. The visible absorption spectra of oxidized and reduced cytochrome oxidase are given in Figure 4. The heme *a* chromophores dominate the spectrum in the near UV and visible regions because of the intense π-π^* transitions of the porphyrin macrocycle. Typically,

Figure 4. Optical absorption spectra of cytochrome oxidase: oxidized ——— and fully reduced - - - -. Extinction coefficients are expressed per unit containing two hemes and two copper ions. (From Halaka, 1981.)

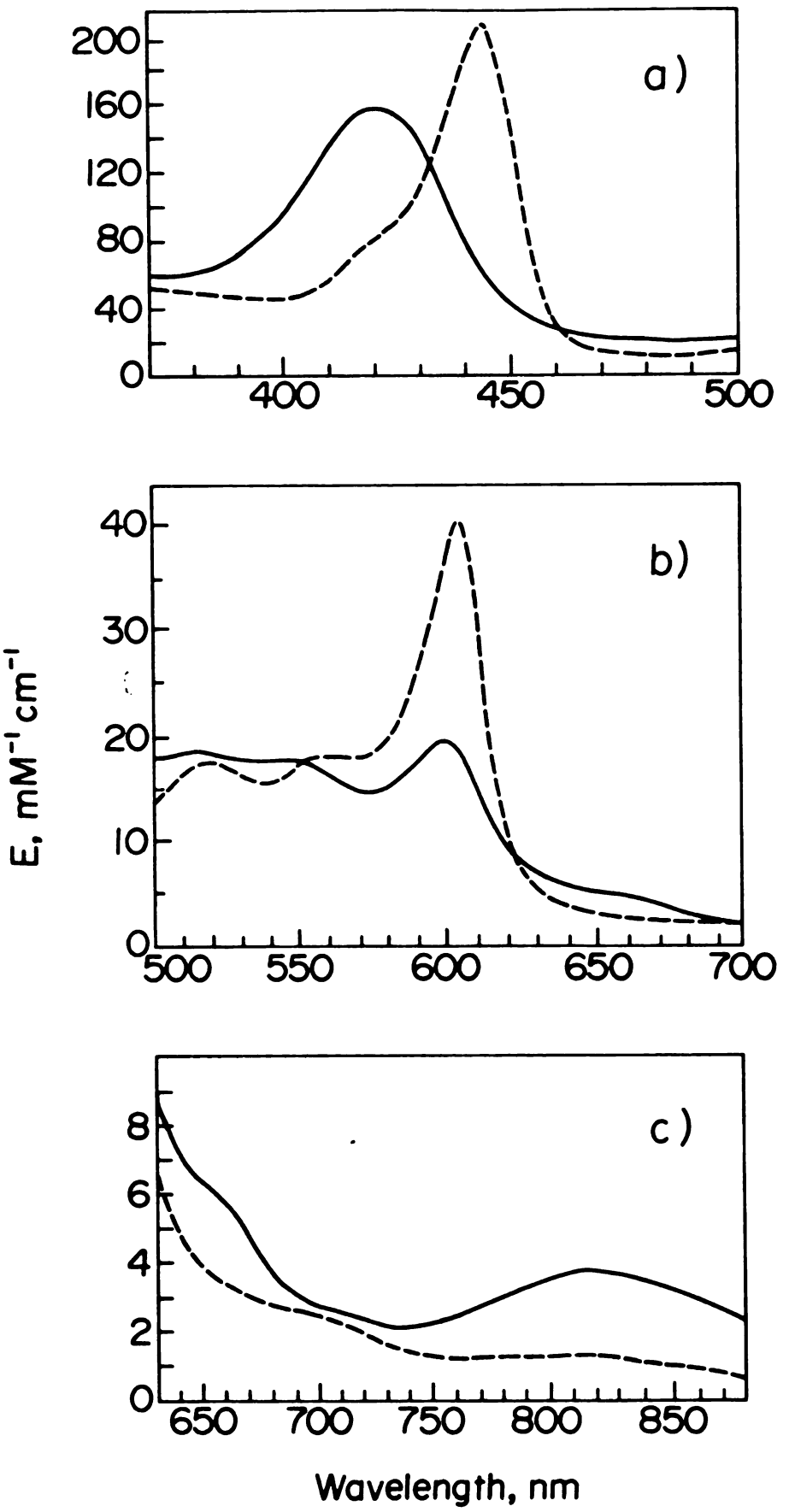
a)
b)
c)
E, mM⁻¹cm⁻¹
Wavelength, nm
200
160
120
80
40
0
400
450
500
40
30
20
10
0
500
550
600
650
700
8
6
4
2
0
650
700
750
800
850

Figure 4

three absorption maxima are observed for metalloporphyrin species, namely, an intense Soret band (also γ band) at 400-450 nm, a weaker α band at 550-600 nm and a β band at approximately 1100 cm^{-1} to higher energy than the α band. A more detailed discussion of heme electronic properties will be given in Chapter 2. The reduced enzyme's absorption maxima are 443, 555, 565, and 604 nm. The Soret maximum of oxidized cytochrome oxidase is broad and centered at 418-424 nm. Its visible spectrum is structureless except for the α maximum at 598 nm and a weak shoulder at 655 nm. The 655 nm band is present only if the enzyme is oxidized in the presence of oxygen rather than other chemical oxidants. In the case of ferricyanide oxidation a transient high-spin heme g6 signal which accounts for 100% of one heme is observed (Beinert and Shaw, 1977). This signal has been assigned to cytochrome $\underline{a}_3^{3+}$. The explanation for these results is that $Cu_{\underline{a}_3}$ is reduced and the exchange coupling between cyt $\underline{a}_3$ and $Cu_{\underline{a}_3}$ is broken, therefore the 655 nm band is present only when the exchange coupling between these two metals in their higher oxidation states, is present.

Aside from the 655 nm shoulder and 830 nm band (which has been assigned to $Cu_{\underline{a}}^{2+}$), the major spectral features arise from cytochrome $\underline{a}$ and cytochrome $\underline{a}_3$ electronic transitions. Because of their similar chemical nature the heme $\underline{a}$ chromophore absorption spectra strongly overlap.

In 1966, Vanneste took advantage of the photodissociability of the electron transfer inhibitor, carbon monoxide, from ferrous cytochrome $\underline{a}_3$. From the photochemical action spectrum he was able to identify the individual contributions of cytochrome $\underline{a}$ and $\underline{a}_3$ to the total absorption spectra. These deconvoluted spectra are shown in Figure 5. In the bottom panel the absorption maxima of cyt $\underline{a}^{3+}$ are 427, 550 and 598 nm and of cyt $\underline{a}^{2+}$ are 443 nm (420 nm shoulder), 520, 555 and 603 nm. Comparison of the extinction coefficients of cyt $\underline{a}$ and cytochrome $\underline{a}_3$ (middle panel) in the visible region show that cyt $\underline{a}$ dominates the spectrum in both oxidation states. In the Soret region, on the other hand, cyt $\underline{a}$ is the major absorber in the oxidized enzyme but the intensities of cyt $\underline{a}$ and cyt $\underline{a}_3$ are comparable in this region for the reduced enzyme. Vanneste's deconvoluted absorption maxima of cyt $\underline{a}_3^{3+}$ are observed at 414, 560 and 600 nm and of cyt $\underline{a}_3^{2+}$ at 442, 565 and 600 nm. The large γ/α intensity ratio for reduced cytochrome $\underline{a}_3$ is indicative of a high-spin species (Lemberg, 1969), which is in agreement with other spectroscopic data (Babcock et al., 1976, 1979). The low-spin character of cyt $\underline{a}$ is indicated by its smaller γ/α intensity ratio. An anomalous aspect of these spectral assignments is the Soret wavelength maxima of the reduced components. In general, the Soret maxima of high and low-spin species are not the same, as is observed for the Soret maxima of cyt $\underline{a}^{2+}$ and cyt $\underline{a}_3^{2+}$ at approximately 443 nm.

Figure 5. Absorption spectral decomposition of cytochromes $\underline{a}$, $\underline{a}_3$ and the CN complex of cytochrome $\underline{a}_3$; oxidized ——— and reduced - - - - - - . (From Vanneste, 1966.)

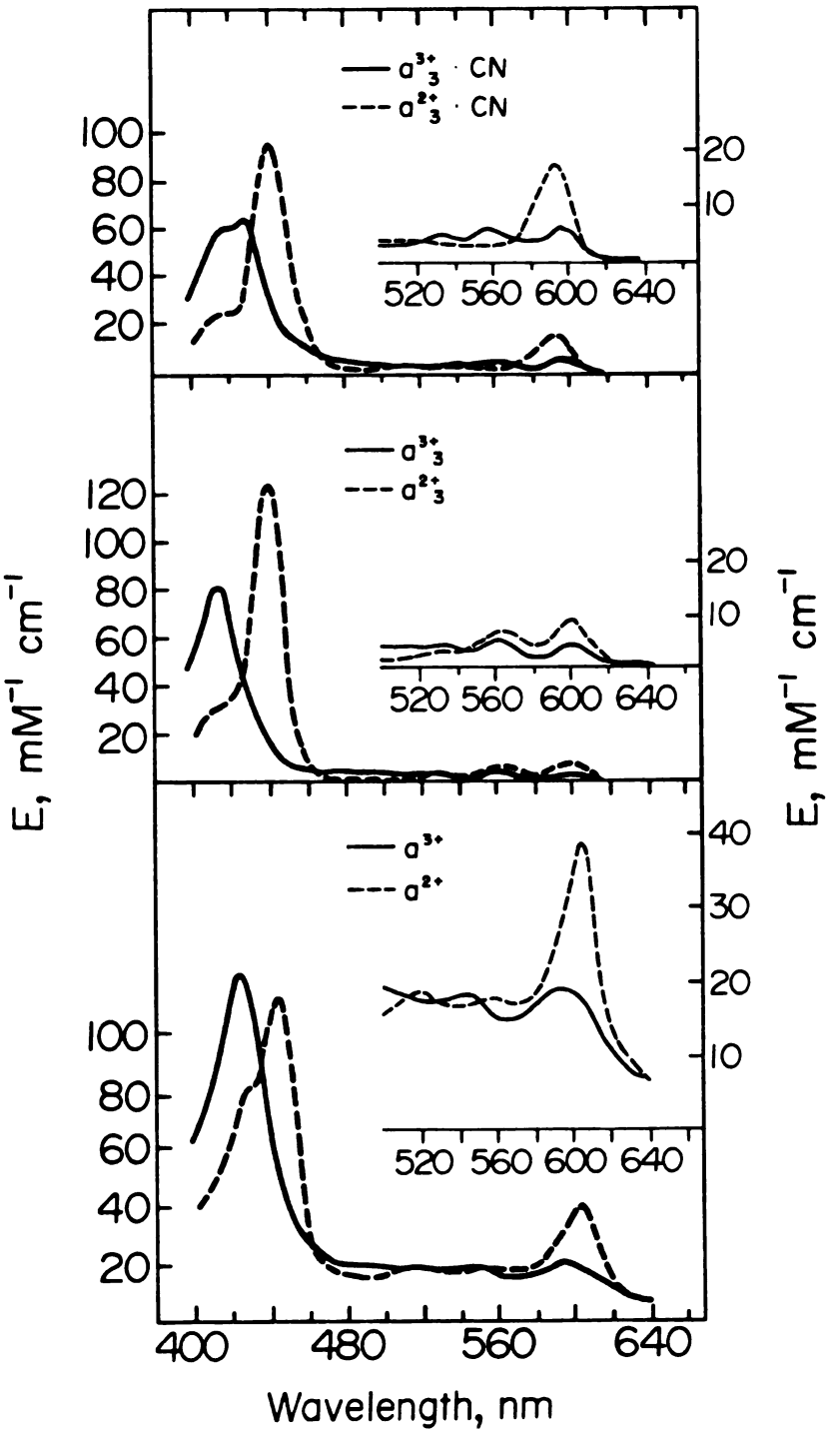
a^{3+}_3 · CN
a^{2+}_3 · CN
a^{3+}_3
a^{2+}_3
a^{3+}
a^{2+}
E, mM^{-1} cm^{-1}
E, mM^{-1} cm^{-1}
Wavelength, nm
400
480
560
640
520 560 600 640

Figure 5

E. Redox Titrations

This spectral decomposition method is valid only if the heme chromophores have independent spectral properties and the redox state of one chromophore does not effect the electronic transitions of another. A controversy on this point arose in the mid-seventies. By monitoring the absorption intensity at 604 nm as a function of redox potential, Wilson et al. (1972) concluded that the heme chromophores have fixed midpoint potentials of 285 mV for the cyt $\underline{a}^{3+/2+}$ couple and 350 mV for cyt $\underline{a}_3{}^{3+/2+}$ and that their spectral properties are strongly interacting. Nicholls and coworkers (1974) and Wikström et al., (1976) presented arguments favoring an alternate description; that is, fixed spectral properties but varying redox potentials. Evidence for the alternate interpretation was given by Babcock et al. (1976, 1978) who established the individual Soret region MCD spectra of the heme a components and monitored both the absorption and MCD spectra of the enzyme during reductive titrations. Their data show that the spectral deconvolution of Vanneste is valid (i.e., non-interacting electronic properties). This conclusion is reached because under all experimental conditions the reduction levels of cytochromes a and $\underline{a}_3$ are comparable. This result cannot be reconciled with a model in which the two heme centers have well resolved potentials.

Addition of one electron to the enzyme lowers the redox

potential of the second heme electron transfer reaction. This negative cooperativity has been estimated to involve an approximate 2 kcal/mole coupling between the heme centers (Carithers and Palmer, 1981). Under the equilibrium conditions present in redox titrations, the two hemes *a* behave essentially as a two electron system in analogy with classical two electron carriers such as ubiquinone (Wikström *et al.*, 1983).

A recent different absorption spectral study involving several different inhibitor complexes of cytochrome oxidase (Blair *et al.*, 1982) also supports the independent chromophore spectral model and Vanneste's deconvolution. This study does, however, point out small spectral interactions especially for the cyt $\underline{a}_3^{3+}$, $Cu_{\underline{a}_3}^{2+}$ and cyt $\underline{a}_3^{3+}$, $Cu_{\underline{a}_3}^{1+}$ species. These results can be understood in terms of an electrostatic effect, whereby the charge on $Cu_{\underline{a}_3}$ effects the absorption properties of nearby cyt $\underline{a}_3$. Although Vanneste's results are generally accepted, simple heme *a* model complexes of the spin and ligation states described above for cytochromes *a* and $\underline{a}_3$ do not reproduce the deconvoluted absorption spectra (Lemberg, 1962). This result will be discussed in Chapters 4 and 5.

III. Catalytic Mechanisms

A. Electron Transfer Intermediates

Up to this point only the structural and spectroscopic properties of the static forms of the enzyme have been discussed. When reduced cytochrome oxidase is reoxidized with O_2 at room temperature, at least three different conformations are sequentially formed. The first which is formed within 2 ms at room temperature and decays in a few seconds is known as the g5 conformation. This form of the enzyme has a Soret maximum at 427 nm, broad absorption at 580 nm when compared to the resting enzyme, a 655 nm absorption band and EPR signals at g=5, 1.78 and 1.69. These EPR transitions were interpreted in terms of an S=5/2 ferric cyt $\underline{a}_3$ interacting with a nearby paramagnetic center ($Cu_{\underline{a}_3}$) (Shaw et al., 1979). Another possible interpretation of the g=5 EPR spectrum involves an S=3/2 system that is composed of ferryl cyt $\underline{a}_3$ and cupric copper (Wikström *et al.*, 1981). Following formation of the g5 species, a second conformation of the enzyme called oxygenated cytochrome oxidase is formed. This is a misnomer in the sense that O_2 is not bound to cyt $\underline{a}_3^{2+}$ as in oxyhemoglobin but the oxygenated description of the form of the enzyme with the following characteristics has become common usage; the absorption maxima occur at 427 nm and 600 nm, the 655 nm band is present, the enzyme requires four electrons for complete reduction, and

the EPR spectrum is identical to that of the oxidized enzyme (i.e., cyt $\underline{a}_3^{3+}$ and $Cu_{\underline{a}_3}^{2+}$ are EPR undetectable). The oxygenated enzyme's reactivity to exogenous ligands is fast and monophasic in comparison to the resting enzyme which binds ligands sluggishly and in a multiphasic manner (Kumar et al., 1983). This suggests that the oxygenated enzyme may be the catalytic starting point for oxygen reduction. On the time scale of hours, the oxygenated enzyme reverts to the resting form.

Since no intermediate oxygen reduction products such as superoxide, peroxide or hydroxyl radical are released from the $\underline{a}_3$ site and because of the unfavorable thermodynamic barrier to transfer of the first or third electron to oxygen, it has been proposed that a concerted two electron transfer process takes place (Malmström, 1974; Babcock et al., 1978; Reed and Landrum, 1979). The initial reaction sequence would then reduce dioxygen to the level of peroxide. The low temperature triple-trapping technique of cytochrome oxidase reaction intermediates developed by Chance and coworkers (Chance et al., 1975) has permitted a preliminary identification of the catalytic mechanism of oxygen reduction. In this technique the enzyme, or mitochondrial suspension, is saturated with carbon monoxide under reducing conditions to form the $\underline{a}^{3+}$ $\underline{a}_3^{2+}\cdot CO$ or $\underline{a}^{2+}$ $\underline{a}_3^{2+}\cdot CO$ compound, and then cooled in the presence of ethylene glycol to about -30°C. Oxygen is then added to the suspension

by stirring or mixing with O_2 saturated buffer. The oxygen will not react with this form of the enzyme owing to the slow dissociation of CO at this temperature in the dark. The oxygenated suspension is then brought to -196°C. The enzymic reaction with oxygen can be initiated by an intense flash of light which photodissociates the CO and allows the oxygen to bind. The reaction proceeds in the temperature range -60 to -130°C and can be stopped at any point by rapid freezing in liquid nitrogen. EPR and absorption spectra of the reaction intermediates prepared in this way have been monitored (Clore and Chance, 1978, Clore et al., 1980).

The stable intermediates that have been formed and characterized by this method are called Compounds A, B and C. Compound A has been identified as an oxy cyt $\underline{a}_3^{2+}$ species (cyt $\underline{a}_3^{2+} \cdot O_2$). This conclusion is reached on the basis of its optical absorption spectrum which is similar to the CO complex but non-photolyzable. Oxy heme a model studies (Babcock and Chang, 1979) are consistent with the spectrum of Compound A. A later intermediate of the mixed-valence ($\underline{a}^{3+}$ $\underline{a}_3^{2+} \cdot CO$) compound called Compound C is characterized by a difference spectrum absorption peak at 607 nm (ε = 12 mM^{-1} cm^{-1}) and weak Soret absorption intensity. This species has been suggested to be the μ-peroxy form of the $\underline{a}_3$ site ($\underline{a}_3^{3+} - O - O - Cu_{\underline{a}_3}^{2+}$) or ferryl iron and cuprous copper ($Fe_{\underline{a}_3}^{4+} = O - O - Cu_{\underline{a}_3}^{1+}$) (Wikström et al., 1981). If the reaction intermediate sequence is begun with fully reduced cytochrome oxidase ($\underline{a}^{2+}$ $\underline{a}_3^{2+} \cdot CO$) a different structural

intermediate is formed (Compound B) following the formation of the oxy intermediate (Compound A). The exact nature of Compound B is difficult to determine because there is partial oxidation of cyt *a* and Cu_a, also (Wikström *et al.*, 1981).

Similar spectral intermediates have been observed by ATP dependent partial reversed electron flow through cytochrome oxidase (Wikström, 1981). In this work, Wikström suggested that the previously observed energy dependent shift of ferric cyt a_3 (Erecińska, et al., 1972) could be attributed to reversed electron transfer. Under highly oxidizing conditions, the addition of ATP to a mitochondrial suspension causes a red-shift in the Soret region of cytochrome oxidase and a broad absorption increase at 580 nm, similar to Compound B described by Chance and coworkers. At a higher phosphorylation potential a moderately intense band in the α region at 607 nm is observed. This spectral form resembles Compound C. These results are good evidence for the physiological nature of the low temperature intermediates.

Much research is now being conducted on the intermediates of the cytochrome oxidase oxygen reduction reaction. The structure of cyt a_3 in the oxygenated enzyme as determined by RRS and a possible reaction mechanism that is consistent with the data obtained to date will be presented in Chapter 4.

B. Energy Transduction

It has been known for thirty years that electron transfer from cyt c to O_2 is linked to ATP formation (Maley and Lardy, 1954, Lehninger et al., 1954). The approximately 500 mV spanned by this reaction contains enough free energy for the energetically uphill proton translocation against a pH gradient. In recent years, isolated cytochrome oxidase reconstituted into liposomes has been shown to generate a chemical potential across the membrane (Hinkle et al., 1972) in agreement with Mitchell's chemiosmotic coupling hypothesis (Mitchell, 1961). Mitchell described the uptake of protons by the a_3 site in the formation of water as the only source of proton motive force in Complex IV (Mitchell and Moyle, 1983). This does not agree with the stoichiometry of protons and charges translocated across the membrane, however (Wikström and Krab, 1979, Reynafarje et al., 1982). This is problematic because cytochrome oxidase contains redox components that are only formal electron carriers (two hemes a and two copper ions) and therefore the result of H^+ translocation by cytochrome oxidase is not completely accepted (Mitchell and Moyle, 1983). Evidence is accumulating, however, that the proton pumping of cytochrome oxidase is a physiological function (Wikström et al., 1983, Casey and Azzi, 1983) and that specific treatments can inhibit this function (Casey et al., 1980; Wikström et al., 1983; Penttilä, 1983 and Maroney and Hinkle, 1983).

Subunit III seems to have a specific role in the translocation of protons. Casey et al (1980) found that dicyclohexylcarbodiimide (DCCD) appeared to block H^+ translocation in cytochrome oxidase reconstituted into liposomes. Under these conditions, DCCD was predominantly bound to subunit III. Treatment of the enzyme to remove subunit III results in the inhibition of proton translocation, (Sarraste et al., 1981; Penttilä, 1983) but the electrochemical proton gradient is formed with only 50% efficiency. This result can be interpreted in the following way: 1) an inhibition of the proton translocating segment of the protein and 2) a continuation of electron transfer and the a_3 site proton uptake necessary for water formation (Wikström, 1983). It is surprising that proton translocation can be decoupled from electron transfer with no effect on the rate of the latter but the possibility of long range interactions between the redox element and the proton source cannot be excluded.

The identification of the redox element of the proton pump as cytochrome a is based on 1) its pH dependent midpoint potential (Artzatbanov et al., 1978) and 2) its kinetic heterogeneity which may reflect two conformational states (Wikström et al., 1981). A necessary element of a redox-linked proton pump is that there must be a connection between the redox component and the polypeptide backbone or proton source. Such a structural connection will be

discussed in Chapter 5 and its possible role in the proton pumping function of the enzyme will be presented in Chapter 6.

CHAPTER 2

HEME ABSORPTION AND RESONANCE RAMAN THEORY

Introduction

A great deal of structural information can be obtained from the absorption spectra of metalloporphyrins. When the absorption spectrum alone fails to identify or characterize a particular sample, the selective vibrational technique, resonance Raman spectroscopy, can supply additional information. Because of the importance of absorption and resonance Raman spectroscopy (RRS) as applied to the heme a chromophores of cytochrome oxidase in this thesis, an understanding of the theoretical considerations is necessary. This chapter will present a description of metalloporphyrin electronic transitions and of resonance Raman spectroscopy as applied to these chromophores.

I. Absorption Spectra

Metalloporphyrins and related compounds are responsible for the red, orange, brown and green coloring of a variety of biological materials; including red blood, green plants and the brilliant coloring of some species of birds. It

has long been recognized that this class of compounds derive their light absorption properties from π-π^* transitions (Platt, 1956).

A. Nomenclature

The basic structure of the porphyrin macrocycle is given in Figure 6. The four pyrrole rings are joined at the methine bridge or meso positions, labelled α, β, γ and δ, and various peripheral substituents can be linked to the β-carbon positions labelled 1-8. The remaining carbon atoms adjacent to the pyrrole nitrogens are called α-carbons. For this specific example of an iron-substituted metalloporphyrin, the molecule is called a heme. In this form the porphyrin ligand exists as a dianionic species which upon removal of the central metal atom is protonated at opposite pyrrole nitrogens to form the free base compound.

B. Electronic Transitions

1. Description of Porphyrin Spectra

The aim of several spectroscopic theories has been to explain the optical absorption spectra of porphyrin and metalloporphyrin species. Typical spectra of these two compounds are shown in Figure 7. An intense band in the near UV ($\varepsilon \approx 100\ mM^{-1}\ cm^{-1}$) called the Soret (or B) band

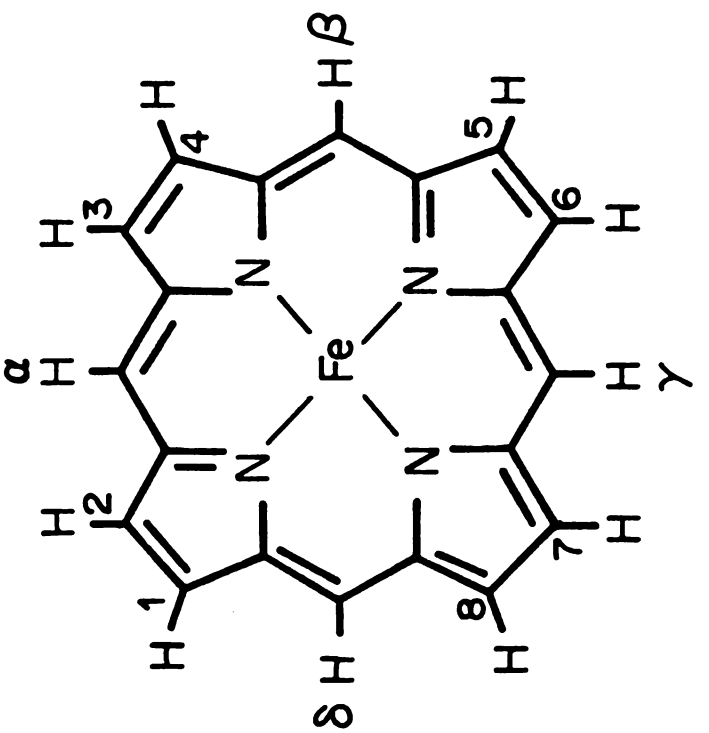

Figure 6. Metalloporphyrin structure including atom labelling pattern.

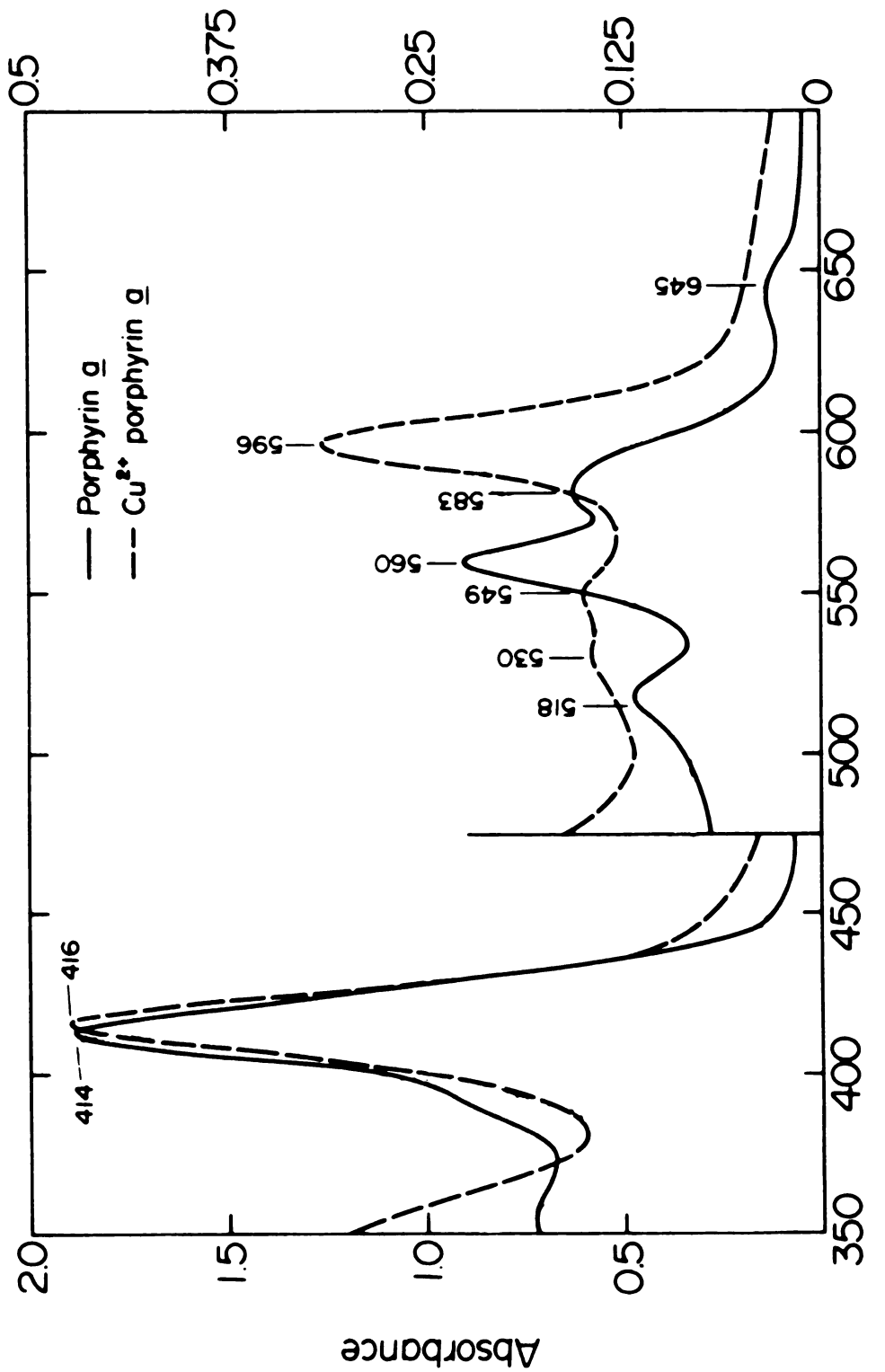

Figure 7. Optical absorption spectra of the indicated heme a derivatives. The solvent is CH_2Cl_2, concentration is ~14 uM, pathlength = 1 cm.

and a weaker ($\varepsilon \approx 20$ mM^{-1} cm^{-1}), α (or Q) band are the two main transitions in metalloporphyrin spectra. The β (or Q_{01}) band at approximately 1100 cm^{-1} higher energy than the α band is a vibronic overtone of the α band. In D_{4h} symmetry these two electronic transitions are of E_u symmetry and therefore doubly degenerate and x, y polarized in the plane of the ring. For the free base porphyrin, the protonation of opposite pyrrole nitrogens lowers the symmetry of the ring to D_{2h} and the x, y degeneracy is lifted causing a doubling of transitions in the visible region (i.e., Q^x_{00}, Q^x_{01}. Q^y_{00}, Q^y_{01}, from low to high energy, respectively).

2. Historical Development

In the free electron model of porphyrin spectra, Simpson (1949) was able to predict the relative energies and relative intensities of the Q and B transitions. By analogy with benzene, the 18 π electrons of the porphyrin ring are placed in orbitals of increasing angular momentum. The top-filled levels have angular momentum, L=4 and the lowest empty orbitals correspond to L=5, therefore these two levels can give rise to transitions of $\Delta L = \pm 1$ or $\Delta L = \pm 9$. By Hund's rule, the forbidden transition, $\Delta L = \pm 9$ lies lower in energy. This development qualitatively predicts the intense B transition ($\Delta L = \pm 1$) and a weak or forbidden transition to lower energy ($\Delta L = \pm 9$). A similar description

of the porphyrin π states, the cyclic polyene model used by Moffitt (1954), reached the same results as the free electron model and also correctly accounted for the splitting of the Q_x and Q_y energy levels in the free base absorption spectra.

In an effort to relate the porphyrin electronic transitions to structure, Longuet-Higgins et al. (1950) employed molecular orbital (MO) calculations. They obtained two top-filled orbitals, a_{2u} and a_{1u} (with a_{1u} of lower energy) and lowest empty degenerate orbitals, e_g (Figure 8). This identifies two electronic transitions, ($a_{2u} \rightarrow e_g$) and ($a_{1u} \rightarrow e_g$), corresponding to the Q and B bands, respectively. However, this development incorrectly predicts equal intensities for the two transitions. The shortcoming of this method lies in the neglect of the fact that since the two calculated transitions are both of E_u symmetry their Coulomb repulsion overlap matrix is finite. This causes the states to mix and drives them apart in energy.

3. The Four-Orbital Model

Gouterman (1959) recognized the necessity of configuration interaction (CI) in the description of porphyrin electronic states. Configuration interaction arises because of the neglect of electron correlation from the restriction to one-center integrals in Hückel MO theory. The solutions then are not solutions of the complete Hamiltonian,

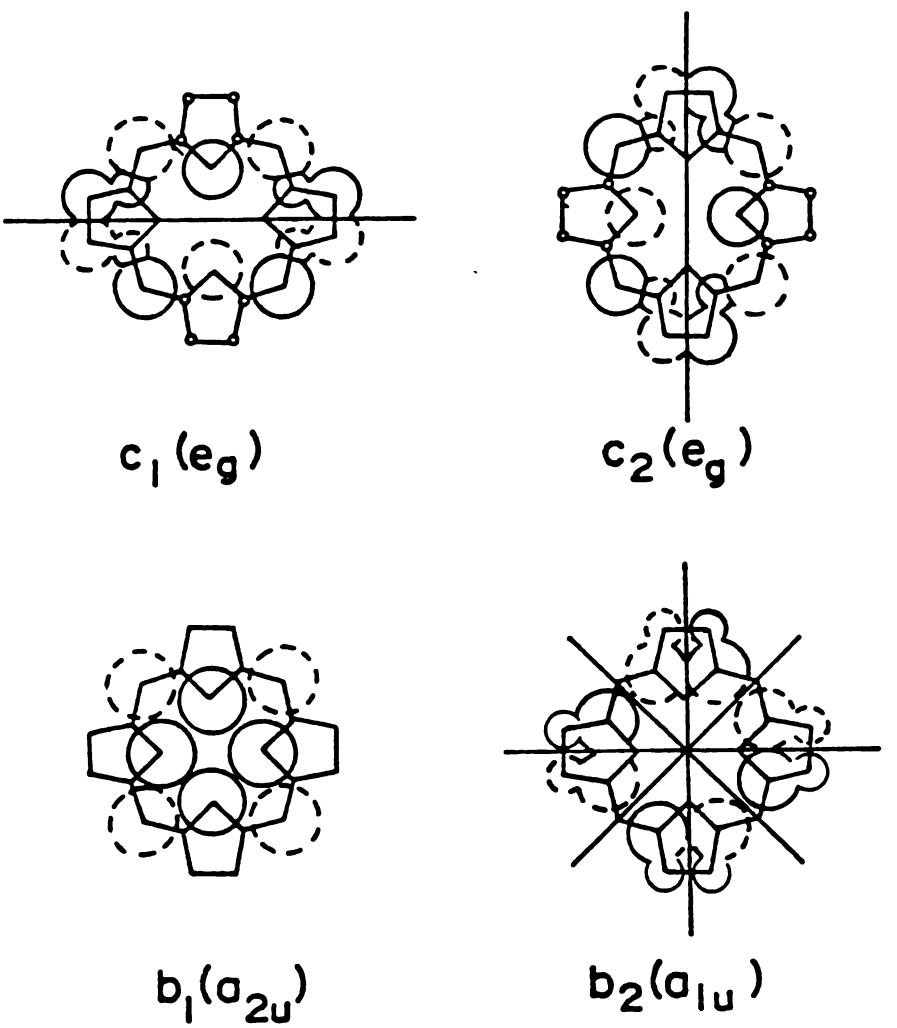

Figure 8. Spatial and nodal characteristics of the lowest unfilled (e_g) and highest filled (a_{1u}, a_{2u}) porphyrin orbitals. (From Gouterman, 1961.)

but rather solutions of an effective Hamiltonian,

$$\hat{H}_{eff}\psi = E\psi.$$

The complete Hamiltonian can be represented as

$$\hat{H} = \hat{H}_{eff} + H',$$

where H' is predominantly the electron repulsion term, e^2/r_{ij}. This Hamiltonian can cause states of the same symmetry to mix, specifically the singly excited configurations $(a_{1u}e_g)$ and $(a_{2u}e_g)$.

Since the singly excited configurations are not an accurate representation of the system, a better starting point for describing the excited states of a metalloporphyrin are linear combinations of the two excited configurations. The components of the zeroth order Q and B electronic states are:

$$|B_y^o\rangle = \frac{1}{\sqrt{2}}\left[(a_{2u}e_{g_y}) + (a_{1u}e_{g_x})\right]$$

$$|Q_y^o\rangle = \frac{1}{\sqrt{2}}\left[(a_{2u}e_{g_y}) - (a_{1u}e_{g_x})\right]$$

$$|B_x^o\rangle = \frac{1}{\sqrt{2}}\left[(a_{2u}e_{g_x}) - (a_{1u}e_{g_y})\right]$$

$$|Q_x^o\rangle = \frac{1}{\sqrt{2}}\left[(a_{2u}e_{g_x}) + (a_{1u}e_{g_y})\right]$$

It can be seen that B_x^o and B_y^o give rise to the allowed Soret transitions while Q_y^o and Q_x^o are the forbidden visible transition. To show this let us define the following transition moments,

$$R_{1y} = \langle a_{1u} e_{g_x} | y | \psi_o \rangle$$

and

$$R_{2y} = \langle a_{2u} e_{g_y} | y | \psi_o \rangle$$

where ψ_o is the ground state wavefunction and integration is over all space. As stated earlier $R_{1y} \approx R_{2y}$, i.e., the intensities are approximately equal. The measure of absorption intensity is the dipole strength which is the square of the transition moment, $\langle q \rangle^2$. For $|B_y^o\rangle$, the transition moment squared equals

$$q^2 = \frac{1}{2}[\langle (a_{2u} e_{g_y}) | y | \psi_o \rangle + \langle (a_{1u} e_{g_x} | y | \psi_o \rangle]^2$$

$$= \frac{1}{2}[R_{2y} + R_{1y}]^2$$

and for $|Q_y^o\rangle$

$$q^2 = \frac{1}{2}[\langle (a_{2u} e_{g_y}) | y | \psi_o \rangle - \langle (a_{1u} e_{g_x} | y | \psi_o \rangle]^2$$

$$= \frac{1}{2}[R_{2y} - R_{1y}]^2 \ .$$

The corresponding dipole strengths of the x-polarized transition can be determined as follows:

let $$R_{1x} = \langle a_{1u} e_{g_y} | x | \psi_o \rangle$$

and $$R_{2x} = \langle a_{2u} e_{g_x} | x | \psi_o \rangle$$

then

$$q^2(|Q_x^o\rangle) = \frac{1}{2}[\langle a_{2u} e_{g_x} | x | \psi_o \rangle + \langle a_{1u} e_{g_y} | x | \psi_o \rangle]^2$$

$$= [R_{2x} + R_{1x}]^2$$

and

$$q^2(|B_x^o\rangle) = \frac{1}{2}[\langle a_{2u} e_{g_x} | x | \psi_o \rangle - \langle a_{1u} e_{g_y} | x | \psi_o \rangle]^2$$

$$= \frac{1}{2}[R_{2x} - R_{1x}]^2 \ .$$

At first glance the x-polarized transition moments seem to contradict the statement that the B transition is strongly allowed and the Q transition forbidden, but we still need to relate the x and y components of the transition moments to each other. This is done by defining an axis system in Figure 8 which leads to the following relations:

$$\hat{C}_4 x \rightarrow y \quad \hat{C}_4 e_{g_x} \rightarrow e_{g_y} \quad \hat{C}_4 a_{1u} \rightarrow a_{1u}$$

$$\hat{C}_4 y \rightarrow -x \quad \hat{C}_4 e_{g_y} \rightarrow -e_{g_x} \quad \hat{C}_4 a_{2u} \rightarrow a_{2u} \; .$$

Therefore,

$$\hat{C}_4 R_{1x} \rightarrow -\langle a_{1u} e_{g_x} | y | \psi_o \rangle = -R_{1y}$$

and

$$\hat{C}_4 R_{2x} \rightarrow \langle a_{2u} e_{g_y} | y | \psi_o \rangle = R_{2y}$$

Using these transformations

$$q^2(|Q_x^o\rangle) = \tfrac{1}{2}[R_{2y} - R_{1y}]^2$$

and

$$q^2(|B_x^o\rangle) = \tfrac{1}{2}[R_{2y} + R_{1y}]^2$$

similar to the y-polarized transitions. The final result is that $R = 1/2\ (R_1 + R_2)^2$ and $r = 1/2\ (R_2 - R_1)^2$ for the B and Q transitions, respectively. For both the x and y-polarized transitions the intensities add in the Soret and subtract and cancel in the visible region.

These 50/50 mixed configurations still do not adequately

represent experimental data. By allowing these zero order wavefunctions to "unmix" depending on the magnitude of a configuration interaction parameter, θ, the intensity of the Q band can be varied continuously relative to the B transition. The coordinate transformation which allows coupling only between states of the same polarization can be defined by:

$$|Q_x\rangle = \cos\theta|Q_x^o\rangle - \sin\theta|B_x^o\rangle$$

$$|Q_y\rangle = \cos\theta|Q_y^o\rangle - \sin\theta|B_y^o\rangle$$

$$|B_x\rangle = \cos\theta|B_x^o\rangle + \sin\theta|Q_x^o\rangle$$

and

$$|B_y\rangle = \cos\theta|B_y^o\rangle + \sin\theta|Q_y^o\rangle$$

The restriction to coupling between states of the same polarization can be relaxed by considering a more complete vibronic description (Shelnutt, 1981).

Previously we defined

$$R_x^o \equiv \langle B_x^o|x|\psi_o\rangle$$

and

$$r_x^o \equiv \langle Q_x^o|x|\psi_o\rangle$$

Similarly we define the unmixed transition moments as

$$R_x \equiv \langle B_x | x | \psi_o \rangle = \sin\theta r_x^o + \cos\theta R_x^o$$

and

$$r_x \equiv \langle Q_x | x | \psi_o \rangle = \cos\theta r_x^o - \sin\theta R_x^o \ ,$$

with analogous equations for the y-polarized transitions. It is usually assumed that r_x^o vanishes as shown in the preceeding section, which results in the approximate transition dipoles

$$R_x \approx \cos\theta R_x^o$$

and

$$r_x \approx -\sin\theta R_x^o \ .$$

This predicts that the Q transition gains intensity at the expense of the B or Soret band. Furthermore, it can be shown that for the case where θ is small, the energy separation between the Q and B transitions is at a minimum; this separation then increases as the configuration interaction parameter increases (Gouterman, 1959). The four-orbital model gives a good qualitative and quantitive

description of metalloporphyrin absorption spectra.

The above description of metalloporphyrin electronic transitions has ignored the effect of changing internuclear coordinates on excited state interactions. Briefly, vibronic coupling effects lead to additional intensity in the α band arising from inter- and intra-manifold coupling of vibrational states of the appropriate symmetry. This will be discussed in Section II of this chapter.

C. Heme Absorption Spectra

Calculation of heme optical absorption spectra are complicated by the presence of the iron d orbitals which are of the appropriate symmetry and energies to couple with the porphyrin π orbitals. Furthermore the range of iron ligation states (four to six ligands are possible) results in several possible crystal field symmetries. In an octahedral field, exemplified by an iron ion ligated by the porphyrin nitrogens and two axial nitrogenous ligands, the five degenerate orbitals are split into two groups. The lower energy group (d_{xy}, d_{yz} d_{xz}) comprises orbitals with axes oriented at 45° to the pyrrole nitrogen axes and those at higher energy ($d_{x^2-y^2}$ and d_{z^2}) are oriented along the pyrrole nitrogen axes and along the axial ligand directions, respectively. From this axis system it can be seen that the high energy d_{z^2} orbital will be most sensitive to axial ligation. Zerner et al., (1966) performed extended

Hückel calculations on ferric and ferrous porphyrins and were able to predict the spin-state of each species. As expected the spin states vary according to the position of the axial ligands in the spectrochemical series. In general this series can be listed from strong field to weak field ligands as: CO, CN^-, nitrogenous ligands, sulfur ligands, oxygen ligands and halogens.

In addition to spin-state variation, several oxidation states of iron are possible in heme species. The two most common are ferric and ferrous iron. Ferric (or oxidized) heme spectra are usually broader and less intense than the ferrous (or reduced) cases. Addition of an electron to the heme π system in the ferrous compound results in population of the π^* antibonding orbitals. This explains the red-shift observed in the Soret maximum upon reduction. In general, however, the wavelength maximum of the α band of low-spin hemes changes very little upon reduction.

Charge transfer (CT) transitions have been shown to be important in the spectra of hemes and heme proteins (Smith and Williams, 1970). Several charge transfer bands exist in the visible and near IR region of the spectrum and are most prominent for high-spin hemes. These bands have been interpreted as porphyrin π to metal d_π (Smith and Williams, 1970) and metal to axial ligand (Asher, 1981) charge transfer transitions.

Three important hemes of physiological significance

significance (heme c found in cytochrome c, protoheme or heme b found in hemoglobin and myoglobin and heme a found in cytochrome oxidase) vary in their pattern of peripheral substituents and absorption maxima. They all have propionic acid residues at position 6 and 7 (Figure 6), presumably to anchor the chromophore to the polypeptide backbone via hydrogen bonding. These acid functionalities are insulated from the porphyrin ring by two carbon atoms and therefore the ring system "sees" these substituents as alkyl groups. Their presence or absence does not affect the spectra. Table 1 summarizes the substituents and absorption maxima of these three species. The optical properties of this series of hemes supports two aspects of Gouterman's formulation of metalloporphyrin spectra. First, the more closely the heme approximates D_{4h} symmetry, the weaker is the intensity of the α band relative to the Soret, and second, the red-shifted α maxima in the lower symmetry cases is an example of the larger splitting between the Soret and α bands predicted by the four orbital model. These symmetry considerations will be important in Chapter 5 for the interpretation of the absorption and Raman spectra of cytochrome a in cytochrome oxidase.

II. Resonance Raman Spectroscopy

Resonance Raman spectroscopy has been widely used in the study of hemes and heme proteins (for reviews see

Table 1. β-Carbon Substituents and Absorption Maxima of Some Low-spin, Ferrous Hemes.

	1	2	3	4	5	6	7	8	Max α	Soret
heme a	Me	HFE	Me	V	Me	P	P	F	595 nm (16807 cm^{-1})	436 nm (22936 cm^{-1})
heme b	Me	V	Me	V	Me	P	P	Me	564 nm (17730 cm^{-1})	430 nm (23256 cm^{-1})
heme c	Me	Th	Me	Th	Me	P	P	Me	550 nm (18182 cm^{-1})	415 nm (24096 cm^{-1})

Side chain abbreviations: Me = methyl, V = vinyl, P = propionic acid, F = formyl,

Th = thioether linkage (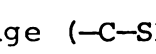), HFE = β-hydroxy

farnesylethyl tail 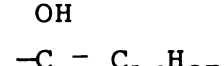

Felton and Yu, 1978; Rousseau et al., 1978; Clark and Stewart, 1979 and Asher, 1981). The selective enhancement of only the vibrations of the resonant chromophore allows protein-associated pigments to be studied owing to the "invisibility" of the protein matrix to the laser excitation. The types of information available from RRS studies of heme proteins are the identification of 1) oxidation and ligation state of the iron, 2) solvent environment of the heme chromophore as indicated by the frequency position of peripheral substituents, 3) covalent or electrostatic interactions at the ring periphery, 4) local protein environment effects arising from symmetry perturbations, 5) the nature of axial ligands, and 6) transient effects (ps, ns) on the heme spectra.

A. Classical Description

Classically, Raman scattering is caused by the interaction of electromagnetic radiation and the molecular polarizability. Light from a laser source at frequency ν_o induces oscillations in the electron cloud of a molecule with an amplitude proportional to the polarizability. The resulting oscillating dipole moment radiates at frequency ν_o; this is called Rayleigh scattering. This oscillating dipole can be modulated by the oscillating field created by harmonic vibrational motion of the nuclei. The resulting beat frequencies occur at $\nu_o \pm \nu_k$ where ν_k is

a normal mode of the molecule. Thus vibrational Raman scattering yields light shifted in energy relative to the incoming laser frequency at lower energy ($\nu_o - \nu_k$) called Stokes scattering and at higher energy ($\nu_o + \nu_k$) called anti-Stokes scattering (Figure 9). Stokes scattering is more intense than anti-Stokes because it arises from the zeroth vibrational level of the ground electronic state, therefore it is the usual experimentally observed process.

The intensity of the Raman scattering process is given by

$$I^{GF}_{scattered} = c(\nu_o - \nu_k)^4 I_o \sum_{\rho,\sigma} |(\alpha_{\rho\sigma})^{GF}|^2 \qquad (2.1)$$

where G and F are ground and final vibronic levels, respectively, I_o is the laser intensity and $\alpha_{\rho\sigma}$ is the $\rho\sigma^{th}$ element of the molecular polarizability tensor (σ,ρ = x, y and z). To describe further the polarizability tensor in terms of wavefunctions of the ground and excited states a quantum mechanical approach must be used.

B. Quantum Mechanical Description of Raman Theory

The Kramers-Heisenberg-Dirac dispersion formula relates the polarizability tensor and quantum theory (Heitler, 1954). The polarizability tensor elements can be described as:

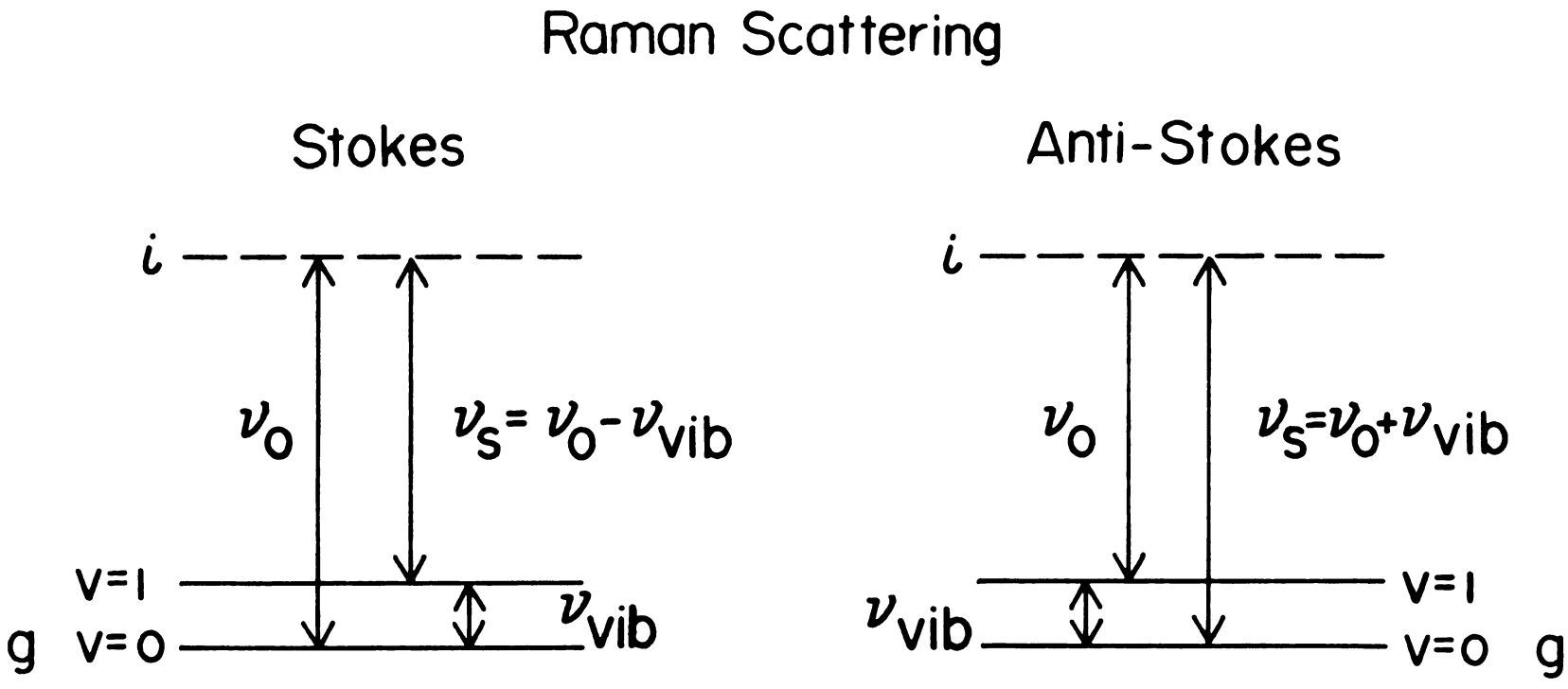

Figure 9. Stokes and Anti-Stokes Raman Scattering Energy Levels: ν_o is the laser excitation frequency, ν_s refers to the scattered photon, ν_k is the frequency between v=0 and v=1 vibrational levels of the ground state, g and scattering occurs from an energy weighted sum of excited states, i.

$$(\alpha_{\rho\sigma})^{GF} = \sum_{I}{}' \left[\frac{\langle G|\mu_\sigma|I\rangle\langle I|\mu_\rho|F\rangle}{(E^I-E^G)-h\nu_o-i\Gamma_I} + \frac{\langle G|\mu_\rho|I\rangle\langle I|\mu_\sigma|F\rangle}{(E^I-E^F)+h\nu_o-i\Gamma_I} \right] \tag{2.2}$$

where G and F are the initial and final vibronic levels as stated before and the summation is over all excited vibronic levels, I. The dipole moment operator, $\mu = \sum_i e_i r_i$ weights the overlap of the initial and final state wavefunctions with all intermediate excited states. E^G, E^F and E^I are the energies of the vibronic levels, Γ_I is the lifetime or bandwidth of state I, and $h\nu_o$ is the laser excitation frequency. The first term in Equation (2.2) is important for resonance Raman and both terms are used in the formulation of normal Raman scattering. The wavefunctions of the vibronic levels, G, F and I are usually not known so the Born-Oppenheimer approximation is made which separates the nuclear and electronic coordinates $|G(r,R_k)\rangle = |g(r;R_k)\rangle|n(R_k)\rangle$ where $|n(R_k)\rangle$ are product harmonic oscillator wavefunctions and the electronic wavefunction $|g(r;R_k)\rangle$ is parametrically dependent on R_k. This approximation enables the integration in Equation (2.2) to be performed over the nuclear coordinates.

For example, the first matrix element is

$$\langle G|\mu_\sigma|I\rangle = \langle g(r;R_k)n(R_k)|\mu_\sigma|i(r;R_k)m(R_k)\rangle$$

$$= M^\sigma_{gi}(r;R_k)\langle n(R_k)|m(R_k)\rangle$$

where we have defined

$$M^\sigma_{gi}(r;R_k) = \langle g(r_j R_k)|\mu_\sigma\ i(r;R_k)\rangle$$

This is the usual description of an electronic transition where M_{gi} specifies the intensity and the band shape is described by the Franck-Condon overlap integrals $\langle n(R_k)\cdot|m(R_k)\rangle$. The M_{gi} are usually weakly varying functions of nuclear coordinates so they can be expanded in a Taylor series about the equilibrium nuclear position, where $R_o = 0$,

$$M_{gi}(R) = M^o_{gi}(R_o) + \left[\frac{\partial M_{gi}}{\partial R_k}\right]_{R_o} R_k + \ldots \qquad (2.3)$$

where

$$M'_{gi} = \left[\frac{\partial M_{gi}}{\partial R_k}\right]_{R_o}$$

and M'_{gi} can be written as

$$M'_{gi} = \sum_{s\neq i} M^o_{gs} \frac{\langle s|\frac{\partial H}{\partial R_k}|i\rangle_{R_o}}{E_i - E_s} \qquad (2.4)$$

This is the key point in the connection between electronic scattering and changing nuclear coordinates. The Raman process is an electron scattering phenomenon yet the frequency of light observed is a direct measure of nuclear vibrational frequencies. This formulation is strictly analogous to vibronic coupling between electronic states in absorption spectroscopy whereby the changing nuclear configuration scrambles the fixed-nuclei electronic wavefunctions. Transitions that originally were weak or forbidden increase in intensity from coupling to nearby allowed transitions. The modes that are group theoretically capable of coupling electronic states may be determined by examining the matrix elements in Equation (2.4). The two excited states s and i in D_{4h} symmetry of hemes are of E_u symmetry. The vibrations that will result in non-zero matrix elements are those contained in the direct product $E_u \times E_u = A_{1g} + A_{2g} + B_{1g} + B_{2g}$.

Substituting Equations (2.2) and (2.3) into (2.4), for the resonant case and considering only one excited electronic state leads to the following expression for the polarizability tensor

$$(\alpha_{\rho\sigma}) = A + B + \ldots$$

$$A = |M_{gi}(R_o)|^2 \sum_k \frac{\langle n|k\rangle\langle k|m\rangle}{(E_{ik}-E_{gn})-h\nu_o-i\Gamma_k} \qquad (2.5)$$

$$B = M_{gi}(R_o)M'_{gi}(R_o) \sum_k \frac{\langle n|R|k\rangle\langle k|m\rangle + \langle n|k\rangle\langle k|R|m\rangle}{(E_{ik}-E_{ev})-h\nu_o-i\Gamma_k} \tag{2.6}$$

These equations indicate that Raman intensity can be produced by two mechanisms, termed A-term (or Franck-Condon) scattering and B-term (or Herzberg-Teller) scattering. The A-term scattering intensity results from three factors; the Franck-Condon overlap integrals, the transition moments M_{gi} and the frequency dependence of the resonance denominator. The Franck-Condon factors are non-vanishing only if there is a displacement of the potential in the excited state along a nuclear coordinate or if there is a change in frequency of a normal mode between ground and excited states. The first mechanism is the predominant cause of A-term intensity and therefore only totally symmetric modes give rise to A-term scattering (Clark and Stewart, 1979).

B-term enhancement results from vibronic borrowing of intensity between the resonant electronic transition and a nearby electronic transition through M'_{gi} in addition to the resonant denominator. Non-totally symmetric modes are enhanced by this scattering mechanism as seen by the harmonic oscillator matrix elements $\langle n|R|k\rangle = \delta_{n,k\pm1}$, *i.e.*, modes along which there is no coordinate displacement in the excited state will have non-vanishing integrals (Clark and Stewart, 1979).

C. Heme Resonance Raman Scattering

The use of the equations obtained in the previous development of resonance Raman theory are not strictly applicable to the electronic transitions of heme species because of their degenerate nature. Use of a more general development yields essentially the same results with bulkier notation (Shelnutt, 1981), so the approximate expressions of the previous section will be used for purposes of discussion.

Franck-Condon scattering is the dominant mechanism for strongly allowed electronic transitions, so this mechanism holds for excitation frequencies in the region of the intense Soret band. Writing out the intensity of the A-term for this electronic state leads to:

$$I \sim |A|^2 \sim \left| \frac{|\langle g0|B0\rangle|}{E_{B0}-h\nu_o-i\Gamma_{B0}} - \frac{|\langle g1|B1\rangle}{E_{B1}-h\nu_o-i\Gamma_{B1}} \right|^2 \qquad (2.7)$$

where the summation over k in Equation (2.5) is carried to the first vibrational overtone and B_o and B_1 refer to the excited state lowest and first vibronic levels, respectively, with energies E_{B0} and E_{B1}.

As stated above, vibrations which display an excited state displacement are active in this scattering mechanism. In D_{4h} symmetry, A_{1g} modes are allowed. Since the Soret transition is of E_u symmetry, those vibrations contained in

the symmetric direct product of $\{E_u \times E_u\} = A_{1g} + B_{1g} + B_{2g}$ may cause a Jahn-Teller distortion in the excited state. B_{1g} and B_{2g} modes can cause shifts of opposite sign in the potential minima of the E_x and E_y components, therefore resulting in enhancement of these modes with Soret excitation (Shelnutt et al., 1977). Examination of the frequency dependence of Equation (2.7), an excitation profile, would reveal two peaks in the intensity, one at the 0-0 vibrational transition and the other at the energy of the active normal mode, $h\nu_k$ to higher energy. Constructive interference between the 0-0 and 0-1 intensity peaks and destructive interference in the wings is observed.

B-term scattering is important for electronic transitions that gain their absorption intensity by vibronic coupling. Excitation into the α band of a heme sample results in the following approximate equation:

$$I \sim |B|^2 \sim \left| \frac{1}{E_{Q0} - h\nu_o - i\Gamma_{Q0}} \pm \frac{1}{E_{Q1} - h\nu_o - i\Gamma_{Q1}} \right|^2 . \qquad (2.8)$$

The vibrations active in the Herzberg-Teller scattering mechanism for D_{4h} symmetry are those active in vibronic coupling. As stated earlier, these vibrations are those contained in the direct product of $E_u \times E_u = A_{1g} + A_{2g} + B_{1g} + B_{2g}$, although A_{1g} modes are expected to be weak or absent (Perrin et al., 1969). The frequency dependence of

the B-term intensity also results in two maxima, and the interference effects are constructive (minus sign in Equation (2.8)) for A_{1g}, B_{1g} and B_{2g} modes and destructive (plus sign) for modes of A_{2g} symmetry.

D. Polarization and Symmetry Effects

The four different symmetry vibrations (A_{1g}, A_{2g}, B_{1g} and B_{2g}) allowed in heme resonance Raman spectra can be identified by their depolarization ratio. Because of the linearly polarized nature of the laser excitation, Raman vibrations can be characterized by the extent to which they retain this polarization. The depolarization ratio is defined as the ratio of the Raman intensity scattered perpendicular to the incoming radiation relative to the intensity of the parallel scattered component, $\rho_\ell = I_\perp / I_{||}$.

Depolarization ratios can be estimated for molecules of a given symmetry by use of the three polarizability tensor invariants: the isotropy G^o, the symmetric anisotropy G^s and the antisymmetric anisotropy G^a. To calculate these tensor invariants it is convenient to define the symmetric and antisymmetric tensors:

$$S_{\rho\sigma} = \frac{1}{2}(\alpha_{\rho\sigma} + \alpha_{\sigma\rho}) \qquad \text{and} \qquad A_{\rho\sigma} = \frac{1}{2}(\alpha_{\rho\sigma} - \alpha_{\sigma\rho}).$$

The relative elements of $\alpha_{\rho\sigma}$ are available (McClain, 1977). Then

$$G^{o} = \frac{1}{3}|Tr\{S\}|^{2}$$

$$G^{s} = Tr\{S\}\{S^{+}\}-G^{o}$$

$$G^{a} = Tr\{A\}\{A^{+}\} \ .$$

For 90° scattering geometry

$$\rho_{\ell} = \frac{I_{\perp}}{I_{||}} = \frac{3G^{s} + 5G^{a}}{10G^{o} + 4G^{s}} \ .$$

In D_{4h} symmetry, A_{1g} modes are polarized (p) with $\rho_{\ell} = 1/8$, B_{1g} and B_{2g} modes are depolarized (dp), $\rho_{\ell} = 3/4$, and A_{2g} modes are anonamously polarized (ap), $\rho_{\ell} = \infty$. Anomalous polarization reflects asymmetry in the scattering tensor and is only observed at resonance with the α band (Rousseau et al., 1978). These depolarization ratios are strictly valid only for molecules of D_{4h} symmetry. For molecules of lower symmetry, there is dispersion in ρ_{ℓ} and the values become $\leq 3/4$ for polarized modes, $=3/4$ for depolarized modes and $>3/4$ for inversely polarized vibrations. The variation in ρ_{ℓ} with excitation frequency provides information about the symmetry and environmental perturbations of the heme macrocycle (Shelnutt 1980, 1981). However, the use of the depolarization ratio obtained at a single excitation frequency to assign mode symmetries can

be misleading because ap modes can be polarized in the Soret, and polarized modes may be depolarized in the visible region (Shelnutt, 1981). None of the physiological relevant hemes is strictly of D_{4h} symmetry. In fact, all of them are C_s, yet the predictions made for D_{4h} molecules are observed in most cases. When deviations occur, a slight reduction in the molecular symmetry classification is usually sufficient to interpret the data. In the worst possible case of C_s symmetry, all mode symmetries are A and their depolarization ratios range from 1/3 to 2.

This description of the factors that influence heme absorption and resonance Raman spectra provides a background for the discussions in the following sections. The experimental aspects of RRS will be covered in the next chapter.

CHAPTER 3

EXPERIMENTAL PROCEDURES

I. Spectroscopy

The setup of a Raman experiment is given in Figure 10. The incident laser frequency impinges upon the sample from the bottom of a clear cuvette and the scattered light is collected at 90° to the incident beam. The scattered light is then focused, passed through a polarization analyzer (optional), a polarization scrambler and a double monochromator to the cathode of a photomultiplier tube. The polarization scrambler is used because of the differential detection of perpendicular and parallel polarized light. The scattered intensity versus frequency data is then displayed on a strip chart recorder. The Raman spectrometer used in the experiments reported here is a Spex 1401 double monochromator in conjunction with the associated Ramalog electronics. Scan speeds of 50, 25 and 10 cm^{-1}/minute were used along with the respective time constants of 1, 2.5 and 5 sec. The delta frequency position was calibrated before each experiment by using benzene as a standard, and the position of the polaroid analyzer was calibrated by reproducing the literature depolarization ratios of

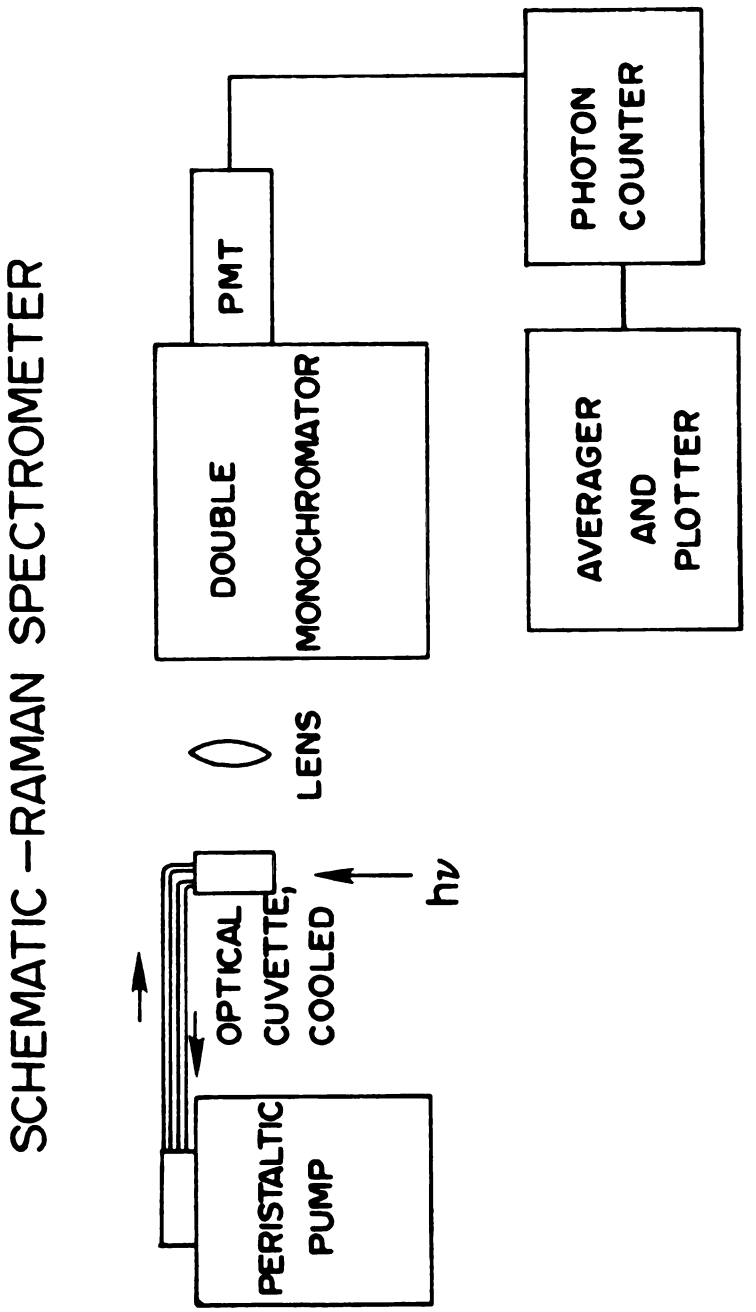

Figure 10. Schematic of the Raman spectrometer and flowing sample arrangement.

benzene and methylene chloride. Static, spinning cell and flowing sample arrangements were used. The spectra of light sensitive model compounds were taken with the spinning cell (constructed at Michigan State University). All model compound samples were monitored at room temperature and all protein samples were obtained at ∿5°C. All samples of oxidized cytochrome oxidase or partially oxidized oxidase were taken with a flowing sample arrangement (Babcock and Salmeen, 1979) to reduce the effects of cytochrome a photoreduction.

Three fixed frequency ion lasers were used; a helium-cadmium (RCA LD2186) on loan from Dr. Irving Salmeen, Ford Motor Company, with λ_{ex} = 441.6 nm, a krypton in Spectra Physics 164-11 equipped with high field magnet which provided 406.7 and 413.1 nm excitation and a Spectra Physics model 165 argon ion laser which provided several lines in the blue-green region. The argon ion laser was also used as a high power source to pump a dye laser. A Spectra Physics model 375 dye laser with Rhodamine 6-G was used to obtain laser excitation in the heme a α band region (∿600 nm). Sample concentrations for Soret excitation resonance Raman spectra were typically 20-40 μM with laser powers of 20-40 mW and those used for visible excitation were approximately 200 μM with typical laser powers of 50-100 mW. Spectral resolution is 5 cm^{-1} and the Raman peak positions are accurate to ∿1.5 cm^{-1}. In the protein

samples used to obtain excitation profile data, the enzyme concentration was maintained at 14 μM and 0.12 M $(NH_4)_2SO_4$ was added as an internal standard. Control experiments showed that the presence of ammonium sulfate did not alter the Raman scattering properties of the enzyme. Reabsorption effects were estimated to lead to maximum errors in the determination of scattered intensity of <8% but were not corrected for. The detector response of the RCA C31034 tube used is essentially frequency dependent over the spectral range of interest.

Absorption spectra of the samples were monitored before and after each experiment to monitor sample integrity. The absorption spectrometer used was either a Cary 17, Cary 219 or McPherson EU707D. The Cary and MCD spectrometers were used in conjunction with a chilled sample holder (∿5°C) for protein work. Magnetic circular dichroic spectra were taken at the University of California, Berkeley by using the computer interfaced spectrophotometer described previously (Sutherland et al., 1974) or at the University of Michigan with a JASCO J-40C recording spectropolarimeter equipped with a MCD-1 electromagnet operating at 16.05 kG, and coupled to a Data General Nova 3 minicomputer and a Tracor Northern PN-1500 digital signal analyzer. MCD sample concentrations were approximately 10 μM. EPR spectra were recorded by using a Bruker ER200D X-band spectrometer; operation at low temperature was achieved by using an Oxford ESR-9

liquid helium cryostat. EPR sample concentrations were typically 200 μM.

II. Protein Sample Preparation

A. Cytochrome Oxidase

Beef heart cytochrome oxidase was isolated by a modified Hartzell-Beinert preparation (Hartzell-Beinert, 1975, Babcock et al., 1976). Cytochrome oxidase isolated from rat liver mitochondria was a gift from Debra Thompson and Prof. Shelagh Ferguson-Miller (Michigan State University) and the bacterial oxidase, cytochrome c_1aa_3 was obtained from Tatsura Yoshida and Prof. James A. Fee (University of Michigan). All samples were prepared at pH 7.4 in 50-100 mM Hepes buffer unless otherwise specified. The inhibitor complexes of the enzyme were formed as previously described (Babcock, et al., 1976), and the oxygenated species was formed by air oxidation of the dithionite or cytochrome c (Sigma, Type VI) reduced enzyme. This procedure yielded a sample with Soret and α maxima at 427 nm and 600 nm, respectively. The 655 nm band was also present. Reduction of the enzyme was achieved by either addition of a few crystals of sodium dithionite (Virginia Smelting) or by addition of 10 mM ascorbate-0.1 mM N,N,N',N',-tetramethyl-paraphenylenediamine (TMPD).

The early work on cytochrome oxidase presented here was

done with Brij 35 as the solubilizing detergent but as of May, 1981 lauryl maltoside was used owing to the monodisperse nature of the enzyme in this detergent (Rosevear et al., 1980). In lauryl maltoside, cytochrome oxidase exists as a dimer whereas in other detergents (Brij, Tween-20, or cholate) it exists as higher order aggregates. The particular detergent used is specified in the figure captions.

In the alkaline pH studies of cytochrome oxidase a different buffer-detergent system was used. This system was 0.5% K-cholate, 50 mM potassium phosphate. The pH induced spectral shifts were also observed in other buffers and detergents, e.g., CHES, CAPS, glycine lauryl maltoside and Tween-20, but the shifts in the pH range 8-11.5 were more dramatic for the cholate-phosphate system and therefore investigated further. The high pH forms of the enzyme were prepared by bringing the enzyme solution to the desired pH level with 1 N NaOH followed by incubation for approximately six hours at 4°C. This incubation period insured that no further spectral shifts could be observed after the spectra were recorded. The slow formation of the alkaline cytochrome oxidase species was a hindrance as noted by Lemberg (1964) but the effects are completely reproducible. For reduced cytochrome oxidase, either the oxidized or reduced enzyme incubated at high pH and then completely reduced with dithionite or TMPD/ascorbate resulted

in the same spectral species as noted by Lemberg and Pilger (1964). For the spectra reported here the enzyme was incubated in the reduced form if the final species was to be a reduced species. The pH values reported are those measured immediately after the experiment was complete.

Dicyclohexylcarbodiimide (DCCD) binding to cytochrome oxidase was performed following the method of Moroney and Hinkle (1983). Experiments done with cytochrome oxidase in D_2O rather than H_2O as solvent were done with isolated enzyme samples which were precipitated one additional time with saturated ammonium sulfate and resuspended in a 0.5% lauryl maltoside, 50 mM Hepes solution in D_2O. There was no change in the absorption spectrum of the oxidized or reduced enzyme in D_2O relative to H_2O.

B. Other Proteins

The preparation of hemoglobin, myoglobin, cytochrome *c* and horse-radish peroxidase samples was carried out as reported in Callahan and Babcock (1981).

III. Heme Model Compound Sample Preparation

A. Hema *a*

The chloride complex of heme *a* was isolated by acid/acetone extraction of purified cytochrome oxidase (Babcock,

et al., 1976). Low-spin ferric heme a complexes in 0.1 M phosphate buffer, pH 7.4, 2% sodium dodecyl sulfate (SDS) or in organic solvents were prepared by addition of 0.7 N-methylimidazole (NMeIM). Six coordinate high-spin ferric heme a was prepared by a procedure analogous to that used in the preparation of high-spin six coordinate Fe^{3+} octaethylporphyrin and Fe^{3+} tetraphenylporphyrin (Dolphin et al., 1977; Zobrist and La Mar 1978; Spiro et al., 1979): heme a perchlorate was prepared from a methylene chloride solution of the heme a^{3+} chloride complex by addition of solid anhydrous $AgClO_4$; following filtration, a sufficient amount of ligand (i.e., DMSO or THF) was added to insure complete formation of the six coordinate high-spin complex as judged by changes in the optical spectrum (Figure 11). Five coordinate ferrous heme a was formed by addition of 0.3 M 2-MeIm and a few crystals of sodium dithionite to an aqueous detergent solution of heme $a^{3+}\cdot Cl^-$.

In order to be able to work at the very acidic conditions needed for protonated Schiff base formation or strong hydrogen bonding to the peripheral aldehyde on the heme a ring, the substitution of the central iron atom for copper was carried out according to the methods of Fuhrop and Smith (1975). Schiff bases readily form between the porphyrin a carbonyl and any primary amine. Protonation or deuteration of the imine linkage follows addition of a slight excess of dry HCl or DCl gas (Ward et al., 1983). Hydrogen

Figure 11. The optical absorption spectra of several of the ferric heme a species used in the present study. The heme a concentration was approximately 13 μM for all samples; the solvent was methylene chloride.

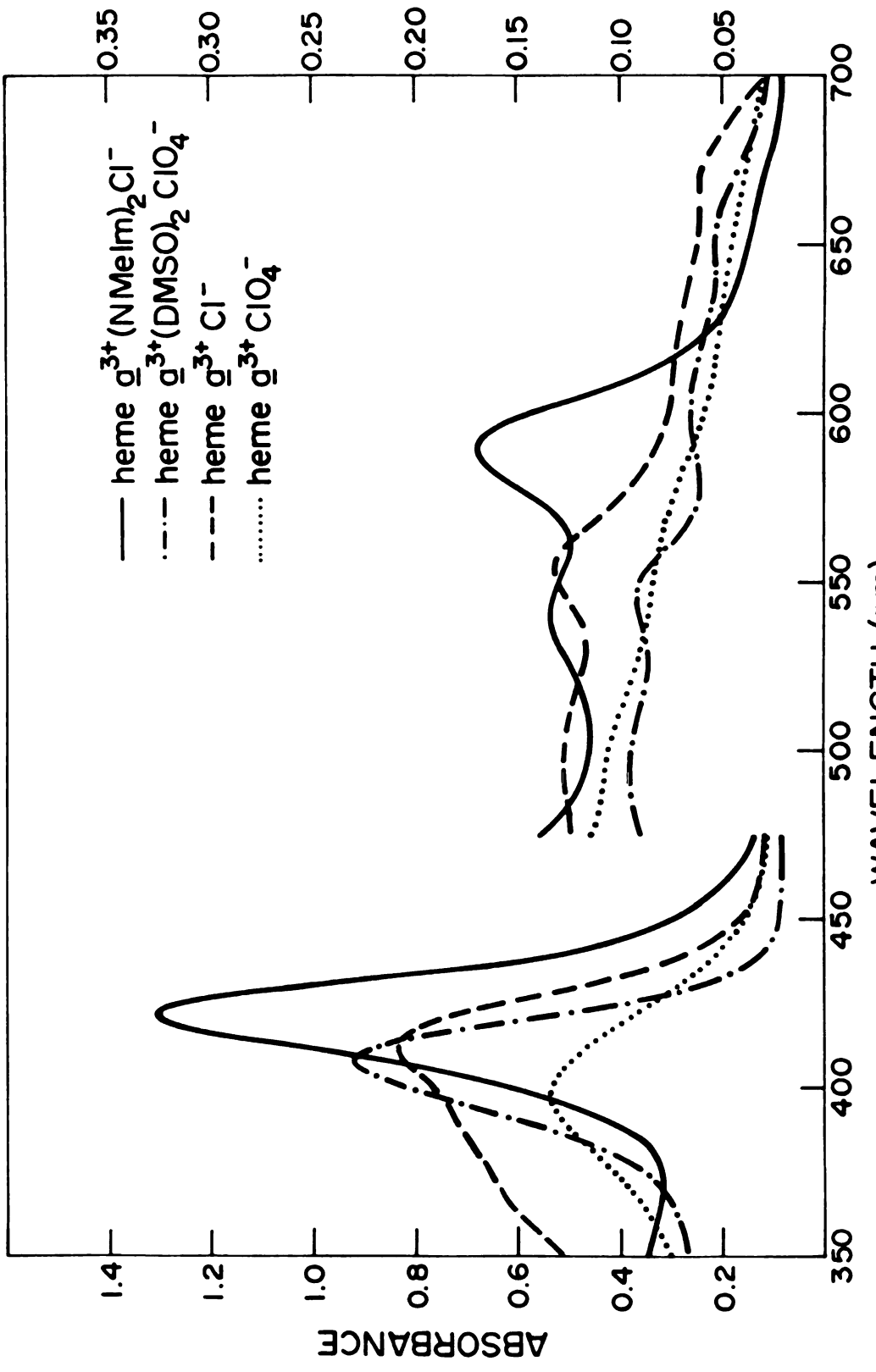
heme $\underline{g}^{3+}$(NMeIm)$_2$Cl$^-$
heme $\underline{g}^{3+}$(DMSO)$_2$ ClO$_4^-$
heme $\underline{g}^{3+}$ Cl$^-$
heme $\underline{g}^{3+}$ ClO$_4^-$
ABSORBANCE
WAVELENGTH (nm)
0.35
0.30
0.25
0.20
0.15
0.10
0.05
1.4
1.2
1.0
0.8
0.6
0.4
0.2
350
400
450
500
550
600
650
700

Figure 11

bonded heme *a* $(NMeIm)_2$ or copper porphyrin *a* model complexes were formed by addition of a hydrogen donor (*e.g.*, phenols, acids and alcohols) until no further spectral shifts were observed. Heme *a* $(NMeIm)_2$ could not be used with acids with pK_a $\sim$5 owing to the preferential protonation of the axial imidazole nitrogens.

Reduction of heme *a* $(NMeIm)_2$ in aprotic solvents was carried out by the method of VanSteelandt-Frentrup *et al.* (1981). For the hydrogen bonded heme *a* model compounds the reduction procedure was slightly different. The heme a^{3+} $(NMeIm)_2$ in solution and hydrogen donor were kept in separate arms of the glassware shown in Figure 12. Following several freeze-pump-thaw cycles and addition of the methanolic solution of 2-2-2 cryptand solubilized sodium dithionite to reduce the heme *a*, the ferrous heme *a* $(NMeIm)_2$ could be mixed with the hydrogen donor. Absorption and Raman spectra were recorded in the attached quartz cuvette. In cases where the hydrogen donor was a liquid, rigorous degassing was necessary before the reduction step. An alternative reduction method involves the use of tetrabutylammonium borohydride. A small amount is placed in the cuvette sidearm of the glassware, the freeze-pump-thaw cycles are performed as before, the heme *a* solution is poured over to mix with the tetrabutylammonium borohydride and then the ferrous heme *a* $(NMeIm)_2$ complex can be mixed with the hydrogen donor present in the third arm. This

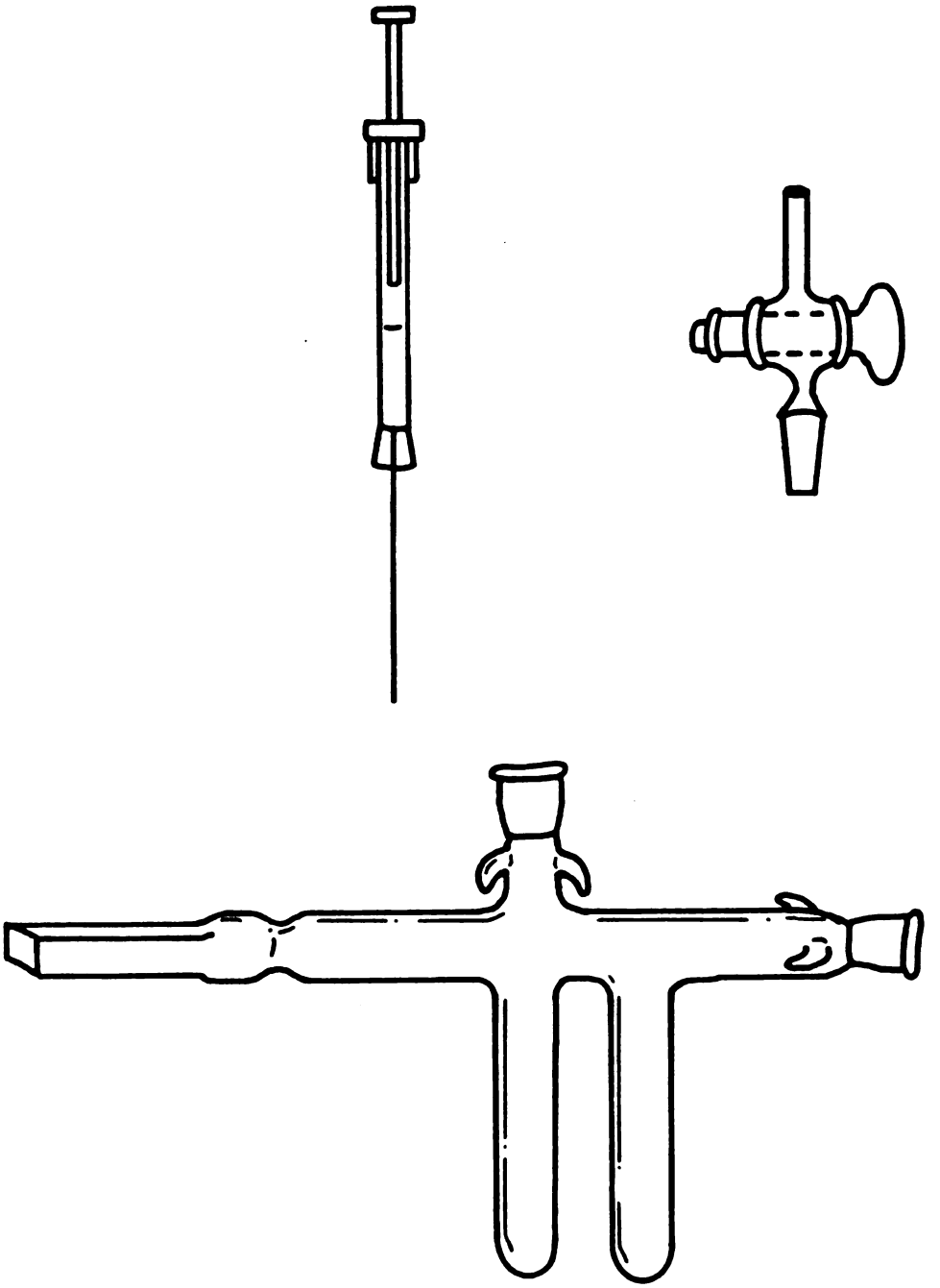

Figure 12. Glassware used for hydrogen bonded heme a reduction.

method eliminates the necessity of any additions once the glassware has been closed off from the atmosphere. Care must be exercised in the amount of tetrabutylammonium borohydride used. Just as with excess sodium dithionite, facile reduction of the heme a peripheral aldehyde is observed. Solvents were of spectral grade and dried over molecular seives prior to use; other reagents were obtained commercially and, when necessary, were further purified by distillation.

B. Other Heme Model Compounds

Hemin chloride was obtained from Sigma and the low-spin ferric bis(NMeIm) complex prepared by addition of 0.7 M N-methylimidazole to a solution of the heme in 0.1 M sodium phosphate, 2% SDS, pH 7.4. Protoporphyrin IX dimethyl ester was obtained from Sigma and the iron insertion was carried out as described by Lemberg et al. (1955) to form the Fe^{3+} protoheme dimethylester chloride compound. Ferric iron etioporphyrin I chloride and ferric iron octaethylporphyrin chloride were the kind gifts of Professor C. K. Chang. Preparation of the six coordinate high- and low-spin species was achieved as described above for the heme a^{3+} complexes. During the preparation of the various derivatives, the optical absorption spectra were monitored to insure complete formation of the species of interest.

CHAPTER 4

COORDINATION GEOMETRIES

I. Reduced Cytochrome Oxidase

A. Introduction

Raman spectroscopy offers the potential to resolve several of the outstanding questions regarding cytochrome oxidase. The technique provides information on both the immediate coordination sphere of the heme-bound iron (Spaulding et al., 1975; Spiro et al., 1979; Callahan and Babcock, 1981) and on the conformation of porphyrin ring peripheral substituents (Salmeen et al., 1973, 1978). Given the unusual formyl substituent of heme a, this latter insight is expected to be extremely useful (Babcock and Salmeen, 1978). The application of Raman spectroscopy to the enzyme, however, is complicated by facile photoreduction of the metal centers in the laser beam (Adar and Yonetani, 1978; Adar and Erecińska, 1979) and by ambiguities in the optical properties of the two heme chromophores. The photoreduction difficulty has been avoided recently by using frozen samples and laser excitation in the visible region (Bocian et al., 1979) or by using flowing oxidase

samples (Babcock and Salmeen, 1979). By using the flow technique and several Soret region laser lines to obtain oxidase Raman spectra, the optical properties of *a* and a_3 have been clarified (Babcock and Salmeen, 1979; Ondrias and Babcock, 1980). Recent oxidase Raman studies carried out by Woodruff *et al.*, (1981) have confirmed these observations. The absorption properties of *a* and a_3 determined by Raman spectroscopy are in close agreement with those originally postulated by Vanneste (1966) but which had been clouded somewhat during the past decade by the uncertain manifestations of heme-heme interaction (Malmström, 1979).

The majority of the oxidase Raman work we have done has used Soret excitation. The scattered intensity under these conditions is controlled by Franck-Condon overlap factors and is distinct from the Herzberg-Teller nature of heme Raman spectra obtained with excitation in resonance with the α and β bands (Felton and Yu, 1978; Rousseau *et al.*, 1979; Clark and Stewart, 1979). In Section II Soret excitation Raman spectroscopy is used to extract heme structural information through the use of model compound data (Callahan and Babcock, 1981). In Section III vibrational band assignments for cytochromes *a* and a_3 are made and in conjunction with heme *a* model compound data the spin and coordination states for the two oxidase iron chromophores are determined. The Soret excitation frequency dependence of the reduced oxidase Raman spectrum has been explored and

the data can be interpreted qualitatively by assuming that the polarizability is dominated by a single electronic state and its Franck-Condon overlap with the ground state. Finally, the mechanism of cytochrome oxidase photoreduction has been studied in some detail in order to clarify the nature of this process.

B. Soret Raman Scattering Frequency Dependence

Studies concerned with the frequency dependence of Raman scattering in the α, β region of heme protein electronic spectra have been carried out, for example on cytochrome c (Friedman et al., 1977), and have been interpreted to first order in terms of a Herzberg-Teller scattering mechanism, and more quantitatively by incorporating both non-adiabatic and Jahn-Teller effects (Shelnutt, 1980). No systematic investigations of this type have been carried out for Soret excitation, with the exception of a study carried out by Champion and Albrecht (1979) of the oxidation state marker band of cytochrome c. Because the Soret absorption spectrum of cytochrome oxidase is considerably red-shifted compared to other hemes and heme proteins, fixed frequency ion laser lines can be used to construct a crude excitation profile in order to explore in more detail the frequency dependence of Soret scattering.

Figure 13 shows the optical spectra of several oxidase derivatives and the relationship of the five available

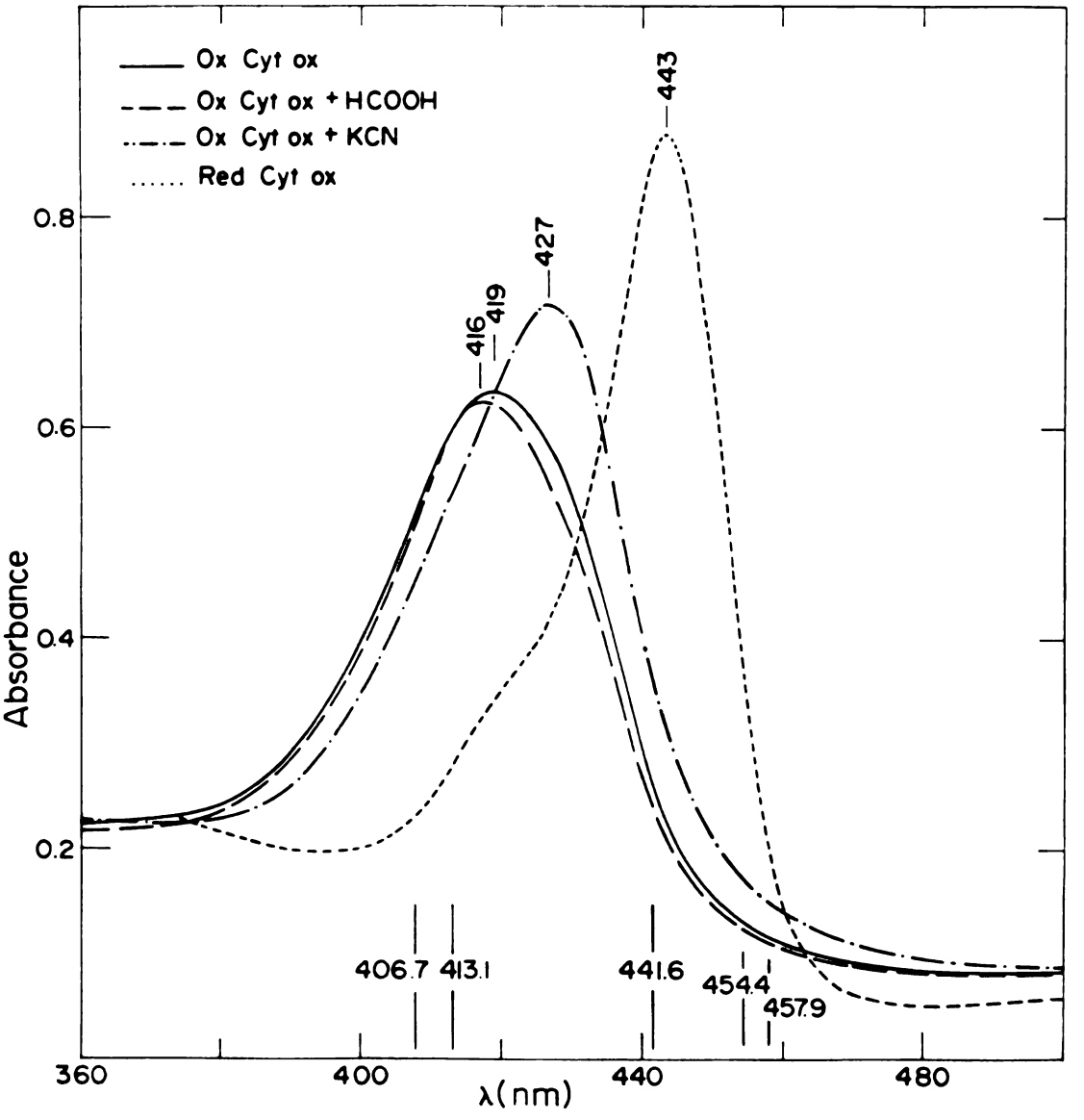

Figure 13. Optical absorption spectra of several of the cytochrome oxidase species used in the Raman experiments. The wavelengths of the laser lines available are also shown in the figure. The cytochrome oxidase concentration was approximately 4 μM (in enzyme) for all four compounds.

laser lines to these spectra. In reduced cytochrome oxidase, both $\underline{a}^{2+}$ and $\underline{a}_3^{2+}$ have maxima at 443 nm (Vanneste, 1966). Two of the laser lines are thus on the long wavelength side of the absorption peak (by 571 and 735 cm^{-1}) and the remaining three are on the short wavelength side of the peak (by 71, 1634, and 2015 cm^{-1}). Figure 14 shows Raman spectra of the reduced oxidase obtained with the three highest frequency lines as well as the Raman spectrum of reduced rat liver cytochrome oxidase with 441.6 nm excitation. The spectra obtained with the 457.9 and 454.5 nm lines were similar to those recorded by Nafie *et al*. (1973).

Equation (2.7) predicts two peaks in the Soret excitation profile for a given mode: one at the absorption peak (*i.e.*, at the 0-0 fundamental) and a second at a frequency given by the sum of the 0-0 fundamental and the vibrational quantum. Constructive interference is predicted in the frequency region between the two peaks and destructive interference is predicted in the wings.

In Figure 15 excitation profiles of six of the modes in Figure 14 are plotted according to a form of Equation (2.7), where the Franck-Condon factors in the numerator are set equal and approximated by the extinction coefficient at the Soret maximum. The bandwidth chosen in Equation (2.7) was 475 cm^{-1}, estimated from the optical data of Vanneste (1966). Two peaks are observed in the calculated excitation profiles unless the bandwidth is of the same magnitude

Figure 14. Raman spectra of reduced beef heart cytochrome oxidase (a,b,c) and of reduced rat liver cytochrome oxidase (d) recorded with the laser lines indicated. Instrumental conditions: resolution, 6 cm^{-1}; time constant, 1s; scan rate, 50 cm^{-1}/min. Raman lines which originate from the buffer systems used are indicated by asterisks; the daggers indicate the Raman line of the sulfate internal standard.

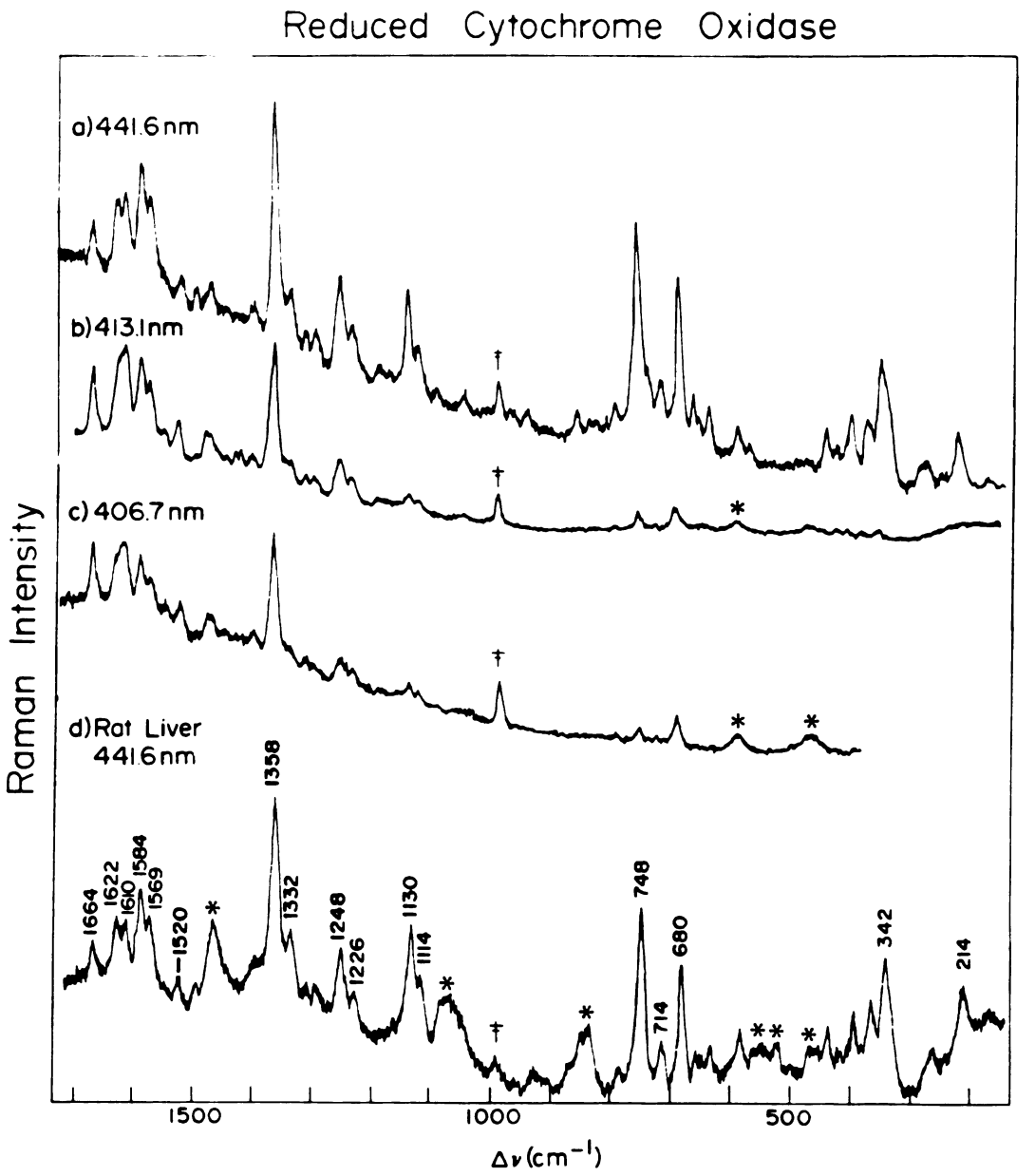
Reduced Cytochrome Oxidase
a) 441.6 nm
b) 413.1 nm
c) 406.7 nm
d) Rat Liver
441.6 nm
Raman Intensity
1664
1622
1610
1584
1569
1520
1358
1332
1248
1226
1130
1114
748
714
680
342
214
1500
1000
500
Δν (cm⁻¹)

Figure 14

Figure 15. Raman excitation profiles for the modes indicated have been calculated from Equation 2.7 in the text and are shown by the solid lines. The experimental data obtained with the five available laser lines are shown by the closed circles and estimated error bars. The experimental and theoretical points are arbitrarily normalized at 441.6 nm. The three low frequency points and the two high frequency points have been connected by dashed lines which have no theoretical basis.

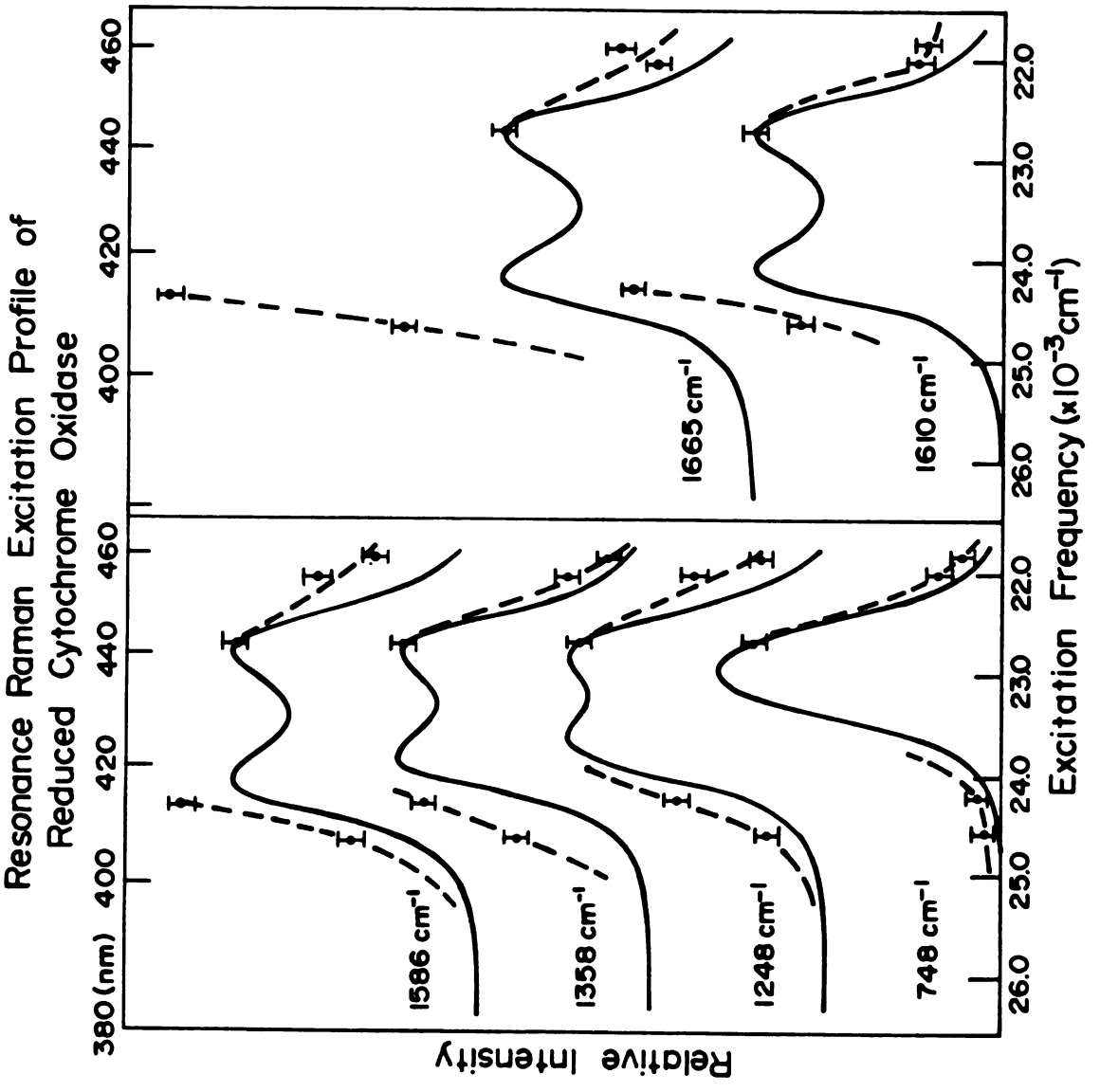
Resonance Raman Excitation Profile of
Reduced Cytochrome Oxidase
Relative Intensity
Excitation Frequency (x10⁻³cm⁻¹)
380(nm) 400 420 440 460
26.0 25.0 24.0 23.0 22.0
1586 cm⁻¹
1358 cm⁻¹
1248 cm⁻¹
748 cm⁻¹
1665 cm⁻¹
1610 cm⁻¹

Figure 15

as the vibrational quantum, in which case the peaks are not resolved. Included in these theoretical plots are data points obtained from the experimental data of Figure 14. There is rough agreement between the calculated and experimental points in that the decreased intensity observed for the low frequency modes with 406.7 and 413.1 nm excitation is predicted. However the experimental data also show deviations from Equation (2.7): a) the scattered intensity on the low frequency side of the 0,0 peak and on the high frequency side of the 0,1 peak is greater than that calculated from Equation (2.7) which predicts destructive interference in these regions, b) the amplitude of the 0,1 scattering is greater than that of the 0,0 and c) the effects in (a) and (b) become more pronounced as the frequency of the vibrations increases. These phenomena have been observed in α band excitation profiles of heme proteins and have been accounted for by including a nonadiabatic term to allow for the effects of Soret excited states (Shelnutt *et al.*, 1976; Rousseau *et al.*, 1979). The dramatic increase in intensity observed for the peripheral aldehyde stretching vibrations of cytochromes *a* and a_3 at 1610 cm^{-1} (see Chapter 5) and 1665 cm^{-1} can be interpreted as arising from nonadiabatic coupling to a transition at higher energy. Carbonyl substitution has been shown to induce additional absorption bands in the spectra of chlorin species (Weiss, 1972). Raman excitation in the

near UV region of these species results in an additional enhancement of the peripheral substituent vibrations (Lutz et al., 1982). A similar mechanism may be operative here for the heme a chromophores in cytochrome oxidase.

With the Franck-Condon nature of the Soret RR spectra established, structural information can be extracted from the spectra by comparison with appropriate model compounds.

II. Soret Excitation RRS of Ferric Heme Model Compounds

A. Previous Structural Correlations

The geometry of the porphyrin macrocycle in hemes and heme proteins is reflected in the frequency positions of several vibrational bands observed by resonance Raman spectroscopy (Spiro, 1974; Felton and Yu, 1978; Kitagawa et al., 1978; Rousseau et al., 1979). One of the most useful empirical correlations between heme structure and Raman frequency has been developed by Spaulding et al., (1975) who showed that an inverse relationship exists between the frequency of an anomalously polarized mode in the 1550-1610 cm^{-1} region and C_t-N, the distance from the center of the porphyrin to the pyrrole nitrogens. This was later confirmed and extended (Huong and Pommier, 1977; Scholler and Hoffman, 1979; Spiro et al., 1979); plots of Raman frequency vs. porphyrin core size (C_t-N) for the ap mode (denoted Band IV) as well as for a polarized mode in

in the 1600-1650 cm^{-1} region (Band IV) could be fit by an empirical equation of the form

$$\bar{\nu}_i = K_i(A_i - d)\ cm^{-1} \qquad (4.1)$$

where $\bar{\nu}_i$ is the frequency of the vibration under consideration, d the C_t-N distance and K_i and A_i are adjustable parameters specific to the i^{th} vibration. Equation (4.1) has thus far been established for the three vibrational bands indicated above, all of which have appreciable methine bridge bond stretching character (Spiro et al., 1979). As a consequence, the correlations indicated by Equation (4.1) are relatively insensitive to the nature of the pyrrole β-carbon substituents, provided that these are linked by $C-C_s$ bonds. However replacement of the hydrogen at the methine bridge carbon by, for example, phenyl groups or deuterium causes shifts in these bands unrelated to core size change and Equation (4.1) is no longer applicable. In addition, Bands II and V are also somewhat sensitive to the nature of the axial ligands and shift to higher frequency as the π acceptor character of the ligands is increased.

With the establishment of sound correlations between porphyrin core size and Raman frequency, it has become possible to interpret scattering data to determine both spin state and iron coordination number for several heme

proteins (Spiro et al., 1979; Seivers et al., 1979). However research which has been done thus far to link porphyrin core size and Raman vibrational frequencies has been carried out with α, β excitation. The vibrations observed upon Soret excitation of hemes and heme proteins are, in general, distinct from those enhanced by α, β excitation and the empirical correlation between core size and Raman frequency described above for Herzberg-Teller active modes may not necessarily apply to the Franck-Condon vibrations.

Sporadic reports have appeared in the literature which relate the frequency of a polarized mode in the 1560-1600 cm^{-1} region, observed with Soret excitation, to heme iron spin state. For example, Yamamoto et al. (1973) reported such a correlation for hemoglobin and myoglobin compounds, Remba et al. (1979) reported analogous data for chloroperoxidase and Babcock and Salmeen (1979) tabulated the frequency of the band as a function of heme a iron spin state. However, a systematic study of this phenomenon has not yet appeared. In this section, the Raman spectra of a number of heme model compounds and heme proteins are investigated and an empirical correlation between the frequencies of the observed modes, the porphyrin core size and the pattern of β-carbon peripheral substituents is established. In the next section this correlation is applied to the interpretation of Soret excitation Raman spectra of cytochrome oxidase and a number of its inhibitor complexes.

B. Peripheral Substituent Dependence of Vibrational Frequencies

1. Protoheme Species

Soret excitation Raman spectra of several protoheme containing species are presented in Table 2A. These have been selected to represent the commonly encountered combinations of spin state and iron coordination: a) six coordinate low-spin, b) six coordinate high-spin, and c) five coordinate high-spin. The Raman spectra of the cyanide and fluoride complexes of ferric HRP have also been investigated and it is found that they resemble the azide and fluoride metmyoglobin complexes, respectively (Babcock et al., 1981). As expected for Soret excitation, the principal vibrational modes observed are polarized ($\rho_\ell \leq .75$) (see Table 3). However the depolarization ratios rarely achieve the 1/8 value expected for D_{4h} symmetry, indicating that the effective symmetry is reduced. This effect, plus the conjugation of the vinyl substituents with the porphyrin π system (Adar, 1975; Choi et al., 1982) contributes additional bands to the high frequency Raman spectra of protoheme derivatives when compared to the symmetric heme species described below.

The Soret excitation spectra are distinct from those obtained for the same compounds with α, β band excitation, particularly in the 1550-1600 cm^{-1} region, where the

Table 2. Spin State, Coordination Geometry, and Selected Raman Frequencies for Various Hemes and Heme Proteins.

Compound	Spin State	Coord.	Raman Frequencies λ_{ex} = Soret			Raman Frequencies* λ_{ex} = visible		
						p	ap	dp
A. Protoheme Species								
MetHbF	5/2	6	1482	1567	1623	1482	1555	1608
MetMbF	5/2	6	1482	1566	1622	1483	1557	1609
$MetMbH_2O$	5/2	6	1482	1565	1622	1481	1562	1611
$PP\text{-}DMEFe^{3+}(DMSO)_2$	5/2	6	1482	1564	1626	1475	1560	1610
oxidized HRP	5/2**	5	1498	1573	1630	1500	1575	1630
$PP\text{-}DMEFe^{3+}Cl^-$	5/2	5	1493	1574	1631	1495	1572	1632
$MetMbN_3^-$	1/2	6	1506	1584	1621, 1640	---	---	---
Protoheme $Fe^{3+}(NMeIm)_2$	1/2	6	1507	1582	1624, 1640	1503	1586	1638
$PP\text{-}DMEFe^{3+}(NMeIm)_2$	1/2	6	1506	1582	1623, 1639	---	---	---
B. Hemes with all Ring Positions Saturated								
$EtioFe^{3+}(DMSO)_2$	5/2	6	1483	1576	1615	1481	1563	1613
$EtioFe^{3+}Cl^-$	5/2	5	1496	1585	1632	1493	1568	1629
$(Fe^{3+}OEP)_2O$	5/2	5	1491	1582	1630	1494	1570	1630
$EtioFe^{3+}(NMeIm)_2$	1/2	6	1506	1593	1640	1505	1584	1641
$OEPFe^{3+}(CN^-)_2$	1/2	6	1505	1590	----	----	----	----
$OEPFe^{3+}(NMeIm)_2$	1/2	6	1507	1591	1640	1506	1587	1640
Cyt $\underline{c}^{3+}$	1/2	6	1506	1588	1640	1502	1582	1636

Table 2. Continued.

Compound	Spin State	Coord.	Raman Frequencies λ_{ex} = Soret			Raman Frequencies* λ_{ex} = visible p	ap	dp
		C. Heme a Species††						
Heme $\underline{a}^{3+}(DMSO)_2$	5/2	6	1482	1572	1615, 1672	----	----	----
Cyt $\underline{a}_3^{3+}$	5/2	6	1478	1572	1615, 1675	----	----	----
Cyt $\underline{a}_3^{3+}\cdot HCOOH$	5/2	6	1478	1572	1615, 1675	----	----	----
Heme $\underline{a}^{3+}Cl^-$	5/2	5	1492	1581	1632, 1676	----	----	----
Heme $\underline{a}^{3+}(NMeIm)_2$	1/2	6	1506	1590	1642, 1670	----	----	----
Cyt $\underline{a}^{3+}$	1/2	6	1506	1590	1641, 1650	----	----	----
Cyt $\underline{a}_3^{3+}\cdot CN^-$	1/2	6	1506	1590	1641, 1674	----	----	----

*From tables compiled by Sievers et al. (1979) and by Spiro et al. (1979).

**The assignment of HRP as pure high-spin is somewhat ambiguous, see Maltempo (1976) and also Sievers et al. (1979).

††The cytochrome a and a_3 assignments are made in Babcock et al. (1980).

structure sensitive anomalously polarized mode (Spaulding et al., 1975) is replaced by polarized modes. Yamamoto et al. (1973) were the first to point out that these polarized modes are sensitive to spin state. For the six coordinate myoglobin derivatives they investigated with 441.6 nm excitation; the ratio of intensities for the bands at 1566 and 1584 increased as the high-spin content increased. The data confirm this correlation and demonstrate that it also applies to six coordinate high-spin and low-spin protoheme compounds. Moreover, five coordinate high-spin protoheme compounds show a strong polarized mode at 1576 cm^{1}, intermediate between the 1584 cm^{-1} low-spin and 1566 cm^{1} six coordinate high-spin marker bands. Thus the high frequency polarized mode showsthe same general dependence on heme structure as reported for Band IV, the high frequency ap mode: as the C_t-N distance increases from six coordinate low-spin through five coordinate high-spin to six coordinate high-spin, the frequency of the band decreases. However, in the case of Band IV the overall decrease amounts to 30 cm^{-1} for the heme complexes examined whereas for the polarized mode the corresponding decrease is only 18 cm^{-1}. This observation indicates a less dramatic C_t-N distance dependence for the polarized mode. Table 2 summarizes the positions of the prominent bands of protoheme, FeOEP and heme a species as well as vibrational frequencies observed for the same compounds with excitation in the visible region.

With α, β band excitation a polarized mode in the 1500 cm^{-1} region is observed (Band II) which is sensitive to heme iron spin and coordination. A band in the same region is also prominent in the Soret excitation Raman spectra we report and exhibits the same dependence; we conclude that Band II is enhanced by both α, β and Soret laser lines. For six coordinate high-spin derivatives Band II occurs at 1482 cm^{-1} and shifts to 1496 cm^{-1} for five coordinate high-spin species. In six coordinate low-spin protoheme compounds the observed frequency is 1507 cm^{-1}. Because other bands are also apparent in the 1470-1510 cm^{-1} region, correlations based only on Band II positions are somewhat tenuous.

2. Hemes with Saturated Ring Substituents

Attempts to extrapolate the correlations developed in the previous section between protoheme structure and Raman frequencies to c-type cytochromes and to heme a containing species were only partially successful. For Band II the same pattern emerges. However for the polarized mode in the high frequency region inconsistencies are apparent. This behavior is demonstrated for species with saturated ring substituents in Table 2B where we have collected data of representative six coordinate high-spin, five coordinate high-spin, and six coordinate low-spin compounds. The Raman spectrum of bis(cyano)Fe^{3+} OEP has also been recorded

and it is found that its vibrational properties are similar to those of the bis(NMeIm) complex; its principal high frequency vibrations occur at 1590 cm^{-1}, 1505 cm^{-1}, and 1376 cm^{-1}. In the 1500 cm^{-1} region, the low-spin species show Band II at 1507 cm^{-1}; for the high-spin compounds Band II occurs at 1496 cm^{-1} for five coordinate complexes and at 1482 cm^{-1} when the iron is six coordinate. In the high frequency region, there is a positive shift of about 10 cm^{-1} in frequency for the structure sensitive polarized mode for the hemes with saturated substituents compared to the corresponding protoheme derivatives. Thus the six coordinate low-spin indicator occurs near 1590 cm^{-1}, the five coordinate high-spin band is at 1584 cm^{-1} and the six coordinate high-spin mode shows at 1575 cm^{-1}. As with the protoheme species, however, the total decrease in the frequency of the high frequency polarized mode as the C_t-N distance increases from its six coordinate low-spin value (1.989 Å, (Collins et al., 1972)) to its six coordinate high-spin value (2.045 Å, Mishiko et al., 1978)) is approximately 18 cm^{-1}.

Protoheme is distinct from the species in Table 2B in that it has unsaturated substituents at two of the β-carbon positions, i.e., vinyl groups at carbons 2 and 4. The Raman data above thus indicate that upon Soret excitation of iron porphyrin compounds the observed frequency of the mode in the 1560-1600 cm^{-1} region reflects three different

structural aspects of the chromophore: (a) the spin state of the iron, (b) the coordination number of the iron, and (c) the nature of the peripheral substituents. For Band IV observed with α, β band excitation, it is apparent that the frequency position reflects only C_t-N distance, i.e., structural features (a) and (b) above, since similar values of A and K in Equation (4.1) can be obtained from Raman data for metalloporphyrins with either saturated or unsaturated β-carbon peripheral substituents. An explanation for the dichotomy in behavior of these two modes can be constructed based on the normal coordinate analysis of Abe et al. (1978) and is considered below.

3. Heme a Species

The data above demonstrate the usefulness of Soret excitation Raman data to the assignment of heme geometries provided that proper account of the pattern of peripheral substituents is taken. In heme a these substituents are distinct from those of protoheme and of the compounds in Table 2B in that a hydroxyfarnesylethyl group occurs at position 2, a vinyl at ring position 4 and a formyl at ring position 8. Thus we have carried out a classification of the structure sensitive heme a modes observed upon Soret excitation and show representative spectra of the various derivatives in Figure 16 and Table 2C. Six coordinate low-spin heme a^{3+} (Figure 16d) shows bands at 1506 cm^{-1} and

Figure 16. Resonance Raman spectra of several heme a model compounds dissolved in methylene chloride. Solvent and non-resonance enhanced ligand vibrations are indicated by asterisks. Instrumental conditions as in Figure 14.

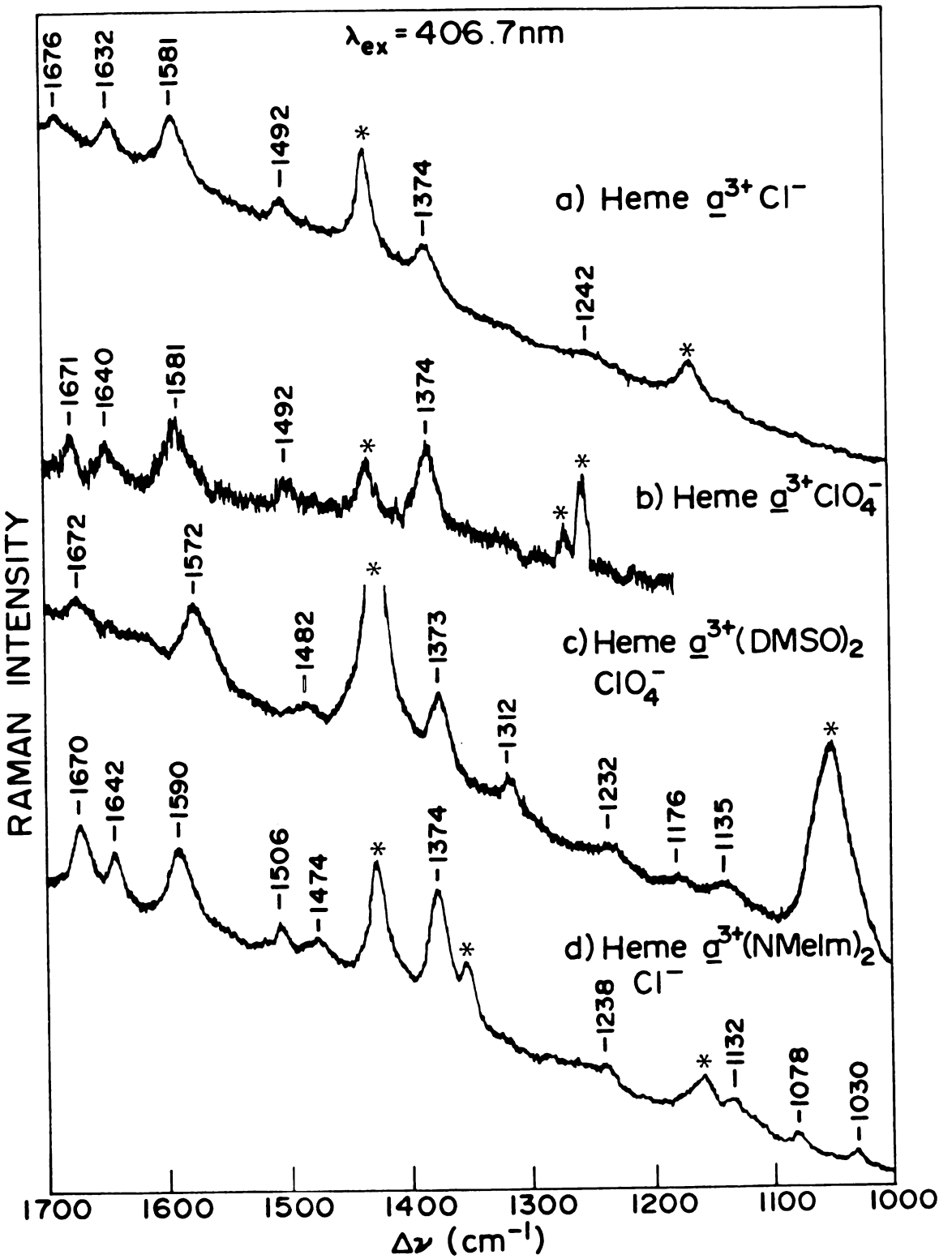
λex = 406.7nm
-1676
-1632
-1581
-1492
-1374
-1242
a) Heme a3+ Cl−
-1671
-1640
-1581
-1492
-1374
b) Heme a3+ ClO4−
-1672
-1572
-1482
-1373
-1312
-1232
-1176
-1135
c) Heme a3+(DMSO)2 ClO4−
-1670
-1642
-1590
-1506
-1474
-1374
-1238
-1132
-1078
-1030
d) Heme a3+(NMeIm)2 Cl−
RAMAN INTENSITY
1700
1600
1500
1400
1300
1200
1100
1000
Δν (cm−1)

Figure 16

1590 cm^{-1} which are replaced by bands at 1492 cm^{-1} and 1581 cm^{-1} in the five coordinate high-spin complex (Figure 16a). For the six coordinate high-spin model compound (Figure 16b), these bands occur at 1482 cm^{-1} and 1572 cm^{-1}. The band observed in the high frequency region near 1670 cm^{-1} in these species is due to the heme a formyl group which is clearly resonance enhanced with Soret laser lines (Salmeen et al., 1978; Tsubaki et al., 1980). The Soret spectra differ markedly from the heme a spectra obtained with α band excitation (Babcock et al., 1979). With λ_{ex} = 592 nm the structure sensitive ap mode is observed and occurs at 1583 cm^{-1} for the six coordinate low-spin species; there is no indication of either a structure sensitive polarized mode in the 1500 cm^{-1} region or of the heme a carbonyl near 1670 cm^{-1}.

C. Vibrational Assignments

Soret excitation Raman spectroscopy offers several advantages over the more commonly employed heme α, β band excitation spectroscopy. These include the use of both lower heme concentrations, generally by a factor of about 10, and lower incident laser powers. This work provides a systematic classification of the iron porphyrin high frequency modes observed when Soret exciting lines are used and of the structural information which can be

extracted from the frequencies of these modes.

It was recognized fairly early in the application of resonance Raman spectroscopy to heme proteins that the scattering mechanism in the Soret was primarily controlled by Franck-Condon overlap factors and hence distinct from the vibronic or Herzberg-Teller mechanism operative when Q band excitation is employed (Nafie et al., 1973; Friedman and Hochstrasser, 1973; Spiro, 1974). Thus modes in which there is origin displacement in the excited state dominate the Raman spectrum obtained with Soret excitation, whereas anomalously polarized and depolarized modes which are active in vibronic mixing are the principal components of heme Raman spectra taken with visible laser lines. Nonetheless for two of the bands observed routinely with Soret excitation of hemes and heme proteins, the polarized oxidation state marker band in the 1345-1380 cm^{-1} region (Band I) and the polarized mode in the 1480-1518 cm^{-1} region, (Band II) are also common features of visible excitation Raman spectra. The data presented above indicate that the correlations between spin, coordination number and oxidation state developed for these two modes are independent of whether the excitation frequency is in resonance with the α, β or γ band transition.

Two other modes, however, the ap mode in the 1550-1600 cm^{-1} region (Band IV) and the dp mode in the 1600-1650 cm^{-1} region (Band V) are not strongly and consistently enhanced

upon Soret excitation. In the Band V region, two effects appear to influence the Soret excitation spectra. For heme species with saturated β-carbon substituents, Table 2 shows that a good correlation exists between the frequency of the dp mode observed with visible excitation and that of the highest frequency mode in our Soret excitation Raman spectra. For a representative compound in this class, OEP Fe^{3+} $(NMeIm)_2$, Table 3 shows that the 1640 cm^{-1} mode is depolarized and thus we conclude that the same vibration (i.e., that which gives rise to Band V) is active with both Soret and visible excitation. The second effect contributing lines in the 1600-1680 cm^{-1} region is apparent when the heme a and protoheme derivatives are considered. For heme a the formyl vibration is observed at 1670-1676 cm^{-1} in aprotic solvents. Band V appears at slightly lower frequencies and shows a dependence of porphyrin core size similar to that of the heme derivatives with saturated substituents (Table 2). For protoheme species the 1600-1650 cm^{-1} region is dominated by a vibration at 1621-1626 cm^{-1}; only in low-spin species is Band V clearly observed. Because vinyl vibrations are expected in the 1620 cm^{-1} region, the mode observed near this frequency in protoheme species is assigned as being due to the carbon-carbon double bond stretching mode.

For the polarized mode in the 1560-1600 cm^{-1} region, the data presented demonstrate a correlation between the

Table 3. Depolarization Ratios: Low-spin Ferric Heme Compounds.*

Fe^{3+}PPIXDME(NMeIm)$_2$		Fe^{3+}OEP(NMeIm)$_2$		heme a^{3+}(NMeIm)$_2$	
Band (cm^{-1})	ρ**	Band (cm^{-1})	ρ	Band (cm^{-1})	ρ
				1670	0.28±0.05
1639	0.57±0.05	1640	0.75±0.05	1642	0.35
1623	0.43				
1582	0.42	1591	0.45	1590	0.40
1506	0.24	1507	0.26	1506	0.20
1472	----	1469	0.50	1474	0.51
1374	0.30	1377	0.34	1374	0.33
1288	----	1286	0.36	1285	0.28
1235	0.49	1230	0.46	1238	0.48
1131	0.49	1138	0.60	1132	0.60
1080	0.38	1078	0.36	1078	0.20
1030	----	1028	0.33	1030	0.26

*Excitation frequency = 406.7 nm

**$\rho = I_{\perp}/I_{||}$

observed frequency and the coordination and spin state of the heme bound iron. In this regard it parallels the behavior of the ap mode in the same region. There are, however, quantitative differences between the two; (a) the position of the polarized mode is also a function of the porphyrin β-carbon substituents; for the ap mode this dependence does not appear to be strong and (b) the shift in the position of Band IV as the heme C_t-N distance is changed is greater than the corresponding shift in the position of the polarized mode. The differences between the various structure sensitive modes is made more apparent by examining the plot of C_t-N distance *vs.* $\Delta\bar{\nu}$ shown in Figure 17. The sensitivity of the 1560-1600 cm^{-1} polarized mode to β-carbon substituents is reflected in the different lines for the indicated classes of hemes; the less dramtic dependence on heme C_t-N distance is evident in the smaller slope of these lines relative to those of the other modes.

The polarized high frequency mode appears to have little or no dependence on the identities of the iron axial ligands, at least for the ferric oxidation state. Table 2 shows that for protoheme species in the low-spin state essentially identical frequencies are observed for bis(N-methylimidazole) and for histidine-azide ligand combinations. A similar insensitivity to ligand identity is apparent for the high-spin compounds. For hemes with saturated peripheral substituents a slight frequency difference is observed when

Figure 17. (C_t-N) A distance plotted versus vibrational frequency for several Soret excitation structure sensitive modes.

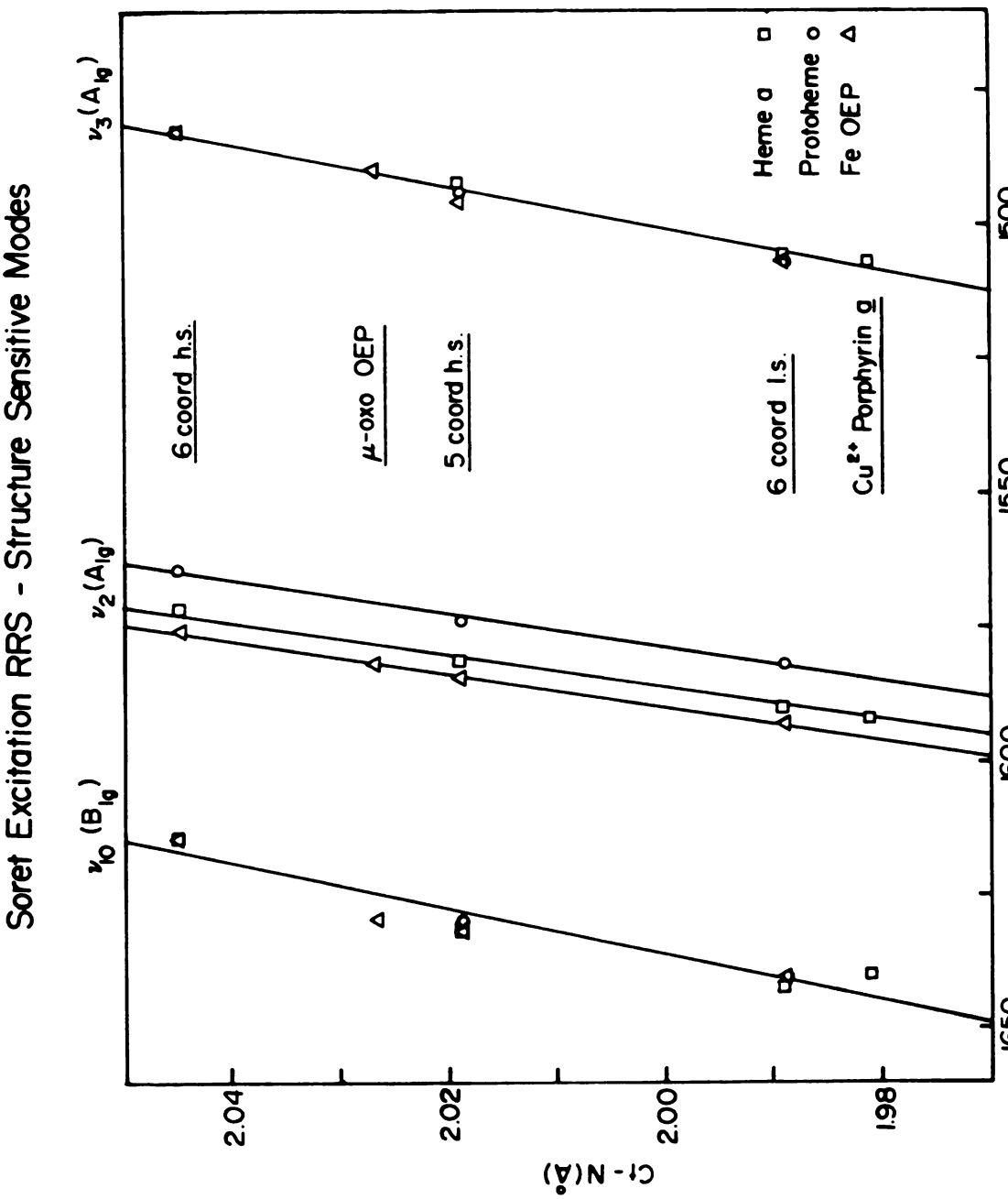
Soret Excitation RRS - Structure Sensitive Modes
ν_{10} (B_{1g})
ν_2 (A_{1g})
ν_3 (A_{1g})
6 coord h.s.
μ-oxo OEP
5 coord h.s.
6 coord l.s.
Cu2+ Porphyrin g
Heme a
Protoheme
Fe OEP
Cγ - N (Å)
2.04
2.02
2.00
1.98
1650
1600
1550
1500
Δν (cm-1)

Figure 17

bis(N-methylimidazole) and bis (cyano) compounds are compared with the histidine methionine combination in cytochrome c. This may reflect a real axial ligand dependence or the fact that the substituents in the 2 and 4 positions on the ring periphery in cytochrome c are involved in thioether linkages.

The observations and differences described above regarding the behavior of the four structure sensitive modes summarized in Table 2 can be rationalized by reference to the recent normal coordinate analysis of Abe et al. (1978). Bands II, IV, and V correspond to vibrations $\nu_4(A_{1g})$, ν_{19} (A_{2g}) and ν_{10} (B_{1g}), respectively, in their normal coordinate analysis and the polarized mode we observe in the 1560-1600 cm^{-1} region with Soret excitation can be assigned as the analog of their ν_2 (A_{1g}). Abe et al. (1978) have shown that ν_3, ν_{19} and ν_{10} have considerable α-carbon/methine-carbon stretching character whereas ν_2 involves primarily β-carbon/β-carbon stretching. Consequently, the more dramatic C_t-N distance dependence of Bands II, IV and V relative to ν_2 is a manifestation of the fact that the pyrrole ring maintains a fairly rigid structure and shifts in porphyrin geometry as a result of core expansion are accommodated largely by distortions in the α-carbon/methine-carbon/α-carbon bond angle. Substituents to the pyrrole β-carbons, on the other hand, are predicted and observed to alter the frequency of ν_2 without perturbing

ν_3, ν_{19} or ν_{10} to a significant extent. In this regard, Kitagawa and coworkers (Abe et al., 1978) have shown that ν_{11}, the B_{1g} mode which represents the out of phase analog to ν_2, is also sensitive to the nature of the β carbon substituents.

The data presented above demonstratethat Soret excitation Raman spectroscopy of hemes and heme proteins can yield structural information analogous to that obtained with visible excitation. This information is, however, somewhat more difficult to extract because the frequency of the structure sensitive modes is also a function of the nature of the peripheral substituents and because the changes in frequency upon change in structure is less dramatic than for Band IV. Nonetheless, there are a number of advantages associated with Soret Raman, particularly in the less severe demands upon protein concentration and laser power. In the following section Soret excitation Raman results of oxidized cytochrome oxidase are presented which apply the structural correlations developed here.

III. Oxidized Cytochrome Oxidase

A. Photoreduction

Photoreduction of resting cytochrome oxidase by the incident laser light at the powers required for Raman spectroscopy is a major obstacle to the application of this

technique to the oxidized enzyme. Moreover, uncertainty exists in the literature regarding both the mechanism (Seiter and Angelos, 1980) and manifestations (Woodruff et al., 1981) of cytochrome oxidase photoreduction. Figure 18 presents results obtained with the flowing sample technique developed to avoid the photoreduction problem (Babcock and Salmeen, 1979). Under flow conditions (Figure 18a) and with 406.7 excitation the oxidation state marker band is observed at 1373 cm^{-1} with no shoulder to lower frequency, the oxidized cytochrome $\underline{a}_3$ modes at 1572 cm^{-1} and 1676 cm^{-1} are present (Ondrias and Babcock, 1980) and the cytochrome $\underline{a}$ modes at 1506 cm^{-1}, 1590 cm^{-1} and near 1650 cm^{-1} are observed. (See Table 4 for a summary of the vibrational properties of cytochromes $\underline{a}$ and $\underline{a}_3$.) When the flow is turned off and the spectrum of the static sample recorded (Figure 18b), a number of changes occur. In particular new bands are apparent at 1622, 1612, 1520 cm^{-1} and a shoulder appears on the low frequency side of the 1372 cm^{-1} band. The cytochrome $\underline{a}_3^{3+}$ bands at 1676, 1572, and 1478 cm^{-1} are still present. The spectrum of the partially photoreduced enzyme in Figure 18b bears a strong resemblance to that of the enzyme in the presence of formate and a mild reductant (Figure 18d), a treatment which is known to generate the species $\underline{a}^{2+}$ $\underline{a}_3^{3+}\cdot HCOOH$ (Nicholls and 976). When the flow is restored the sample again exhibits the spectrum of the oxidized enzyme (Figure 18c).

Figure 18. Resonance Raman spectra of several cytochrome oxidase species recorded with 406.7 nm excitation. Instrumental conditions: resolution, 6 cm^{-1}; time constant, 1 s; scan rate, 50 cm^{-1}/min. The instrument gain was constant in recording spectra a, c, d and e; for spectrum b this was increased by a factor of three.

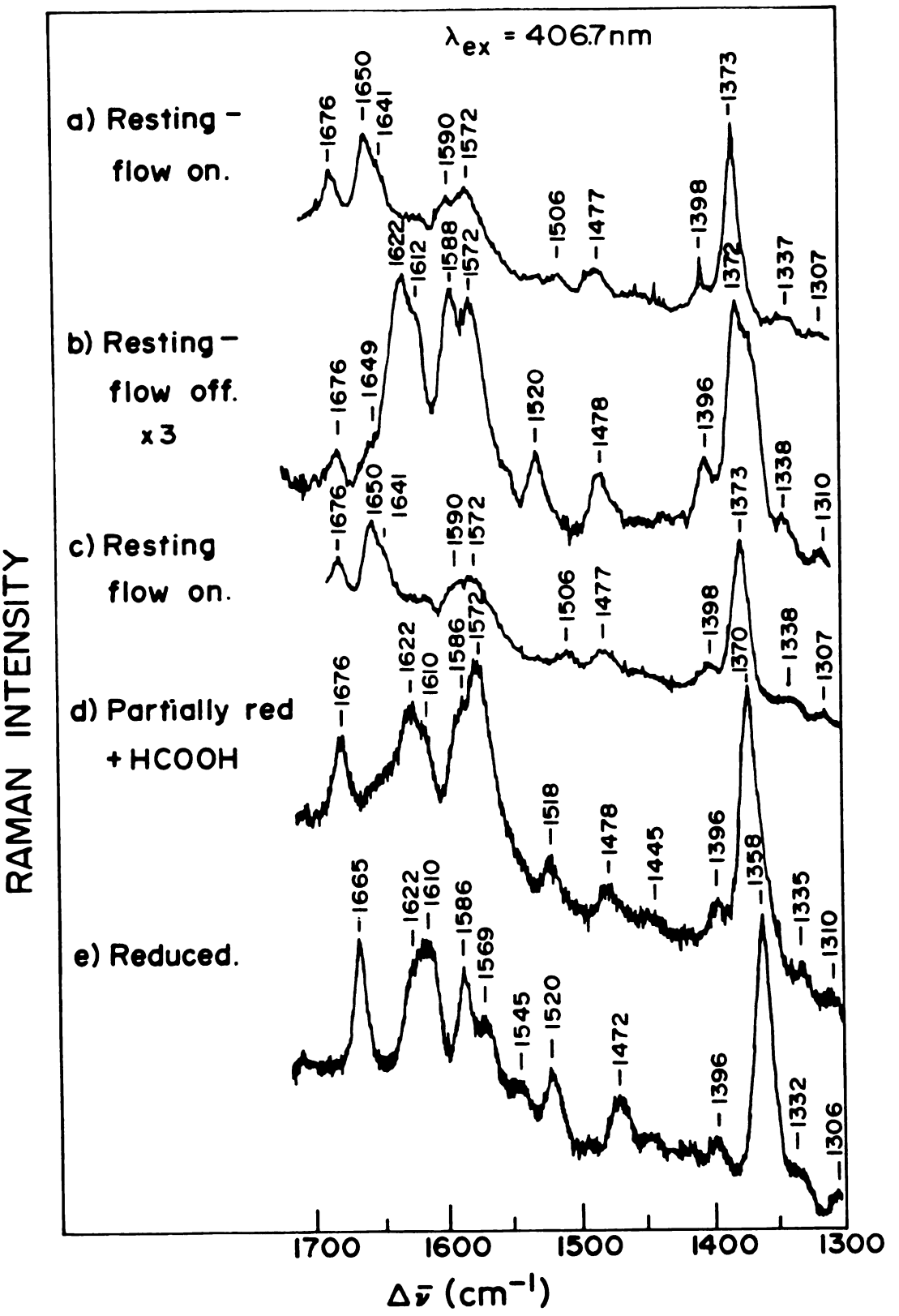
λex = 406.7nm
a) Resting – flow on.
b) Resting – flow off. x3
c) Resting flow on.
d) Partially red + HCOOH
e) Reduced.
RAMAN INTENSITY
Δν̄ (cm⁻¹)
1700
1600
1500
1400
1300

Figure 18

The results in Figure 18, particularly the comparison between 18b and 18d indicate that in aerobic samples of cytochrome oxidase, the photoreduction process leads first to reduction of cytochrome *a* followed by reduction of cytochrome a_3. This redox situation, *i.e.*, reduced cytochrome *a* and oxidized cytochrome a_3, corresponds to that found in the aerobic steady state (Nicholls and Petersen, 1974) and suggests the following mechanism for the photoreduction process. Illumination produces reducing equivalents external to the oxidase (most likely via a flavin contamination (Adar and Yonetani, 1978)) which subsequently reduce the enzyme. In the presence of oxygen the predominate species is that corresponding to the aerobic steady state (a^{2+} a_3^{3+}). Upon depletion of O_2, full reduction is achieved (Adar and Yonetani, 1978). This proposal is compatible with previous results with 441.6 nm excitation which showed minimal formation of reduced cytochrome a_3 upon illumination of static oxidase samples (Salmeen *et al.*, 1978), with the observations of Adar and Erecinska (1979) who saw a delay in the appearance of the 1665 cm^{-1} band, characteristic of reduced cytochrome a_3 in the initial stages of photoreduction at -10°C, and with the results of Bocian *et al.* (1979) who showed that Soret excitation of frozen oxidase samples produced photoreduction but that visible excitation did not. This latter result is expected if the photoactive species is a flavin, which has a strong absorption in the blue but not in the red region (>550 nm)

of the spectrum.

The photoreduction process has been studied in more detail by carrying out laser power studies on flowing oxidase samples (Babcock et al., 1981). At low to moderate powers of 406.7 and 413.1 nm excitation (Figure 19) the spectrum of the oxidized enzyme is observed. Only at 55 mW incident power do photoreduction effects, notably the increase in the intensity of bands at 1622 cm^{-1}, 1610 cm^{-1} and 1520 cm^{-1}, become evident. This work demonstrates that the use of the oxidation state marker band as a judge of photoreduction is a poor criterion. Even with appreciable photoreduction (Figure 19d) there is little obvious change in this band. This observation, as well as the fact that photoreduction produces its first noticeable effects in the 1600 cm^{-1} region with 406.7 and 413.1 nm excitation, can be rationalized by reference to the excitation profile data presented above. Under conditions of partial photoreduction the predominant form of the enzyme is identified as the aerobic steady state: cytochrome $\underline{a}_3$ oxidized and cytochrome $\underline{a}$ reduced. The $\underline{a}^{2+}$ species has an absorption peak at 443 nm which is 2015 cm^{-1} and 1634 cm^{-1} to the red of the 406.7 and 413.1 nm laser lines, respectively. Consequently, from Equation (2.7), we expect that vibrations in these frequency regions will be more strongly enhanced than those to lower frequency and that photoreduction will be apparent first in the high frequency

Figure 19. The incident laser power dependence of the resonance Raman spectrum of resting cytochrome oxidase. The excitation frequency and power incident on the sample are indicated. Instrumental conditions: resolution, 6 cm^{-1}; time constant 1 s; scan rate, 50 cm^{-1}/min. From Babcock _et al_. (1981).

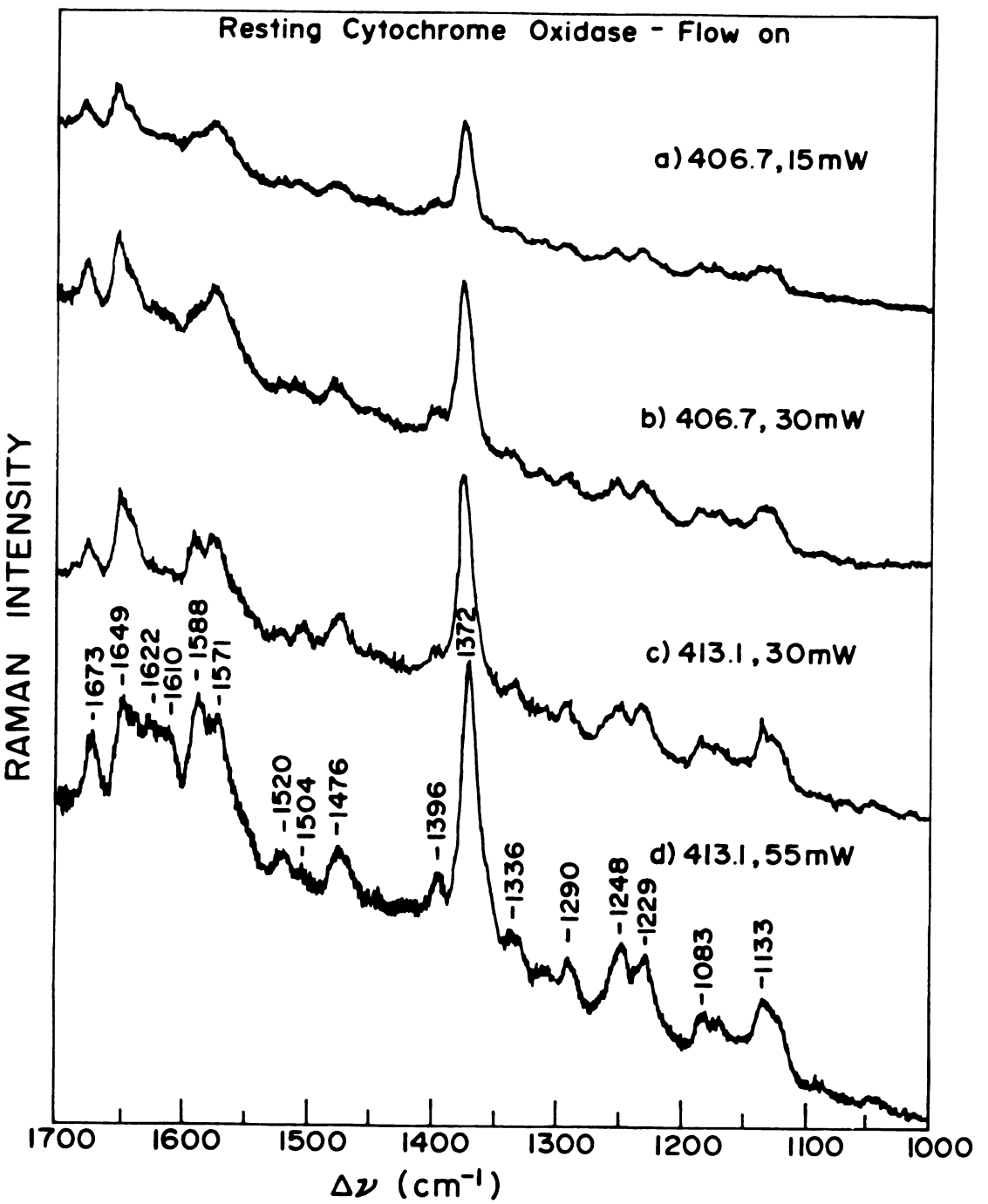
Resting Cytochrome Oxidase - Flow on
a) 406.7, 15mW
b) 406.7, 30mW
c) 413.1, 30mW
d) 413.1, 55mW
RAMAN INTENSITY
1673
1649
1622
1610
1588
1571
1520
1504
1476
1396
1372
1336
1290
1248
1229
1083
1133
1700
1600
1500
1400
1300
1200
1100
1000
Δν (cm⁻¹)

Figure 19

modes. As more of the enzyme is reduced, this process also becomes evident in the 1360 cm^{-1} region (Figure 18b). These excitation profile arguments also rationalize earlier observations on the photoreduction of the oxidized enzyme (Salmeen *et al.*, 1978) in which excitation at 441.6 nm (72 cm^{-1} from the 443 nm $\underline{a}^{2+}$ peak absorption) resulted in the observation of cytochrome $\underline{a}^{2+}$ modes throughout the Raman spectrum.

B. Raman Spectra of Inhibitor Complexes of Cytochrome Oxidase and of its Oxygenated Form

Figure 20 presents Raman spectra of several derivatives of cytochrome oxidase; the vibrational assignments from these data are summarized in Table 4. In the formate complex of the oxidized enzyme, cytochrome $\underline{a}_3^{3+}\cdot$HCOOH is high-spin whereas cytochrome $\underline{a}^{3+}$ remains low-spin (Babcock *et al.*, 1976). There is thus no change in spin state in going from the resting enzyme to the formate complex and correspondingly the Raman spectra of these two oxidase species are similar (compare Figure 18a with Figure 20a). Upon reduction of cytochrome *a* in the presence of formate, the mixed valence species, $\underline{a}^{2+}\ \underline{a}_3^{3+}\cdot$HCOOH, is formed (Figure 20b). The $\underline{a}_3^{3+}\cdot$HCOOH bands at 1676 cm^{-1}, 1572 cm^{-1} and 1478 cm^{-1} remain constant whereas the oxidized *a* bands at 1648 cm^{-1}, 1590 cm^{-1} and 1507 cm^{-1} are replaced by bands at 1622, 1610, 1586 and 1518 cm^{-1} as reduction of

Figure 20. Resonance Raman spectra of the oxidized (a,d) and partially reduced (b,e) complexes of cytochrome oxidase with formate and cyanide. In c, the spectrum of oxygenated cytochrome oxidase, formed by air oxidation of the dithionite reduced enzyme, is shown. Instrumental conditions: resolution, 6 cm^{-1}; time constant, 1 s; scan rate, 50 cm^{-1}/min.

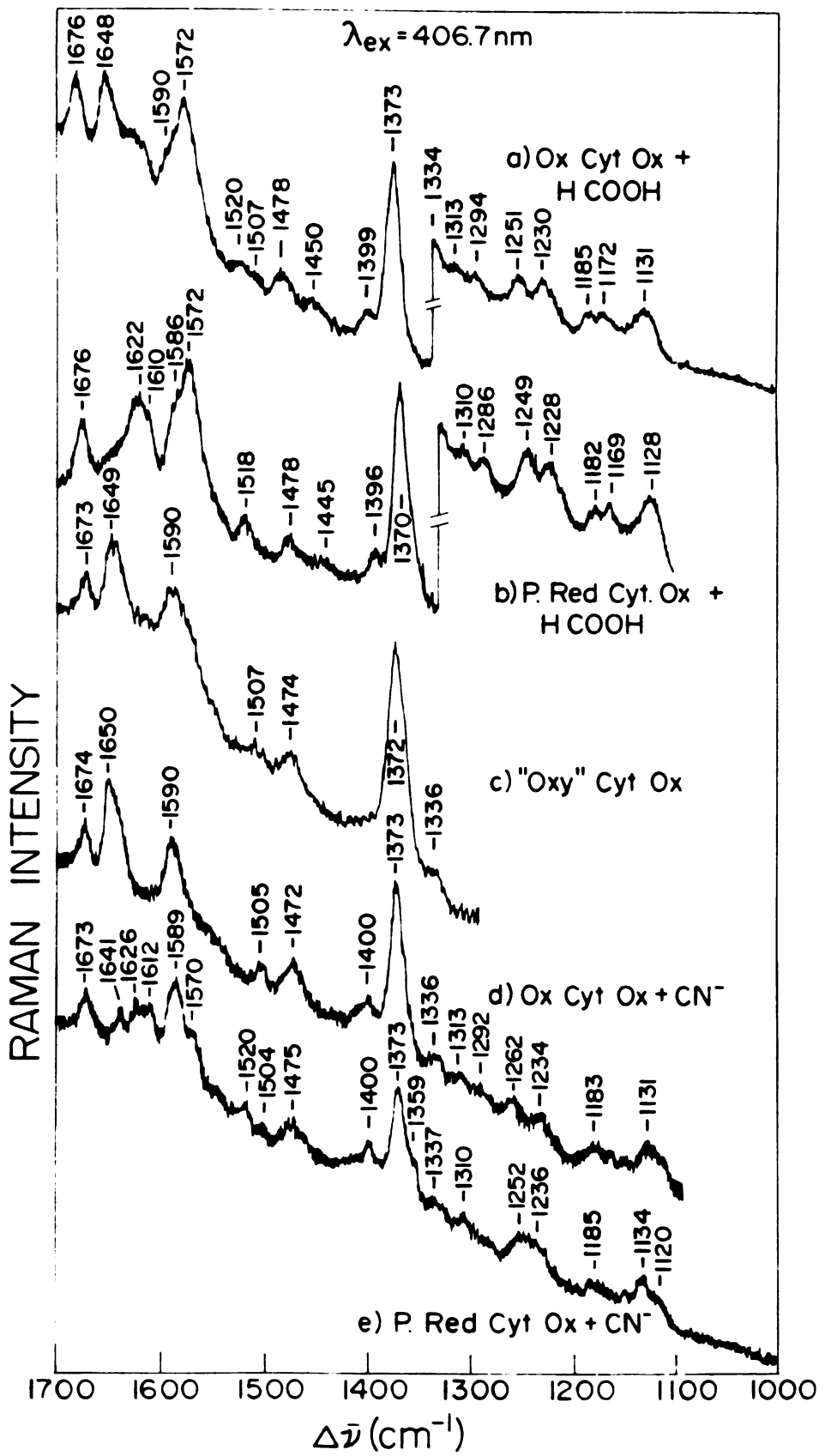
λex = 406.7nm
a) Ox Cyt Ox + H COOH
b) P. Red Cyt. Ox + H COOH
c) "Oxy" Cyt Ox
d) Ox Cyt Ox + CN⁻
e) P. Red Cyt Ox + CN⁻
RAMAN INTENSITY
Δν̄ (cm⁻¹)
1700
1600
1500
1400
1300
1200
1100
1000

Figure 20

Table 4. Optical, Coordination and Vibrational Properties of Cytochrome $\underline{a}$ and $\underline{a}_3$ in Various Cytochrome Oxidase Species.

Species	Spin	Coord.	λ_{max}	Characteristic Vibrations (cm^{-1})
$\underline{a}_3^{3+}$	5/2	6	414	1373, 1478, 1572, ∿1615, 1676
$\underline{a}_3^{3+}\cdot HCOOH$	5/2	6	414	1373, 1478, 1572, ∿1615, 1676
$\underline{a}_3^{3+}\cdot CN$	1/2	6	427	1373, 1474, 1506, 1590, 1641, 1676
$\underline{a}^{3+}$	1/2	6	427	1373, 1474, 1506, 1590, 1641, 1650
$\underline{a}^{2+}$	0	6	443	1358, 1521, 1622
$\underline{a}_3^{2+}$	2	5	443	215, 364, 1230, 1358, 1472, 1666
*heme $\underline{a}^{3+}Cl^-$	5/2	5	414	1374, 1492, 1581, 1632, 1676
*heme $\underline{a}^{3+}(DMSO)_2$	5/2	6	410	1373, 1482, 1572, 1615, 1672
*heme $\underline{a}^{3+}(NMeIm)_2$	1/2	6	422	1374, 1474, 1506, 1590, 1642, 1670

*From Callahan and Babcock (1981).

cytochrome a occurs. Upon CN^- addition to the oxidized enzyme, the species, a^{3+} $a_3^{3+}\cdot CN^-$, is formed and the a and a_3 species occur in the low-spin state. In the Raman spectrum of this derivative (Figure 20d), the high-spin a_3^{3+} band at 1572 cm^{-1} is absent and both a^{3+} and $a_3^{3+}\cdot CN^-$ show the low-spin ferric heme a marker band at 1590 cm^{-1}. The 1478 high-spin band of the oxidized enzyme is also absent, having been replaced by the low-spin band at 1505 cm^{-1}. The latter change is somewhat obscured by the appearance of the 1472 cm^{-1} band which occurs in low-spin heme a^{3+} complexes (Callahan and Babcock, 1981). Upon reduction of cytochrome a in the oxidized, cyanide complexed enzyme, the mixed valence species, a^{2+} $a_3^{3+}\cdot CN$, is formed (Figure 20e). As with the partially reduced formate species, the a^{2+} modes at 1626, 1610, 1520 and 1359 cm^{-1} appear. The low-spin $a_3^{3+}\cdot CN^-$ modes remain at 1673, 1641, 1589, 1504, 1475 and 1373 cm^{-1}.

C. Discussion

1. Optical Properties of Cytochrome Oxidase

The Raman data presented here and elsewhere (Salmeen et al., 1978; Babcock and Salmeen, 1979; Ondrias and Babcock, 1980), as well as the Raman observations made by Woodruff et al. (1981), provide strong evidence in support of Vanneste's (1966) original decomposition of the optical

properties of cytochrome oxidase into separate cytochrome $\underline{a}$ and $\underline{a}_3$ contributions (Table 4). Thus laser excitation (441.6 nm) on the long wavelength side of the oxidized oxidase Soret band generates the Raman spectrum of cytochrome $\underline{a}^{3+}$ (Babcock and Salmeen, 1979). Laser excitation (413.1 nm, 406.7 nm) on the short wavelength side produces the Raman spectrum of cytochrome $\underline{a}_3^{3+}$ through the first term of Equation (2.7) and those vibrational modes of cytochrome $\underline{a}^{3+}$ which are in resonance according to the second term of this equation. The cytochrome $\underline{a}^{3+}$ absorption peak occurs at 427 nm, which is 790 cm^{-1} away from the 413.1 nm krypton line. Thus the observation that the low frequency modes in the Raman spectrum of the oxidized enzyme obtained with 413.1 nm excitation are those of cytochrome $\underline{a}_3^{3+}$ (Babcock and Ondrias, 1980; Woodruff *et al.*, 1981) can be rationalized.

2. Coordination Geometries of $\underline{a}$ and $\underline{a}_3$

Cytochrome $\underline{a}$ is low-spin in both valence states (Tweedle *et al.*, 1978) and consequently six coordination is expected. This expectation is borne out by a comparison between the Raman properties of heme $\underline{a}^{3+}(NMeIm)_2$ and cytochrome $\underline{a}^{3+}$ in the 1500-1600 cm^{-1} region and is in agreement with earlier EPR (Blumberg and Peisach, 1979; Babcock *et al.*, 1979) and MCD (Nozawa et al., 1979) observations. An interesting anomaly for cytochrome $\underline{a}$ involves the behavior

of its formyl group. The formyl vibration is observed in the bis(imidazole)heme $\underline{a}^{3+}$ model compound at 1670 cm^{-1}. For cytochrome $\underline{a}^{3+}$, however, the highest frequency mode is observed at 1650 cm^{-1} with a second vibration apparent at 1641 cm^{-1} (Figure 18a; Babcock and Salmeen, 1979). Thus, even though the bis(imidazole) heme $\underline{a}^{3+}$ species has the EPR crystal field parameters of cytochrome $\underline{a}^{3+}$, it does not have the vibrational properties of the *in vivo* formyl group.

Because cytochrome $\underline{a}_3^{3+}$ is high-spin (Tweedle *et al.*, 1978) and can exist as either five or six coordinate, the model compound data for heme *a* are extremely useful in the determination of its geometry. In the resting enzyme cytochrome $\underline{a}_3^{3+}$ contributes vibrations at 1676, 1572, and 1478 cm^{-1} in the high frequency region. A weak feature near 1615 cm^{-1} is also due to the $\underline{a}_3^{3+}$ chromophore (Figure 18a). A comparison of these frequency positions with those of the high-spin five and six coordinate model compounds of Figure 17 and Table 4 clearly shows that the heme $\underline{a}^{3+}(DMSO)_2$ complex reproduces the cytochrome $\underline{a}_3^{3+}$ spectrum well; the five coordinate model, heme $\underline{a}^{3+}\cdot Cl$ does so much less adequately. Thus we conclude that in the resting enzyme, the $\underline{a}_3^{3+}$ species occurs in the high-spin, six coordinate state. The absorption spectrum of heme $\underline{a}^{3+}(DMSO)_2$ (Figure 11) also agrees well with Vanneste's spectral assignments of the Soret and visible region absorption

maxima. Table 4 also indicates that the frequency positions assigned to the $\underline{a}_3^{3+}\cdot CN^-$ complex and those of the low-spin heme $\underline{a}^{3+}$ $(NMeIm)_2$ compare well, confirming the assignment of cyanide derivative as six coordinate, low-spin. Finally $\underline{a}_3^{3+}\cdot HCOOH$ can be seen to occur as the six coordinate high-spin species consistent with the idea that formate serves as a ligand to the iron in this inhibitor complex (Nicholls, 1976).

Our finding that cytochrome $\underline{a}_3^{3+}$ in the resting enzyme is six coordinate has interesting ramifications with respect to the structure of the oxygen reducing site and the mode by which the proposed exchange coupling between the iron of $\underline{a}_3$ and the associated copper (Van Gelder and Beinert, 1969; Palmer, et al., 1976) is mediated. Two general models are available in the literature. These can be classified as "backside" bridging in which the copper of the heme a ring to which O_2 binding occurs and "front-side" bridging in which the copper is coupled to the iron by a ligand which occupies the reduced protein dioxygen binding site (See Figure 21 a,b). A specific "back-side" model has been proposed in which the bridging ligand is a histidine residue (Palmer et al., 1976). This is represented in Figure 21c where a water molecule has been incorporated in the iron sixth ligand position to account for the Raman data. A "front-side" model has also been proposed which postulates a μ-oxo bridging ligand (Blumberg and Peisach,

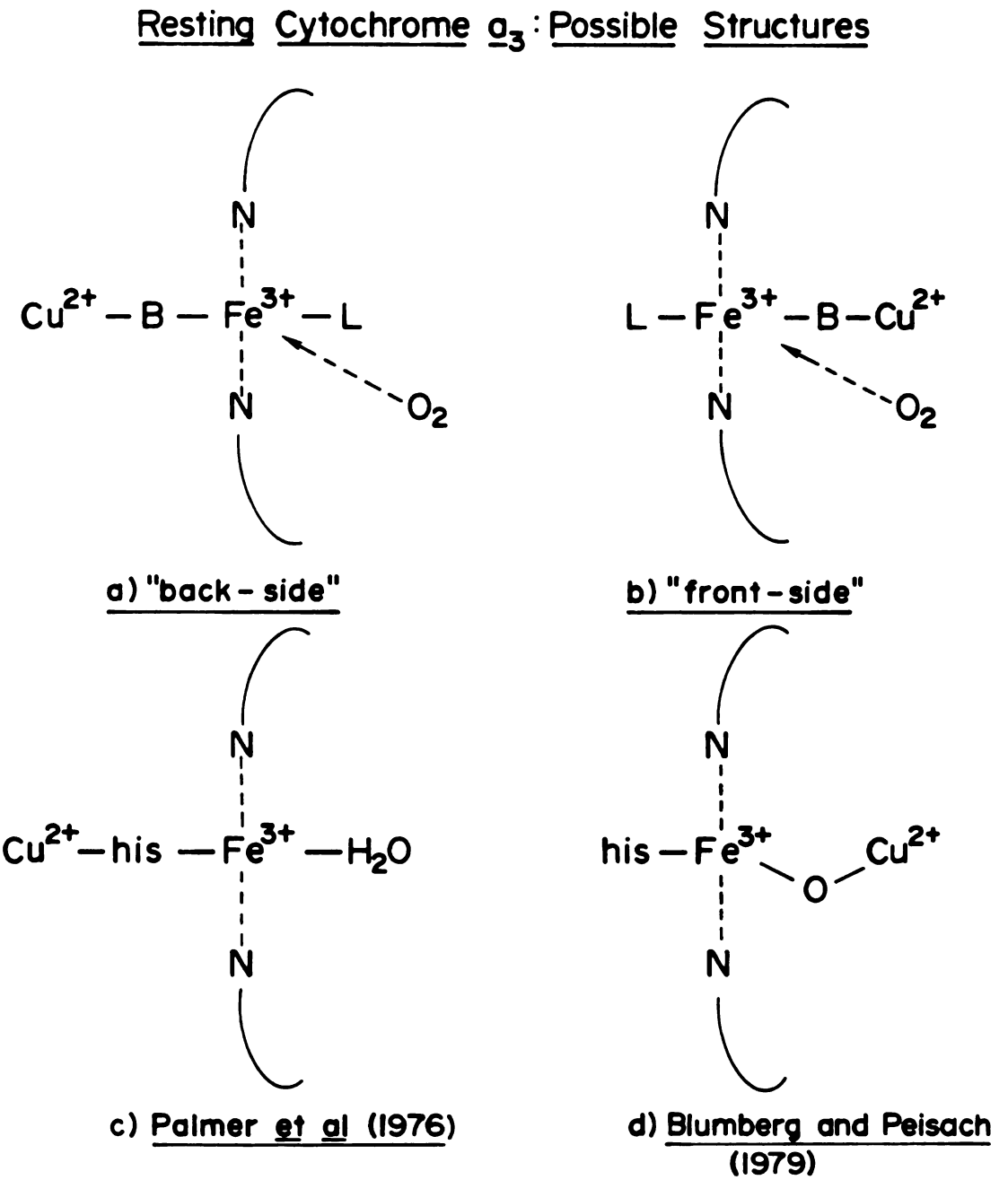

Figure 21. Possible structures for the cytochrome a_3 dioxygen reducing site.

1979) and is shown in Figure 21d; here a histidine residue is incorporated as the sixth ligand to maintain the iron in the six coordinate state.

Of these two structures, the "front-side" bridging model has received experimental support from the fact that: 1) imidazole bridging ligands are generally unable to support exchange coupling with magnitudes as large as those found in the enzyme ($|2J|>200$ cm^{-1}) (Kolks et al., 1976; Landrum, et al., 1978; Haddad and Hendrickson, 1978; Petty et al., 1980), whereas μ-oxo exchange couplings are well within this range (O'Keeffe et al., 1975) and 2) CO photolyzed from the a_3 heme has been shown to bind to the Cu_{a_3} site (Alben et al., 1981). These results support the "front-side" bridging model although μ-oxo ligand structures generally force the iron to adopt a five coordinate, out-of-plane geometry (O'Keeffe et al., 1975). Other ligands, particularly carbonate, have been proposed in lieu of the μ-oxo bridge (Seiter, 1978). Since the resting form of the enzyme is formed on a time scale slow with respect to the turnover of the enzyme, this structure may not be important in the catalytic process. Oxygenated cytochrome oxidase (Orii and King, 1976) which is formed on a much faster time scale may provide insight into the oxygen reduction mechanism.

The shoulder at the low frequency side of the 1590 cm^{-1} band in oxygenated cytochrome oxidase in Figure 20c has

been resolved in higher resolution studies to be a peak at 1574 cm^{-1}. This indicates a structure with approximately the same core size as $\underline{a}_3^{3+}$ in the resting enzyme. The dramatic reduction in intensity in the 1572-1574 cm^{-1} band between oxygenated and oxidized cyt $\underline{a}_3$ may be caused by a large decrease in the extinction coefficient of this heme. The Soret absorption maximum of this species shifts to 427 nm from ∿420 nm without an increase in intensity as is observed for the cyanide inhibited enzyme where cyt $\underline{a}_3$ is low-spin. Thus the absorption properties of the oxygenated enzyme seem to reflect predominantly the transition energies of cytochrome $\underline{a}$ with only a small contribution from cyt $\underline{a}_3$. A mixed-spin (S=3/2) species as suggested by Shaw *et al.*, 1978, and Woodruff *et al.*, 1982 may account for these observations.

In the reduced protein, only cytochrome $\underline{a}_3^{2+}$ is paramagnetic and occurs in the high-spin state. The MCD properties of this species are quite similar to those of deoxyhemoglobin and deoxymyoglobin (Babcock *et al.*, 1976) as are its ligand binding properties (Erecińska and Wilson, 1978). These observations suggest that $\underline{a}_3^{2+}$ is five coordinate in the reduced enzyme in the absence of an added ligand. This conclusion is consistent with previous Raman results which identified specific vibrations associated with $\underline{a}_3^{2+}$ (Salmeen *et al.*, 1978) including a vibration at 215 cm^{-1}. This mode has been assigned to the Fe-histidine

stretching mode by analogy to the 215 cm^{-1} vibration in deoxyhemeglobin and deoxymyoglobin (Nagai et al., 1980; Hori and Kitagawa, 1980).

An additional conclusion can be reached concerning the nature of the a_3 site from the Raman results presented here and in previous reports (Salmeen et al., 1978; Ondrias and Babcock, 1980; Babcock and Salmeen, 1979; VanSteelandt et al., 1981). In both the oxidized and reduced states of the enzyme the formyl vibration of a_3 is clearly enhanced and occurs at a frequency typical of a free, non-hydrogen bonded C=O. These observations indicate that the a_3 site, at least in the vicinity of pyrrole ring IV, is hydrophobic and that bulk H_2O is excluded.

3. Cytochrome a_3 Catalytic Model

This structural information concerning cytochrome a_3 can be combined and a speculative model for dioxygen reduction proposed. Figure 22 depicts a schematic of the a_3 oxygen reducing site. The resting form of the enzyme is shown in the upper left hand corner where the sixth ligand to cyt a_3, B, mediates the strong exchange coupling between cyt a_3 and Cu_{a_3}. Reduction of the enzyme results in the structure in the upper right corner where cyt a_3 is five coordinate and high-spin. It is this form, which is similar to the active site of hemoglobin, that binds oxygen (Figure 22, lower right). This enzyme-substrate complex, called

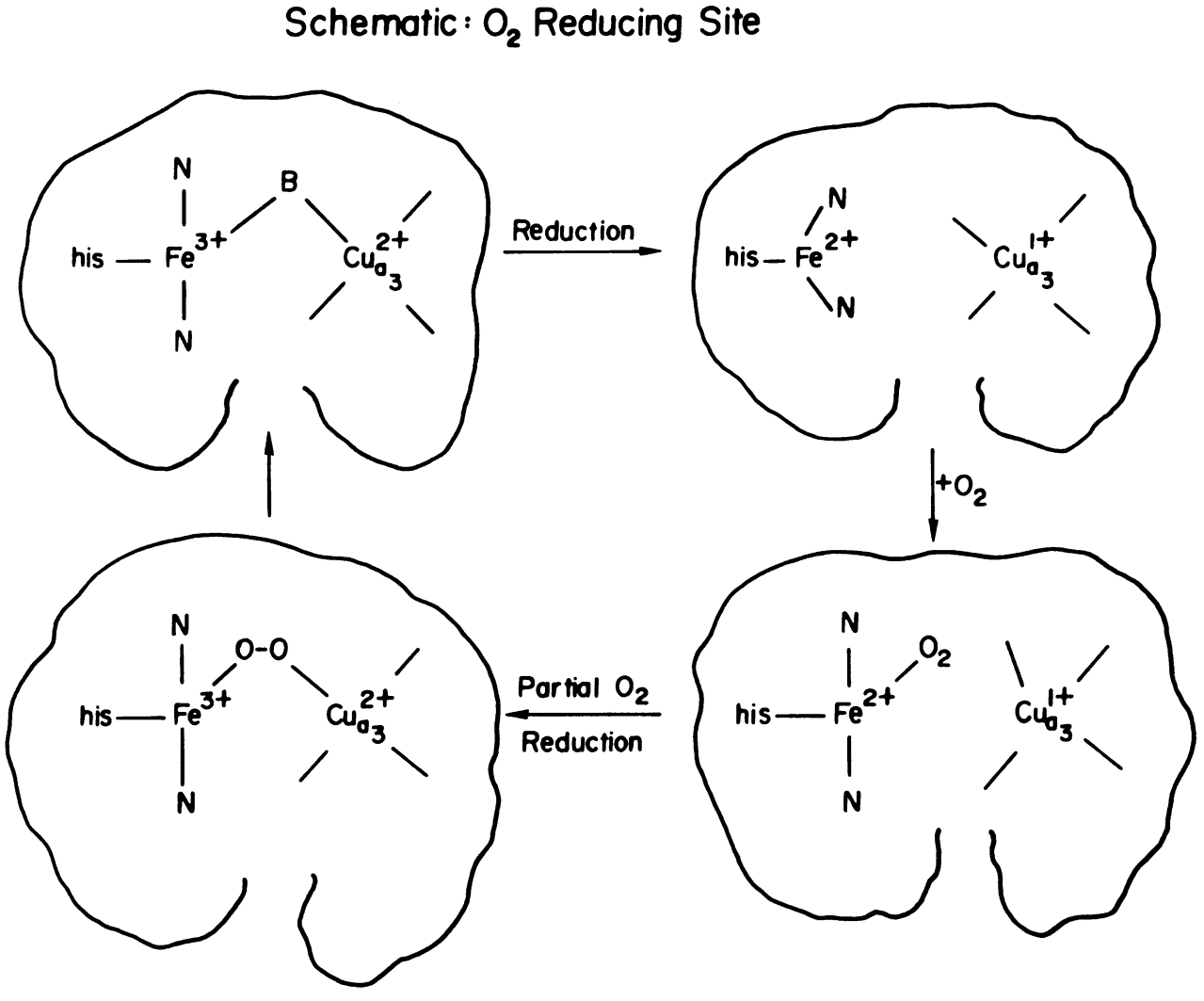

Figure 22. Schematic of the Cytochrome Oxidase oxygen reducing site.

Compound A (Chance et al., 1975) has been shown to be spectroscopically similar to $(NMeIm)_2$ heme $a^{2+} \cdot O_2$ (Babcock and Chang, 1979). Following partial O_2 reduction a μ-peroxy structure (lower left) has been postulated to be important in the catalytic cycle (Wikström et al., 1983). Further electron transfer, uptake of protons, and release of H_2O eventually leads to the resting structure (upper left). However, the details of the reaction mechanism, have not been established.

CHAPTER 5

THE ORIGIN OF THE CYTOCHROME A ABSORPTION RED-SHIFT

I. Introduction

The longer wavelength absorbance maxima of cytochrome oxidase relative to protoheme containing proteins results from its formyl-containing heme a chromophores (Figure 1). The individual contributions of cytochromes a and a_3 to the overall protein spectrum have been resolved by evidence from several laboratories (Wikström et al., 1976; Wilson, et al., 1978; Babcock and Salmeen, 1979; Scott and Gray, 1980; Halaka et al., 1981; Babcock et al., 1981; Woodruff et al., 1981) which support an independent chromophore model and indicate that the spectral deconvolution carried out by Vanneste (1966) provides reasonably accurate spectra of cytochromes a and a_3. By using the information described in the previous chapter on the coordination geometries of cytochromes a and a_3, it should be possible to prepare heme a model compounds which duplicate the optical properties of the in situ chromophores. The results of our efforts to accomplish this are summarized in Table 5 along with Vanneste's spectral data on cytochromes a and

Table 5. Absorption Maxima and Formyl Stretching Frequencies of Cytochromes a and a_3 with Corresponding Heme a Model Compounds.

Heme a Species	Solvent	Soret (nm)	α (nm)	ν(C=O) cm^{-1}
cytochrome a_3^{3+}		414[a]		1676[b]
heme a^{3+} $(DMSO)_2$[c]	CH_2Cl_2	410		1672
cytochrome a_3^{2+}		443[a]		1665[d]
heme a^{2+} (2MeIm)[e]	CH_2Cl_2	442		1660
	H_2O	434		1640
cytochrome a^{3+}		425[a]	595	1650[g]
heme a^{3+} $(NMeIm)_2$[c]	CH_2Cl_2	422	588	1670
	H_2O[h]	422	590	----
cytochrome a^{2+}		444[a]	604	1610[g]
heme a^{2+} $(NMeIm)_2$[e]	CH_2Cl_2	436[e]	588	1642
	H_2O	436[f]	594	1633[g]

From:

[a]Vanneste (1966); [b]Ondrias and Babcock (1980); [c]Callahan and Babcock (1981); [d]Salmeen et al. (1978) [e]Van-Steelandt-Frentrup et al. (1981); [f]Babcock et al. (1979b); [g]this work (see below); [h]Babcock et al. (1979a).

$\underline{a}_3$. Heme $\underline{a}$ model compounds of the appropriate spin, coordination, oxidation state and solvent environment reproduce well the spectral properties of the high-spin species, cytochrome $\underline{a}_3$. Discrepancies arise, however, in the comparison of cytochrome $\underline{a}$ and low-spin heme $\underline{a}$. The deconvoluted α band and Soret maxima of ferric and ferrous cytochrome $\underline{a}$ are considerably red-shifted relative to oxidized and reduced bis-N-methylimidazole heme $\underline{a}$, which by EPR standards, is an appropriate cytochrome $\underline{a}$ model (Blumberg and Peisach, 1979; Babcock *et al.*, 1979). Moreover, the model compound spectra are only slightly sensitive to solvent and thus, the unusual red-shift of cytochrome $\underline{a}$, which was originally noted by Lemberg (1962), may involve a fairly complex chromophore/protein interaction.

A second anomalous spectral characteristic of cytochrome $\underline{a}$ is apparent when the vibrational properties of its peripheral formyl group are compared with those of cytochrome $\underline{a}_3$, and their respective model compounds (Babcock and Salmeen 1979; Babcock *et al.*, 1981). For high-spin cytochrome $\underline{a}_3$, the same heme $\underline{a}$ models which reproduce the optical properties also mimic the formyl stretching frequency (Table 5), thus indicating that the position 8 aldehyde is free in a hydrophobic environment (VanSteelandt-Frentrup et al., 1981). On the other hand, the characteristic formyl vibration stretching frequencies observed for low-spin ferric and ferrous heme $\underline{a}$ model compounds are not apparent in the resonance Raman spectra of the

enzyme (Table 5).

Thus the Raman data suggest a protein-induced alteration of the heme a formyl group in the cytochrome a binding site which, in turn, may be linked to the absorption red-shift commented upon above. Such protein-chromophore interactions have been shown to be responsible for in vivo versus in vitro spectral differences in other protein systems. For example, both the absorption red-shift and vibrational properties of retinal in rhodopsin and bacteriorhodopsin have been accounted for to first order by the presence of a protonated Schiff base linkage between a lysine residue of the protein and the retinal aldehyde (Aton et al., 1977; Mathies et al., 1977; Marcus et al., 1979). Point charges in the vicinity of the chromophore have been advanced to explain further spectral differences (Honig et al., 1979; Sheves et al., 1979). Similarly, in photosynthetic systems, shifts in chlorophyll absorption spectra relative to model compounds have been attributed, in part, to perturbations induced by the protein environment (Davis, et al., 1981). Finally, spectral differences between various formylated hemes when incorporated into apomyoglobin have been attributed to differences in local protein environments (Tsubaki et al., 1980).

Insight into such a protein-chromophore interaction in cytochrome oxidase can be obtained from data reported by Lemberg (1964) which showed that upon alkalinization

of cytochrome oxidase solutions the spectrum of the reduced enzyme shifts to shorter wavelength in two distinct steps. In the first, the absorption maxima move to (Soret, α) (436 nm, 596 nm) followed by a further blue shift to (428 nm, 575 nm). The latter species is clearly established as the Schiff's base adduct of the heme a aldehyde which is stable at pH levels greater than 12 (Lemberg, 1964, Takemori and King, 1965). The basis of the initial absorption spectral shift to yield Soret and α maxima typical of low-spin ferrous heme a in an aqueous environment was attributed to an unspecified conformational change of the protein. This work was extended in Soret excitation resonance Raman experiments by Salmeen et al. (1978) who observed several changes in vibrational frequencies as the pH was raised and noted that the species absorbing at (436 nm, 595 nm), formed at pH 11.5, gives rise to a spectrum that is similar to the resonance Raman spectrum of heme $a^{2+}(Im)_2$ in aqueous detergent solution.

These pH induced effects on the optical properties of cytochrome oxidase have been reinvestigated by using resonance Raman, MCD and EPR spectroscopies as probes to understand the anomalous spectral features of cytochrome a. The magnetic techniques are useful in that changes in heme a spin state may be monitored. Resonance Raman spectroscopy provides similar information of coordination geometries through analysis of the structure sensitive vibrations of the porphyrin macrocycle (Callahan and

Babcock, 1981). Moreover, Raman detection of the formyl stretching vibration provides additional insight into the chromophore because this mode is sensitive to solvent effects, covalent interactions and hydrogen bonding effects. By using this approach, we have been able to detect and assign the cytochrome a formyl stretching vibration. The combination of red-shifted absorption spectrum and altered formyl vibration is interpreted as arising from a pH dependent hydrogen bonding interaction between a protein residue, possibly tyrosine, and the cytochrome a formyl group.

II. pH Dependent Spectral Shifts

A. Oxidized Cytochrome Oxidase

For oxidized cytochrome oxidase, the pH dependence of the resonance Raman spectrum is shown in Figure 23 and of the visible absorption spectrum in Figure 24. At pH 7.4, the high frequency vibrations of cytochrome a^{3+} occur at 1650, 1641, 1590, 1506, 1474 and 1373 cm^{-1} and those of cytochrome a_3^{3+} are observed at 1676, 1615, 1572, 1477 and 1373 cm^{-1} (Babcock et al., 1981). At pH 11 vibrational band shifts are observed as follows: (a) a decrease in intensity of the cytochrome a_3^{3+} 1572 cm^{-1} band, (b) increases in intensity at 1590 and 1641 cm^{-1} and (c) a decrease in intensity and frequency shift in the a_3 formyl

Figure 23. Resonance Raman spectra of oxidized cytochrome oxidase at several pH levels obtained with 413.1 nm excitation. Enzyme concentration was approximately 30-50 μM (heme a basis). Instrumental conditions: resolution, 6 cm^{-1}; time constant 1s, scan rate 50 cm^{-1}/min.

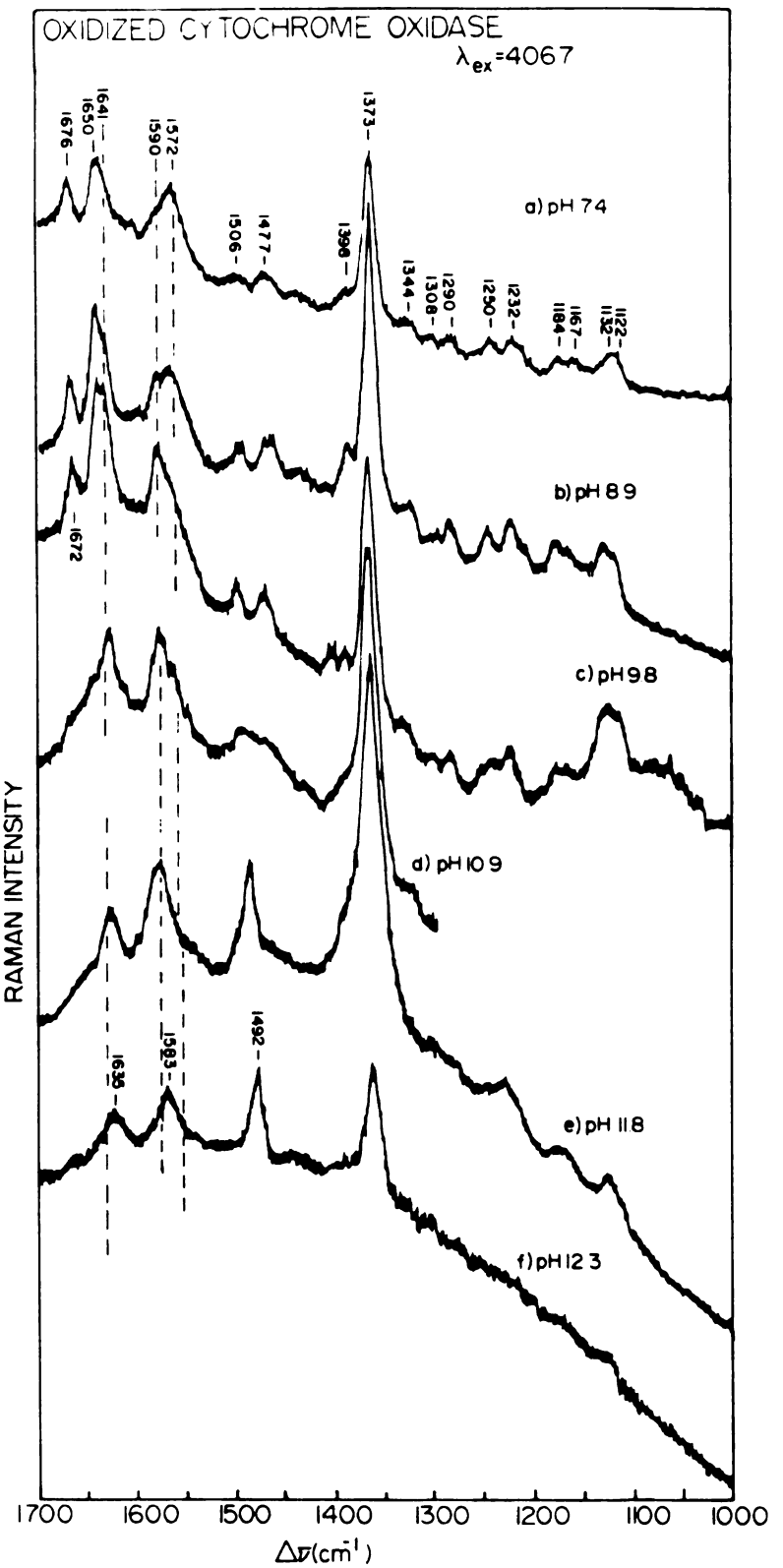
OXIDIZED CYTOCHROME OXIDASE
λ_{ex}=4067
1676
1650
1641
1590
1572
1506
1477
1373
1344
1308
1290
1250
1232
1184
1167
1132
1122
a) pH 7.4
b) pH 8.9
1672
c) pH 9.8
d) pH 10.9
1636
1583
1492
e) pH 11.8
f) pH 12.3
RAMAN INTENSITY
1700
1600
1500
1400
1300
1200
1100
1000
$\Delta\bar{\nu}$(cm^{-1})

Figure 23

Figure 24. Optical absorption spectra of oxidized cytochrome oxidase at several alkaline pH levels. Enzyme concentration was approximately 10-15 μM (heme a basis) for all samples.

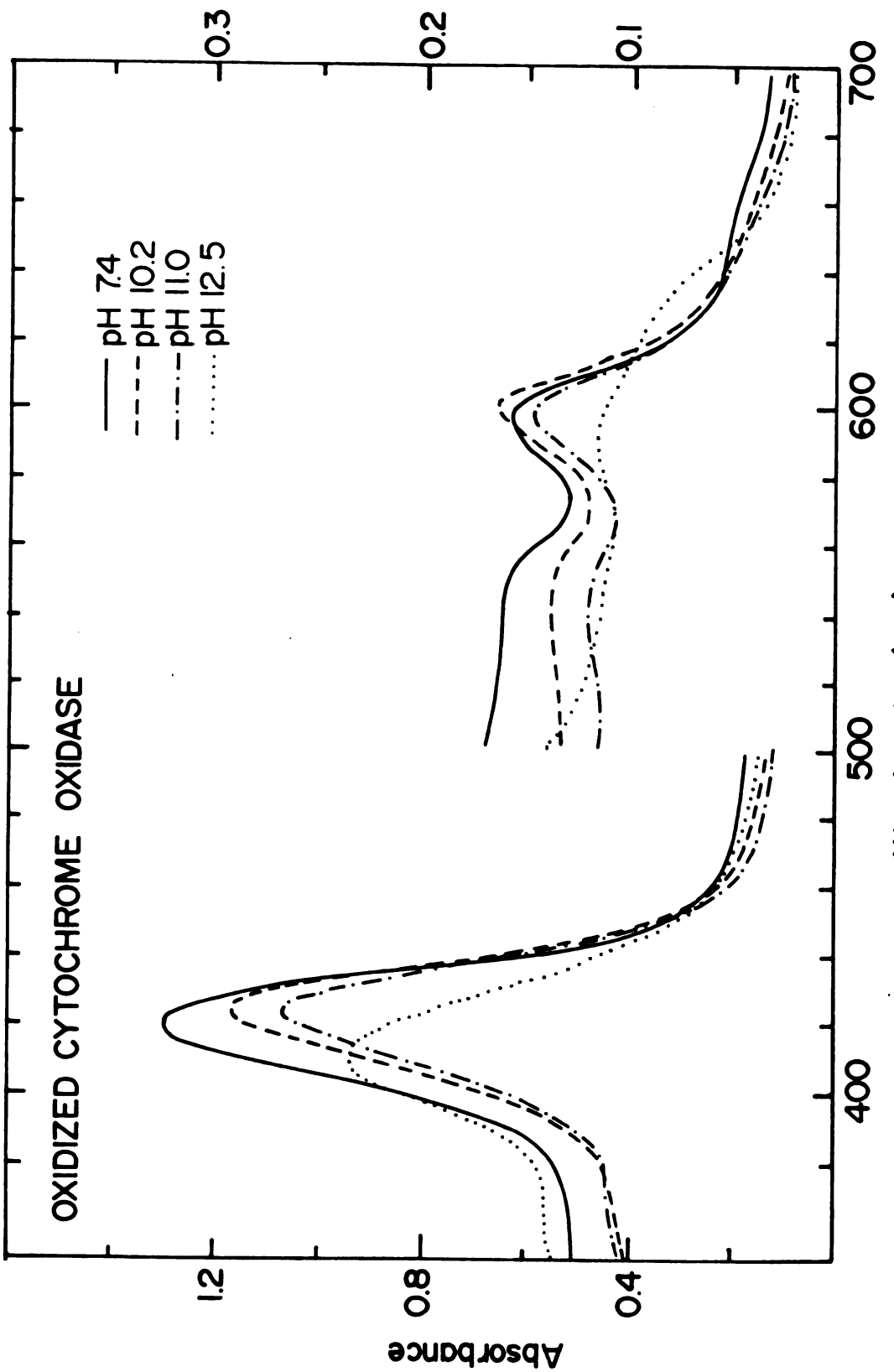
OXIDIZED CYTOCHROME OXIDASE
pH 7.4
pH 10.2
pH 11.0
pH 12.5
Absorbance
1.2
0.8
0.4
0.3
0.2
0.1
400
500
600
700
Wavelength (nm)

Figure 24

vibration from 1676 cm^{-1} to 1673 cm^{-1}. The changes that occur in the optical absorption spectrum in this pH range (Figure 24) are (a) decreased absorbance at 655 nm, (b) increased absorbance at 600 nm and (c) a red-shift in the Soret maximum from 420 nm to 425 nm. The apparent mid-point for this shift is ∿9.5. These changes are consistent with a high to low-spin transition of the cytochrome $\underline{a}_3$ chromophore as the pH is increased. The core-size marker vibrations of a six coordinate high-spin heme $\underline{a}$ model at 1572 and 1615 cm^{-1} disappear and are replaced by increased intensity in the corresponding modes of a six coordinate, low-spin heme $\underline{a}$ species at 1590 and 1641 cm^{-1} (Callahan and Babcock, 1981). The shift in the cytochrome $\underline{a}_3^{3+}$ formyl vibration from 1676 cm^{-1} to 1673 cm^{-1} and the optical absorption spectral shifts are also indicative of increased low-spin character at alkaline pH (Callahan and Babcock, 1981; see below). EPR spectra of a similar series of enzyme samples (data not shown) taken under low power (2 mW), low temperature (10K) conditions show a low-spin heme absorption in the pH range 8.5-10.8 with g values of 2.58, 2.3 and 1.80, indicative of the low-spin hydroxide form of heme $\underline{a}^{3+}$ (Wever *et al.*, 1977). The spin concentration represented by this signal increases with increasing pH up to 10 and subsequently decreases as the pH is increased further. Even at maximum intensity, however, it represents considerably less than one heme per cytochrome

oxidase. Similar behavior in the EPR spectrum was observed at moderately alkaline pH by Hartzell and Beinert (1974). No observable changes in the Raman intensity of the anomalous cytochrome $\underline{a}^{3+}$ vibration at 1650 cm^{-1} occur in this pH range; only under strongly denaturing conditions is this vibration affected.

At very high pH (>12), the Soret is broadened and blue-shifted to 413 nm. The visible region shows no distinct maxima although there is an increased absorbance at 635 nm. The major vibrational frequencies observed at pH 12 for the oxidized enzyme are 1635, 1583, 1492 and 1373 cm^{-1}. These band positions are similar to those observed for five coordinate, high-spin heme $\underline{a}^{3+}$ (Callahan and Babcock, 1981). Electron paramagnetic resonance spectra of alkaline pH enzyme samples result in a gradual decrease and disappearance in the low-spin cytochrome $\underline{a}^{3+}$ resonance at g=3, with an apparent pK in the range 10-10.5, in agreement with the RR observations which show the absence of any low-spin species at pH 12. Although the Raman and optical absorption spectra at pH 12 suggest five coordinate high-spin heme $\underline{a}^{3+}$ species, no high-spin EPR signal is observed at alkaline pH. This suggests severe protein denaturation in this pH range with release and subsequent aggregate, possibly μ-oxo dimer, formation by the free heme $\underline{a}$ chromophores. Supporting evidence for this configuration of the heme $\underline{a}$ chromophores lies in the

similarity of the optical absorption properties of oxidized cytochrome oxidase at pH 12 and the previously reported data for heme a μ-oxo dimers (Caughey et al., 1975).

B. Reduced Cytochrome Oxidase

Reduced cytochrome oxidase also shows a series of absorption shifts as the pH of the medium is raised (Figure 25). The Soret and α maxima gradually shift from (Soret, α), (443 nm, 604 nm) at pH 7.4 to (436 nm, 595 nm) at pH 11.5 (Table 6). In the Soret region, cytochromes a and a_3 make roughly equal contributions to the absorption at neutral pH (Vanneste, 1966). In the α band region, however, cytochrome a^{2+} is the dominant absorber. Thus, the shift of the oxidase α maximum from 604 nm to 596 nm as the pH of the reduced enzyme is raised implies that cytochrome a is being perturbed, as noted originally by Lemberg and Pilger (1964). The pH dependence of the half bandwidth at half-height of the visible absorption band is shown in Figure 27. This titration curve has a pK of approximately 10.5. The half-bandwidths of ferrous low-spin heme a model compounds vary with solvent from approximately 300 cm^{-1} in non-polar solvent to 500 cm^{-1} in an aqueous environment (Babcock et al., 1979). Similarly, the two extremes of the titration curve correspond to half-bandwidths of approximately 300 to 500 cm^{-1} for the α band of cytochrome oxidase at neutral and alkaline pH. This observation

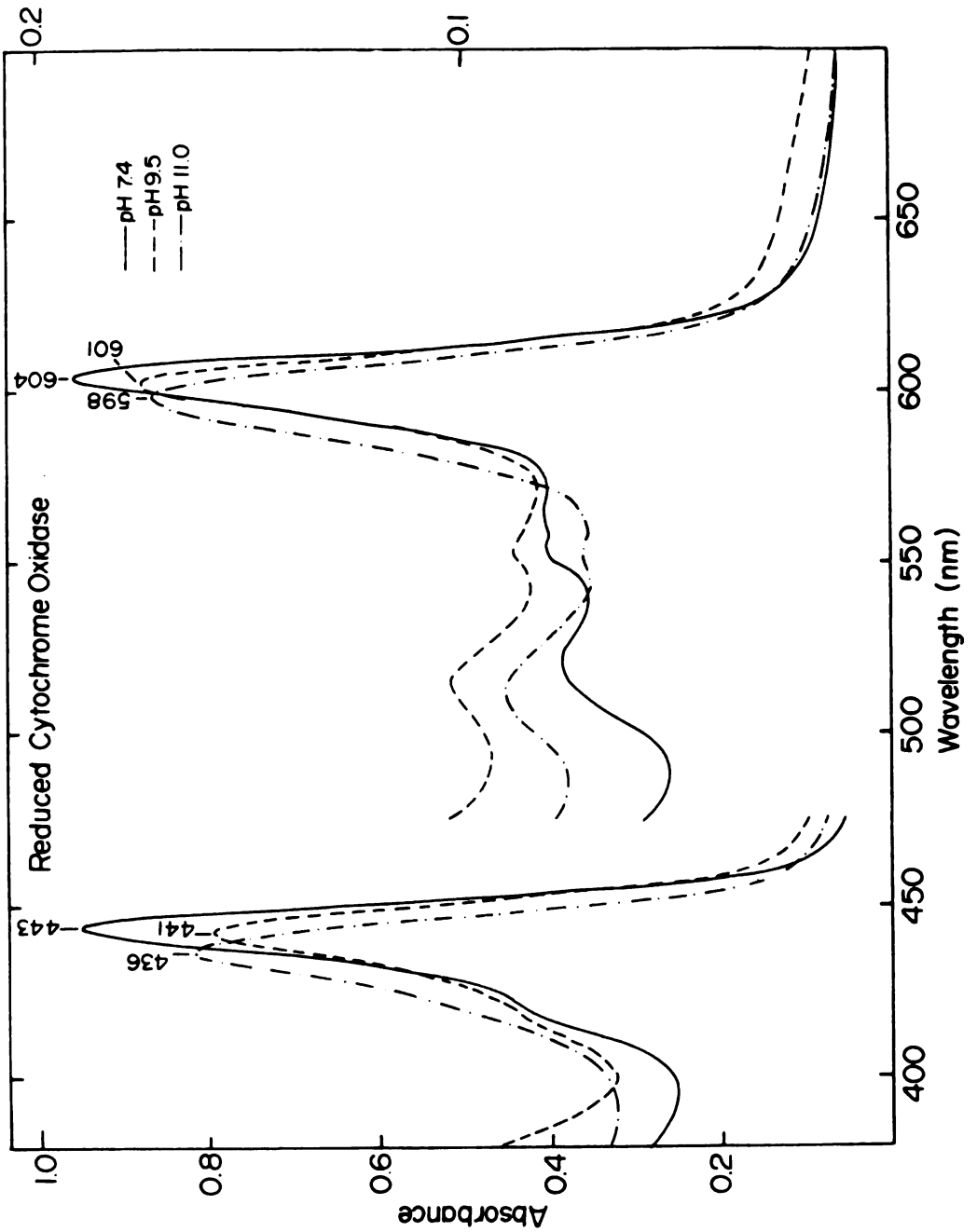

Figure 25. Optical absorption spectra of reduced cytochrome oxidase at several pH levels. Enzyme concentrations are approximately 6-8 μM.

Table 6. Absorption Maxima and Individual Chromophore Formyl Vibrational Assignments of Reduced Cytochrome Oxidase at Neutral and Alkaline pH.

pH	Soret (nm)	α (nm)	$\nu(C=O)\underline{a}_3^{2+}$ (cm^{-1})	$\nu(C=O)\underline{a}^{2+}$ (cm^{-1})
7.4	443	604	1665	1610
9.5	441	601	1633	1610
11.5	436	596	1633	1633
12.5	428	575	----	----

suggests that a solvent environment change occurs at the low-spin heme chromophore, cytochrome $\underline{a}^{2+}$ as the pH is increased. Because of the overlapping absorption spectra of the oxidase heme $\underline{a}$ chromophores and because alkaline modification of cytochrome $\underline{a}^{2+}$ was suspected as well (Salmeen et al., 1978), three other spectroscopic probes have been used to identify more conclusively the shifts arising from the individual heme centers.

The MCD spectrum of reduced cytochrome oxidase has distinct contributions from cytochromes $\underline{a}^{2+}$ and $\underline{a}_3^{2+}$, thus offering a probe of the structural changes which occur at each of the individual chromophores at alkaline pH. An intense ($\Delta\varepsilon/T$ = 79.3 $(M\cdot cm\cdot T)^{-1}$ at 446.7 nm) asymmetric A- and C- term MCD spectrum is observed for the native enzyme (Figure 26), which arises mainly from high-spin cytochrome $\underline{a}_3^{2+}$ (Babcock et al., 1978). Spectra obtained for low-spin species, cytochrome $\underline{a}^{2+}$ and heme $\underline{a}^{2+}(NMeIm)_2$ are less intense ($\Delta\varepsilon/T$ = 35.0 and 27 $(M\cdot cm\cdot T)^{-1}$ at 452 nm, respectively) and more symmetric (Babcock et al., 1979). In addition to the MCD intensity differences, the various coordination and spin-states of cytochromes $\underline{a}^{2+}$ and $\underline{a}_3^{2+}$ and isolated heme $\underline{a}$ complexes have characteristic Soret region trough/peak ratios: cytochrome $\underline{a}_3^{2+}$, 0.5; high-spin heme $\underline{a}^{2+}$ in ethylene glycol, 0.5; cytochrome $\underline{a}^{2+}$, 0.75; and low-spin heme $\underline{a}^{2+}(NMeIm)_2$, 1.0. These features can be used to monitor the properties of cytochromes $\underline{a}$ and $\underline{a}_3$

Figure 26. MCD spectra of reduced cytochrome oxidase at pH 7.4 and 11.5. Enzyme concentration of enzyme is 10 μM.

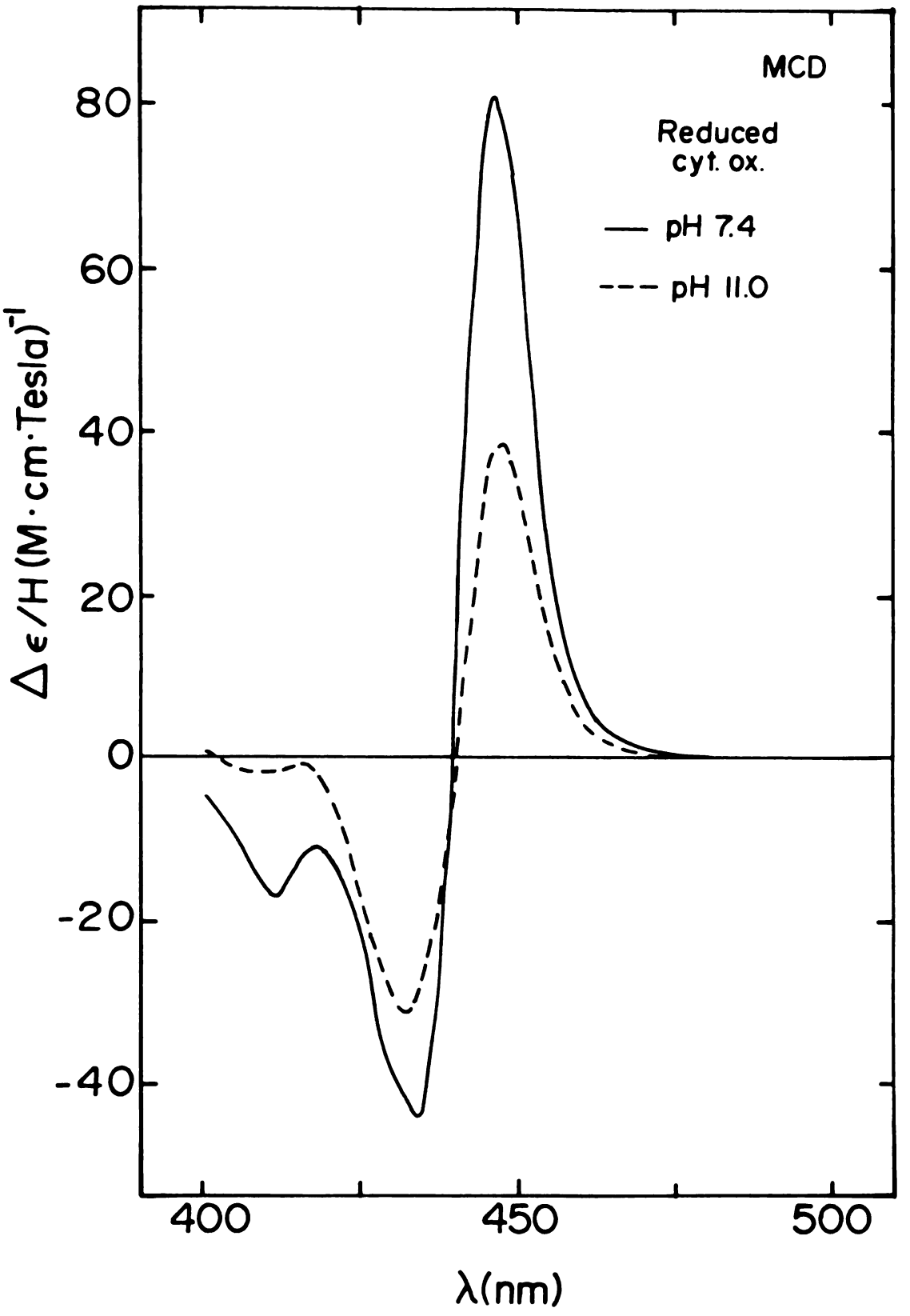
MCD
Reduced
cyt. ox.
pH 7.4
pH 11.0
80
60
40
20
0
-20
-40
400
450
500
λ(nm)
Δε/H (M·cm·Tesla)⁻¹

Figure 26

as the pH is changed. Figure 26 reproduces MCD spectra of reduced cytochrome oxidase at neutral and at alkaline pH. The variation of the Soret MCD trough/peak ratio versus pH is summarized for the reduced enzyme in Figure 27. The initial value of 0.5 increases gradually to a value of 0.7 in the pH range 9.5-10. This MCD ratio of 0.7 and the absorption spectrum of reduced cytochrome oxidase at pH 10 are similar to the spectral properties obtained for the fully reduced enzyme plus cyanide (Babcock *et al.*, 1976). The minor absorption band in the reduced enzyme optical spectrum at 565 nm, which is absent in inhibitor complexes that convert cytochrome $\underline{a}_3$ to a low-spin species (HCN, CO), is also absent at pH 10 (Figure 25). These two pieces of data suggest that cytochrome $\underline{a}_3^{2+}$ undergoes a high- to low-spin transition in the pH range 8.5-11.5. The trough/peak ratio further increases to a value of 1.0 at pH 11.5. This pH dependent step is responsible for the shift from a trough/peak ratio characteristic of cytochrome $\underline{a}^{2+}$ (0.7) to a ratio typical of a low-spin heme $\underline{a}^{2+}$ model compound (1.0). This final species also has absorption maxima corresponding to those of isolated low-spin heme *a* (Soret, α), (436 nm, 596 nm), respectively. Further increases in this MCD parameter at strongly alkaline pH's ($\sim$12) can be attributed to Schiff's base formation at the hemes *a* aldehydes as determined by the characteristic α band absorption maximum of 575 nm.

Figure 27. Titration curves as a function of pH for several spectral parameters of reduced cytochrome oxidase. Open circles are normalized α band half-widths at half height. The solid line is that calculated for pK = 10.5. Filled circles represent data points of MCD trough/peak (436/446.7 nm) ratio. Open triangles represent the normalized intensity ratio of $\nu(C{=}O)/\nu_4$; the solid line is that calculated for pK = 9.3.

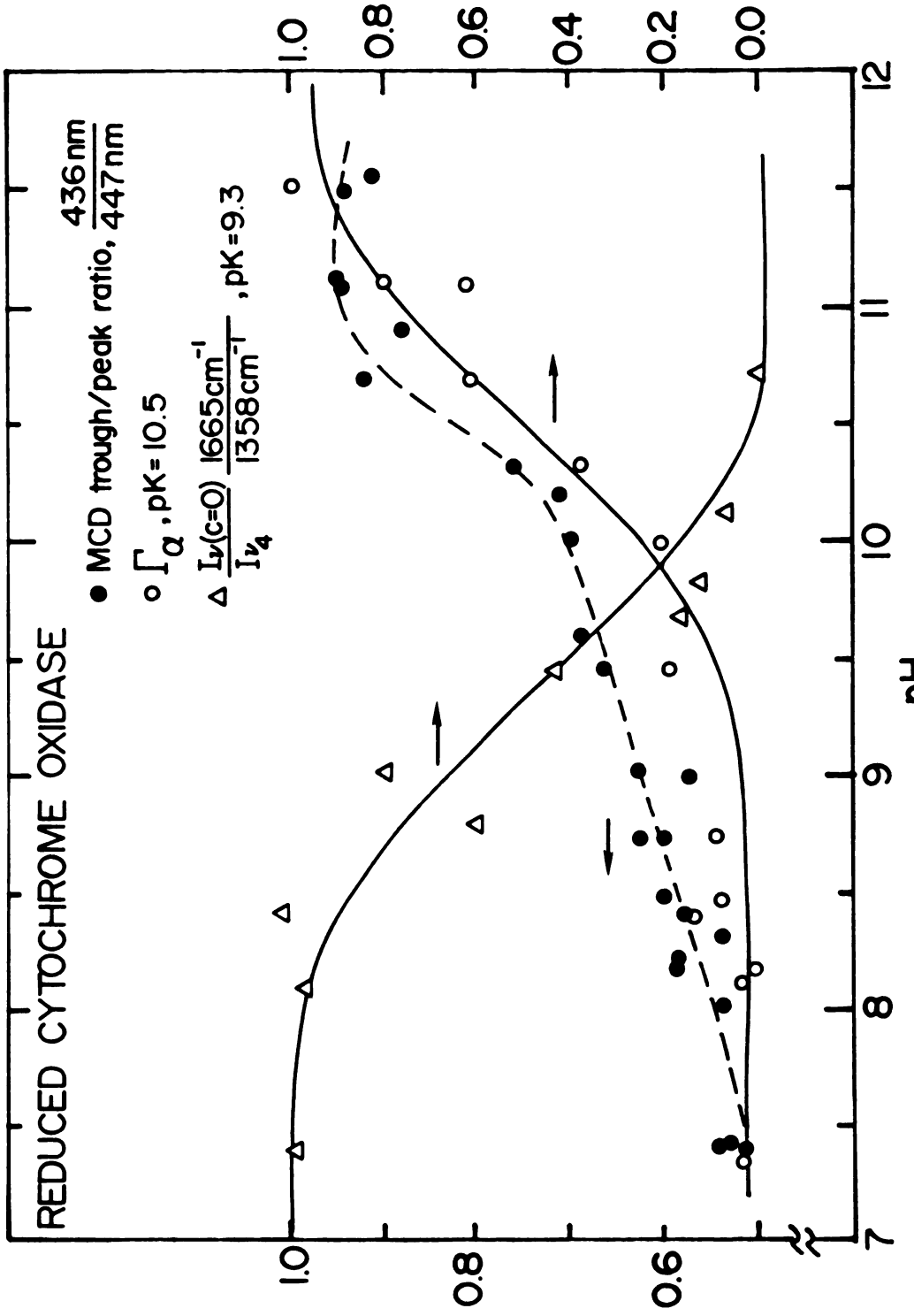
REDUCED CYTOCHROME OXIDASE
● MCD trough/peak ratio, 436nm/447nm
○ ∫α, pK= 10.5
Δ Iν(c=0) 1665cm⁻¹ / Iν4 1358cm⁻¹, pK=9.3
1.0
0.8
0.6
0.4
0.2
0.0
7
8
9
10
11
12
pH

Figure 27

Attempts to calculate a titration curve of the MCD trough/peak ratio from contributions of the individual chromophores were unsuccessful in mimicking the observed results. This may be a reflection of the heterogeneity of sites (Brudvig et al., 1981) or of the time dependence of the alkaline pH effects (Lemberg and Pilger, 1964).

Visible excitation resonance Raman spectroscopy provides a second probe and a more exact separation of the cytochrome $\underline{a}^{2+}$ and $\underline{a}_3^{2+}$ pH dependent spectral shifts owing to the selective enhancement of the vibrations of one chromophore over the other. Figure 28 shows the resonance Raman spectra of reduced cytochrome oxidase and its partially reduced inhibitor complexes (Figure 28a, b and c) obtained with α band excitation at 605 nm. The Raman spectra are similar regardless as to whether cytochrome $\underline{a}_3$ is ferrous, five coordinate and high-spin (Figure 28a) or ferric, six coordinate and low-spin (Figure 28b) or high-spin (Figure 28c) (Bocian et al., 1979). Because of the well documented dependence of resonance Raman band position and intensity upon heme coordination geometry and extinction coefficient in the Herzberg-Teller scattering region (Spaulding et al., 1975; Spiro, et al., 1979) we would expect these alterations in cytochrome $\underline{a}_3$ spin and valence states to be reflected by shifts in the Raman spectrum if it were a strong absorber in the α band region. However, the visible excitation resonance Raman spectra of Figure 28 are essentially identical, independent of

Figure 28. Visible excitation resonance Raman spectra of reduced cytochrome oxidase a), and partially reduced inhibitor complexes b) and c). The spectrum in c) was obtained with a flowing sample arrangement. Enzyme concentration was approximately 200 μM. The sample conditions in d) are ∿200 μM heme a, 0.5 M 2-methylimidazole, in 0.07 M CTAB, 0.1 M sodium phosphate, 0.001 M EDTA, pH 7.4, with sodium dithionite as reductant. Instrumental conditions: resolution 5 cm^{-1}; a)-c) time constant 1s, scan rate 50 cm^{-1}/min; conditions in d) time constant 2.5 s, scan rate 20 cm^{-1}/min.

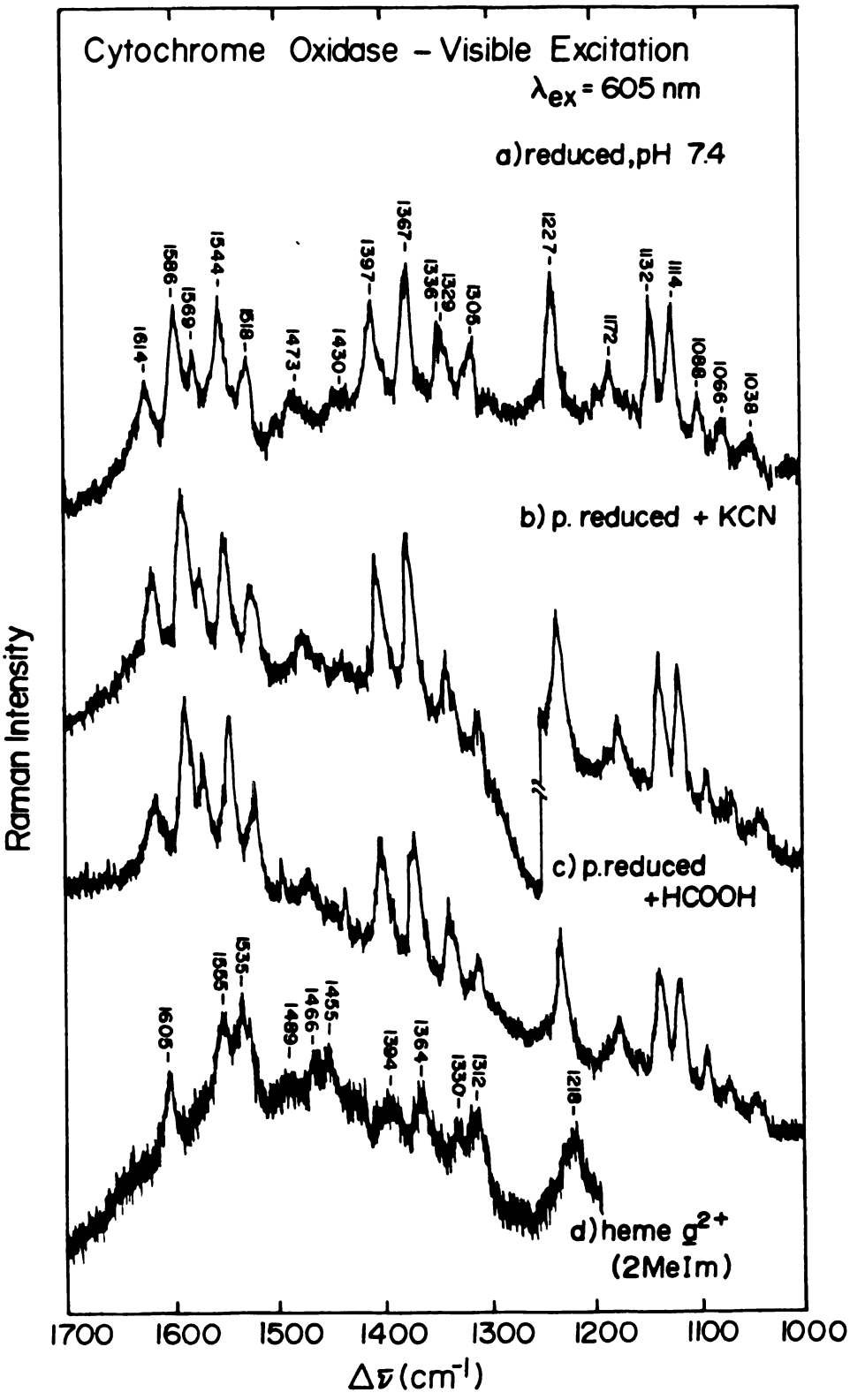
Cytochrome Oxidase – Visible Excitation
λ_{ex} = 605 nm
a) reduced, pH 7.4
1614
1586
1569
1544
1518
1473
1430
1397
1367
1336
1329
1306
1227
1172
1132
1114
1088
1066
1038
b) p. reduced + KCN
c) p. reduced +HCOOH
1605
1585
1535
1499
1466
1455
1394
1364
1330
1312
1218
d) heme g^{2+} (2MeIm)
Raman Intensity
1700
1600
1500
1400
1300
1200
1100
1000
$\Delta\bar{\nu}$ (cm^{-1})

Figure 28

oxidation, coordination or spin-state of cytochrome $\underline{a}_3$, and therefore we attribute the vibrations observed to cytochrome $\underline{a}$ and make the corollary conclusion that it is the dominant absorber in this region. Furthermore, the prominent vibrations of heme $\underline{a}^{2+}$ (2MeIm), (Figure 28d) at 1533, 1555 and 1605 cm^{-1}, a model for the coordination and spin-state of cytochrome $\underline{a}_3^{2+}$ (VanSteelandt *et al.*, 1981), are not observed in the RR spectra of reduced cytochrome oxidase; thereby providing additional evidence that vibrations of cytochrome $\underline{a}^{2+}$ alone are observed under these conditions. Visible excitation Raman spectra, then, can be used to monitor the pH dependence of a single heme chromophore, cytochrome $\underline{a}^{2+}$. Resonance Raman spectra obtained with visible excitation of reduced cytochrome oxidase at several pH levels are shown in Figure 29. The changes observed are (a) a reduction in intensity of the 1569 cm^{-1} and 1329 cm^{-1} bands and (b) a decrease in intensity and shift in frequency of the 1114 cm^{-1} vibration to 1109 cm^{-1}. These pH effects titrate over the pH 10-11.5 range. Since the vibrations observed with visible excitation of the reduced enzyme at neutral pH arise solely from cytochrome $\underline{a}^{2+}$ and noting the fact that no new vibrations are observed with visible excitation at alkaline pH, this suggests that the spectral shifts occurring with a pK $\sim$ 10.5 arise from a pH dependent modification of cytochrome $\underline{a}^{2+}$.

Figure 29. Visible excitation resonance Raman spectra of reduced cytochrome oxidase at several pH levels, with excitation wavelength as noted in the figure. Enzyme concentration was 200-300 μM (heme a basis). Instrumental conditions: resolution 5 cm^{-1}, time constant 2.5 s, scan rate 20 cm^{-1}/min.

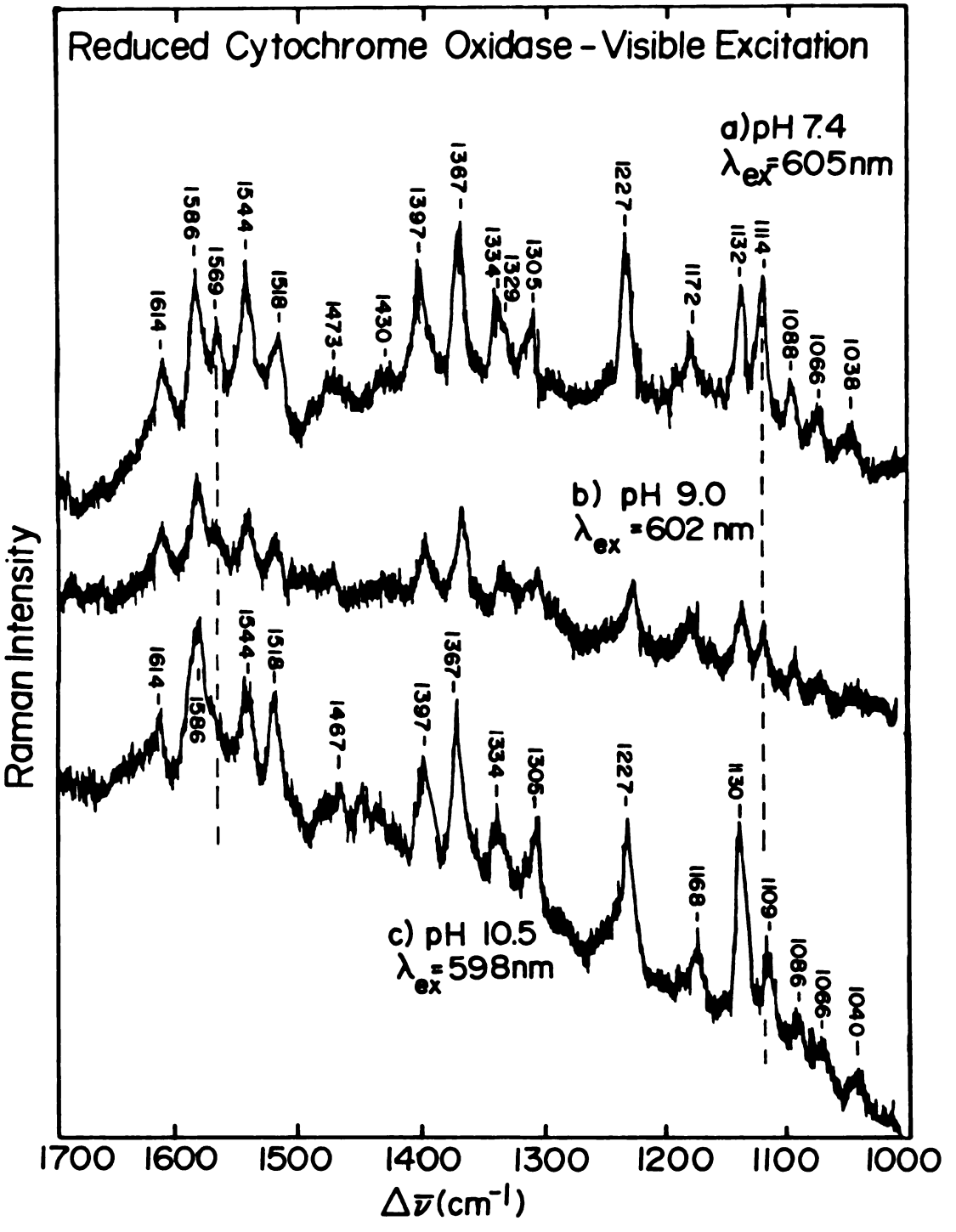
Reduced Cytochrome Oxidase - Visible Excitation
a) pH 7.4
λex=605nm
1614
1586
1569
1544
1518
1473
1430
1397
1367
1334
1329
1305
1227
1172
1132
1114
1088
1066
1038
b) pH 9.0
λex=602 nm
1614
1586
1544
1518
1467
1397
1367
1334
1306
1227
1168
1130
1109
1086
1066
1040
c) pH 10.5
λex=598nm
Raman Intensity
1700
1600
1500
1400
1300
1200
1100
1000
Δν̄(cm⁻¹)

Figure 29

To document the pH dependencies of the two heme centers further, Soret excitation resonance Raman spectroscopy has been employed as a third technique. The selective enhancement of the vibrations of a single chromophore by proper choice of excitation frequency for the partially reduced inhibitor complexes of cytochrome oxidase is not feasible at alkaline pH because of the unfavorable pH values of HCN and HCOOH. For this reason, we are limited to the study of the fully reduced enzyme. Although complicated by the fact that vibrations of both chromophores are enhanced, Soret excitation resonance Raman spectra can yield significant structural information. The Soret resonance Raman spectra of reduced cytochrome oxidase at several alkaline pH levels are shown in Figure 30. At pH 7.4, with excitation at 406.7 nm, the characteristic vibrations of cytochrome $\underline{a}^{2+}$ at 1622, 1610, 1586, 1569, 1520 and 1358 cm^{-1} and of cytochrome $\underline{a}_3^{2+}$ at 1665, 1610, 1569 and 1358 cm^{-1} are observed (Table 7). The changes that occur as the pH is raised to 9.5 are (a) decreases in intensity at 1665, 1610 and 1115 cm^{-1}, (b) an increase in intensity at 1633 cm^{-1} and (c) a shift in intensities in the 1220-1250 cm^{-1} region. Since the formyl stretching vibration of cytochrome $\underline{a}_3^{2+}$ at 1665 cm^{-1} is well separated from the other ring vibrations, its intensity ratioed to the intensity of ν_4 at 1358 cm^{-1} establishes a titration curve for the pH dependent changes

Figure 30. Soret excitation resonance Raman spectra of reduced cytochrome oxidase at neutral and alkaline pH (a-e). Enzyme concentration was approximately 40 μM. Sample conditions in f) are ~50 μM heme a, 0.7 M N-methyl imidazole, 0.07 M CTAB, 0.001 M EDTA, 0.1 M sodium phosphate, pH 7.4. Instrumental conditions: resolution 6 cm^{-1}; a)-e) time constant 2.5 s, scan rate 20 cm^{-1}/min; f) time constant 1s, scan rate 50 cm^{-1}/min.

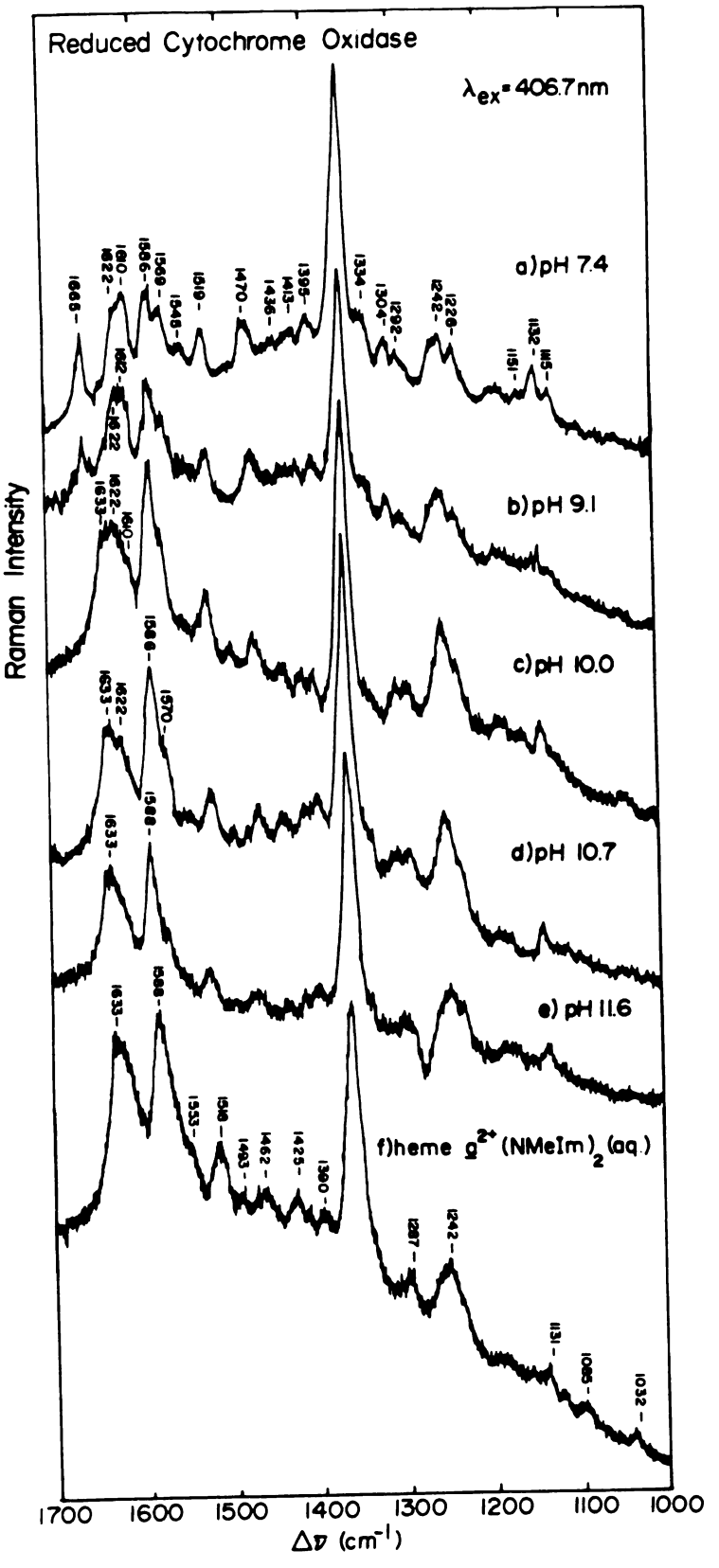
Reduced Cytochrome Oxidase
λex=406.7nm
a)pH 7.4
b)pH 9.1
c)pH 10.0
d)pH 10.7
e) pH 11.6
f)heme g2+ (NMeIm)2 (aq.)
Raman Intensity
1700
1600
1500
1400
1300
1200
1100
1000
Δν (cm-1)

Figure 30

Table 7. Reduced Cytochrome Oxidase Soret Excitation Heme Chromophore Vibrational Assignments.[a]

------cytochrome $\underline{a}^{2+}$------		------cytochrome $\underline{a}_3^{2+}$------	
$\Delta\bar{\nu}$ (cm^{-1})	Assignment (#)	$\Delta\bar{\nu}$ (cm^{-1})	Assignment (#)
		1665	ν(C=O)
1622	B_{1g}, ν_{10}	1610	B_{1g}, ν_{10}
1610	H-bonded ν(C=O)		
1586	A_{1g}, ν_2	1575	A_{1g}, ν_2
1569	B_{1g}, ν_{11} or E_u, ν_{38}[b]	1565	B_{1g}, ν_{11} or E_u, ν_{37}[b]
1520	A_{1g}, ν_3	1473	A_{1g}, ν_3
1358	A_{1g}, ν_4	1358	A_{1g}, ν_4

[a] Symmetries and mode numbers from Abe et al., 1978 for further documentation of these assignments, see Salmeen et al., 1978.

[b] See Choi et al., 1982.

of cytochrome $\underline{a}_3^{2+}$ (Figure 27). This band decreases in intensity with an apparent pK = 9.3 corresponding to the pH range of the initial changes observed by MCD. After complete disappearance of the native cytochrome $\underline{a}_3^{2+}$ formyl vibration (1665 cm^{-1} band) at pH 10, further band changes in the high frequency region are observed. These consist of an additional decrease in intensity in the 1610 cm^{-1} band with a concomitant increase at 1633 cm^{-1}; the shoulder at 1570 cm^{-1} is no longer strongly observed at pH 11.5. The vibrational spectrum of reduced cytochrome oxidase at pH 11.5 is essentially identical with that of a low-spin ferrous heme a model compound in an aqueous environment (Figure 30f) and the band at 1633 cm^{-1} is characteristic of the formyl vibration of heme a under these conditions. This second set of vibrational shifts occur in a pH range comparable to the range of cytochrome $\underline{a}^{2+}$ pH dependent shifts as determined by visible excitation Raman data. As the pH is increased above 11.5, vibrations characteristic of the Schiff's base species are detected (Salmeen, et al., 1978).

III. pH Dependent Structural Changes

A. Reduced Cytochrome Oxidase

The original optical/Raman work on cytochrome oxidase at high pH (Salmeen et al., 1978) was somewhat paradoxical

in that the major apparent alteration as detected by Raman spectroscopy appeared to occur at cytochrome $\underline{a}_3$ while the primary optical shift appeared to involve cytochrome $\underline{a}$ (Lemberg and Pilger, 1964). The present, more detailed study resolves this paradox and shows that for reduced cytochrome oxidase both heme $\underline{a}$ chromophores are gradually modified in structure by alkaline pH. Moreover, these alterations show different pH dependencies which allow us to determine the structural changes responsible for the spectral shifts. The MCD, visible and Soret excitation Raman data identify three pH dependent steps: a change in cytochrome $\underline{a}_3$ which occurs with a pK $\sim$9.3, an alteration of cytochrome $\underline{a}$ with a pK $\sim$10.5, and at pH >11.5, formation of the Schiff's base adducts of both chromophores. For the pH range 8.5-10, the optical absorption, MCD and Soret excitation resonance Raman data suggest a high- to low-spin transition and a solvent environment change at the $\underline{a}_3$ site. It has been reported that redox titrations of cytochrome oxidase, monitored by MCD, display unusual behavior above pH 9 (Carithers and Palmer, 1981). This shift in thermodynamic behavior may be a reflection of the structural changes induced in cytochrome $\underline{a}_3$ by mildly alkaline conditions.

Cytochrome $\underline{a}$ is affected by somewhat more alkaline conditions. With pK $\sim$10.5, its spectral characteristics shift to those of an isolated low-spin heme $\underline{a}^{2+}$ model

compound in an aqueous environment. Soret excitation resonance Raman spectra offer the most insight into the structural changes which occur during this process (Figure 30). One of the major band shifts that occurs in this pH range is the decrease in intensity of the anomalous cytochrome $\underline{a}^{2+}$ vibration at 1610 cm^{-1} and concomitant increase at 1633 cm^{-1}. From the fact that the 1633 cm^{-1} band arises from a low-spin heme $\underline{a}^{2+}$ formyl vibration exposed to an aqueous environment (Figure 30f) and from the mirrored shifts in the 1610 and 1633 cm^{-1} vibrations, we assign the 1610 cm^{-1} band observed in the native protein to a perturbed formyl vibration of the cytochrome a chromophore. The largest optical absorption changes, from (441 nm, 601 nm) to (436 nm, 595 nm), also occur in this pH range, which indicate that the optical properties of cytochrome $\underline{a}^{2+}$ and the physical state of its formyl group are linked. In view of the significant perturbation of heme optical properties induced by peripheral aldehydes (Gouterman, 1959), such a linkage is not surprising.

The argument above indicates that the absorption red-shift of cytochrome a *in vivo* at neutral pH relative to its model compounds and the structural alteration of its formyl group are related. This observation, coupled with earlier results which showed that low-spin heme a models accurately produce other vibrations of cytochrome a, particularly its core size marker bands (Callahan and Babcock, 1981),

provides criteria with which to judge possible models for the structure of the cytochrome a site. For example, the presence of nearby polarizing amino acids capable of forming π complexes with the heme a system may be expected to alter the spectral properties of cytochrome a by analogy with the absorption red-shift observed by Mauzerall (1965) for π complexes between aromatic rings and uroporphyrin. However, Shelnutt (1981) has shown that formation of a π complex is accompanied by vibrational frequency changes of several wavenumbers in the high frequency core-size marker bands. Such frequency shifts are not apparent in the cytochrome a Raman spectrum. In addition, metalloporphyrin a complexes with π acceptors show only small spectral shifts which are unable to account for the differences between isolated heme a and *in vivo* cytochrome a spectral properties. A second possible model involves the occurrence of strained or hindered axial ligands to the cytochrome a iron which may perturb the optical properties of the chromophore. Carter *et al.* (1981) have shown that hindered axial ligands shift heme EPR ligand field parameters in a characteristic manner and used their observation to rationalize the liganding in mitochondrial b cytochromes. Such an explanation is unlikely for cytochrome a owing to our previous EPR results on the chromophore and its models (Babcock *et al.*, 1979a). Moreover, Raman core size marker bands are perturbed by sterically

hindered axial ligands (Frentrup, J., unpublished); such perturbations are not observed in the Raman spectrum of the *in vivo* chromophore. A third possible means to account for the red-shifted cytochrome *a* absorption spectrum is suggested by studies on rhodopsin and bacteriorhodopsin (Honig, *et al.*, 1979; Sheves *et al.*, 1979) and involves the specific arrangement of point charges in the heme *a* binding site of cytochrome *a*. The extension of the external point charge model to tetrapyrrole-based systems has resulted in reports of a range of absorption spectral shifts (Davis *et al.*, 1981; Eccles and Honig, 1982), but such a model would not be able to account for the altered formyl vibrational frequencies in cytochrome *a* without additional *ad hoc* assumptions. Point charge effects, however, may be important for the spectroscopy of cytochrome a_3 in isolated cytochrome oxidase and could account for the effects of Ca^{2+} on the absorption properties of various heme *a* species reported by Wikström and coworkers (Saari *et al.*, 1980).

It appears, therefore, that a perturbation to the cytochrome *a* ring system which only indirectly influences the formyl group will not account for the combined optical, Raman and EPR data; rather, a specific interaction at the carbonyl seems necessary in order to rationzalize the spectroscopic results. Structural modifications of the cytochrome *a* formyl group which may explain the observed

phenomena include the following: (a) protonated Schiff's base formation at the peripheral formyl group, (b) non-planarity of the position 8 aldehyde with the porphyrin π-system, and (c) hydrogen bonding to the peripheral aldehyde. The previously suggested structure of a protonated Schiff base between the cytochrome $\underline{a}^{3+}$ aldehyde and an ε-amino group of a lysine residue of the protein (Ondrias and Babcock, 1980) is not supported by model compound studies (Ward et al., 1983) and can therefore be eliminated as a likely explanation. Non-planarity of the peripheral aldehyde and porphyrin ring π-systems also seems unlikely for two reasons. First, the fact that we observe a high frequency vibration from a perturbed formyl group indicates that the carbonyl and porphyrin π-systems must have some degree of overlap for resonance enhancement to occur. Secondly, it is difficult to rationalize a red-shifted heme absorption spectrum in both the Soret and α-band regions when the perturbation invoked decreases the extent of conjugation of the porphyrin π-system.

In order to effect both a red-shifted absorption spectrum and a decreased formyl stretching frequency, a greater electron-withdrawing capability at the peripheral formyl group is needed. A hydrogen bonding interaction in which the formyl C=O acts as the proton acceptor provides a reasonable structure within which such effects could occur. The decrease in carbonyl stretching frequency upon hydrogen

bond formation is well known and, because the visible and Soret absorption bands of heme a are $\pi \rightarrow \pi^*$ transitions, an absorption red-shift is predicted to result from hydrogen bonding (Pimentel and McClellan, 1960). Moreover, because the hydrogen bond is a specific perturbation to the formyl group, the major porphyrin ring vibrations would not be modified to any great extent, in agreement with earlier observations. Therefore, we conclude that a hydrogen bond between an amino acid residue and the peripheral aldehyde can explain the spectra of cytochrome a and the observed pH dependent behavior. We suggest that tyrosine may be the proton-donating group involved in the hydrogen bond interaction with the cytochrome a peripheral aldehyde based on the ability of phenol as hydrogen donor to low-spin heme a model compounds to mimic the cytochrome a^{3+} absorption spectrum. A schematic of the proposed structure of the heme a binding site in cytochrome a at neutral pH is given in Figure 31.

The pH dependence of the hydrogen bonded form of cytochrome a presented above could arise from either a titration of the proton donor group or a disruption of the hydrogen-bonded structure by an alkaline pH-induced conformational change of the protein. Since we can monitor only the hydrogen acceptor (C=O) stretching frequency by RRS and not the donor (R-H) stretching frequency we are unable to distinguish experimentally between these two

Figure 31. Schematic of proposed structural changes of the oxidized and reduced heme a chromophores at several pH levels.

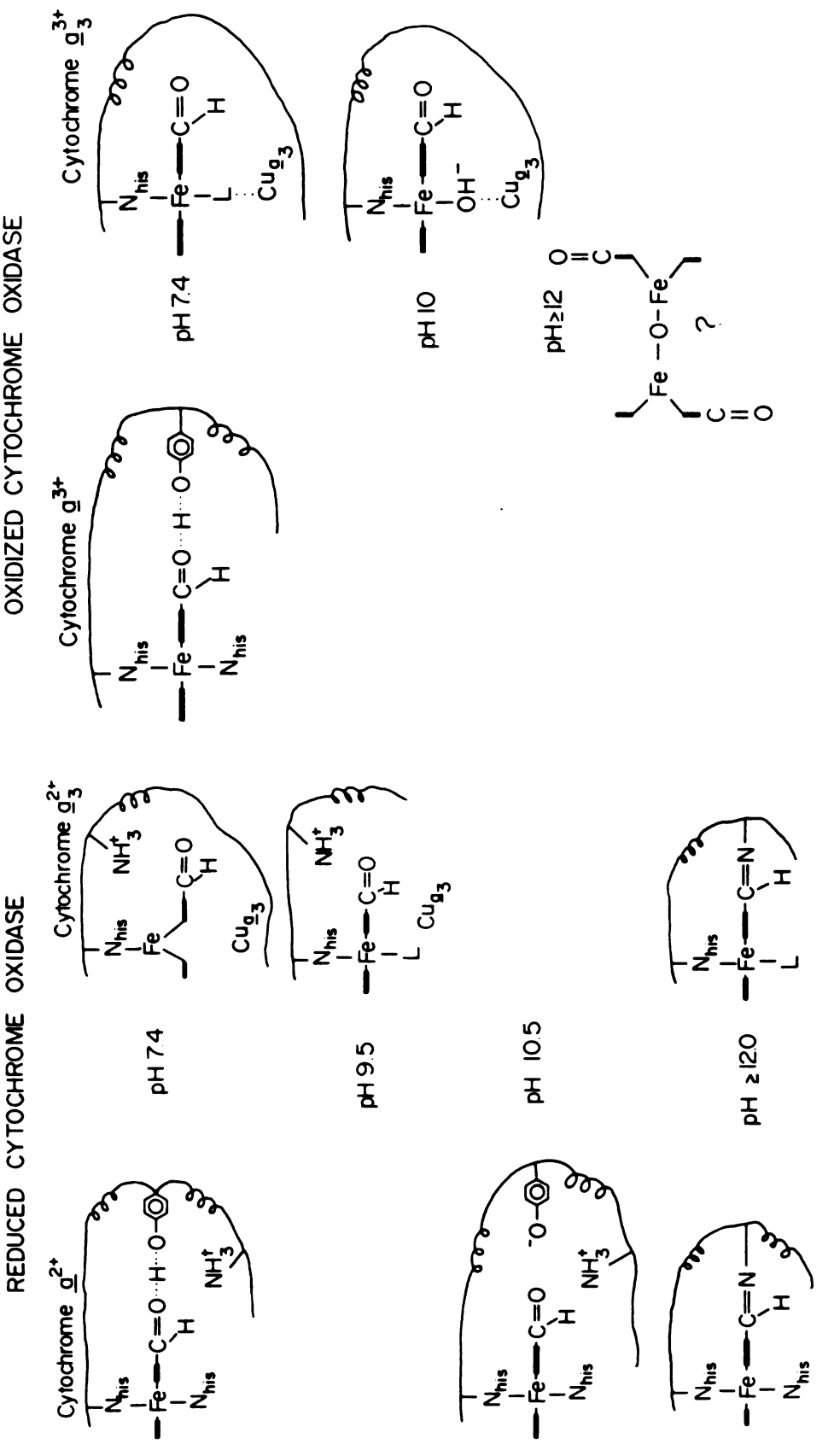
OXIDIZED CYTOCHROME OXIDASE
REDUCED CYTOCHROME OXIDASE
Cytochrome g3+
Cytochrome g2+
pH 7.4
pH 10
pH≥12
pH 9.5
pH 10.5
pH ≥12.0

Figure 31

alternatives. However, the ability to shift the titration curves of the pH dependent spectral changes to higher pH values by using non-denaturing neutral detergents (Tween 20 and lauryl maltoside, see above) or to lower pH values under more strongly denaturing conditions ($NaDodSO_4$ treatment (Criddle and Bock, 1959), 8 M urea, pH 7.4 (Lemberg and Pilger, 1964) or heat treatment (Person and Zipper, 1964)) suggests that these effects are most likely due to an unfolding of the protein tertiary structure.

By combining this information with the conclusions on the behavior of cytochrome a_3 under alkaline conditions, the overall effects of pH on reduced cytochrome oxidase can be summarized as in the schematic in Figure 31. The first pH dependent step, pK ∿9.3, involves a structural shift at cytochrome a_3, apparently arising from a ligation and solvent environment change. The second pH dependent step involves cytochrome a and is a consequence of the disruption of the hydrogen bond between the position 8 formyl group of the cytochrome a ring and the postulated tyrosine residue. This seems to be a result of a protein conformational change caused by the denaturing alkaline conditions. At this pH both cytochromes a and a_3 have similar spectral characteristics, that of low-spin ferrous heme a in an aqueous environment. Above pH 12, Schiff base formation between the heme a aldehydes of both chromophores and ε-amino groups of lysine residues

is observed (Lemberg, 1964; Takemori and King, 1965). At this point denaturation of the protein may proceed to such an extent that migration of the hemes a to other loci on the protein occurs. If this is the case, then the location of lysine residues within the heme pockets of cytochromes a and a_3 is not mandatory in our model.

B. Oxidized Cytochrome Oxidase

As in the reduced enzyme, cytochrome a_3 is first affected by alkaline pH treatment of the oxidized enzyme. The resonance Raman and optical data indicate that a six-coordinate high- to low-spin transition takes place in this chromophore over the pH range 8.5-10. This conclusion rationalizes the decrease in absorbance at 655 nm, which has been attributed to the high-spin cytochrome a_3^{3+}-Cu_3^{2+} site (Hartzell et al., 1973), and accounts for the shift in the cytochrome a_3^{3+} core size band from 1572 cm^{-1} to 1590 cm^{-1}. In a recent study of H_2O_2 binding to cytochrome oxidase, Bickar et al. (1982) reported a change in the optical spectra of the native enzyme and of the peroxide bound form at pH 9.8. These spectral shifts may be a reflection of the spin-state transition induced in cytochrome a_3^{3+} by moderately alkaline pH as reported here. No changes in cytochrome a^{3+} in this pH range are observed. At strongly alkaline pH ($\geq$12), both heme chromophores have similar vibrational properties indicative of five

coordinate, high-spin heme $\underline{a}^{3+}$. Aggregate or μ-oxo dimer formation at pH 12, as suggested above, is a possible configuration that is consistent with both the EPR and Raman data. Although several structural changes are observed for the heme a chromophores in oxidized cytochrome oxidase under alkaline conditions, the 10 nm red-shift in the α band maximum of cytochrome a and its anomalous high frequency vibration at 1650 cm^{-1} relative to low-spin heme a model compounds (Table 5) are not modified in such a manner as to reveal the nature of these spectral shifts. Noting the fact that heme $\underline{a}^{3+}$ with the exception of the formyl vibration (Babcock et al., 1981) and by reference to the proposed structure of ferrous cytochrome a in which a hydrogen bonded aldehyde structure (Figure 33) lowers the formyl stretching frequency by ∿30 cm^{-1}, the 1650 cm^{-1} band of cytochrome $\underline{a}^{3+}$ is assigned to a perturbed formyl vibration in the oxidized enzyme. The ability of low-spin heme $\underline{a}^{3+}$ model compounds in the presence of hydrogen donors (e.g., phenol) to mimic the optical and resonance Raman vibrational properties of cytochrome $\underline{a}^{3+}$ provides additional support for the proposal that the 1650 cm^{-1} band of cytochrome $\underline{a}^{3+}$ arises from a hydrogen bonded formyl group. Therefore, it is concluded that the hydrogen bonded formyl configuration is also present in the oxidized enzyme.

A schematic summary of the pH effects on oxidized cytochrome oxidase is shown in Figure 31. The native enzyme

displays the cytochrome a formyl group: tyrosine hydrogen bonding interaction. As the pH is raised, the optical, Raman and EPR data indicate that cytochrome a_3 undergoes a spin-state transition. In this case, the cytochrome a formyl hydrogen bonded structure remains intact until strongly denaturing conditions are reached, at approximately pH 12, where Raman, optical and EPR data suggest that the heme a chromophores occur as five coordinate and high-spin hemes, possibly in the configuration of μ-oxo dimers.

The ability to alter the cytochrome a formyl/protein interaction at lower pH in the reduced protein than in the oxidized enzyme suggests that the latter is a more compact, stable structure. Further evidence for this protein structural feature lies in the determination of the relative sizes and conformations of different forms of cytochrome oxidase by sedimentation velocity experiments (Cabral and Love, 1972). These results indicate that the reduced enzyme occupies a 3% larger volume than the fully oxidized form of cytochrome oxidase. A further significant difference between the oxidized and reduced forms of the enzyme lies in the shift in the α band maximum upon reduction. In most heme absorption spectra the position of the α band is unchanged or only slightly modified (±2 nm) upon redox state change. The 5 nm red shift in the α band of cytochrome oxidase (essentially the α band of cyt a) from

599 nm to 604 nm upon reduction, indicates a stronger interaction of the cytochrome a formyl with the H-donor group of the protein in the reduced versus the oxidized protein (Pimentel and McClellan, 1960; Baum and McClure, 1979). Initial estimate of the shift in hydrogen bond energy upon iron redox state change is roughly 2 kcal/mole. This energy shift and the presumed change in hydrogen bond length which accompanies it provide a pathway by which electron transfer events at the redox active cytochrome a iron may be communicated to the surrounding protein matrix.

CHAPTER 6

REDOX-LINKED HYDROGEN BOND STRENGTH CHANGES IN CYTOCHROME A

I. Introduction

While the existence of the proton pump appears to be accepted by most researchers in the field (see, however, the recent article by Mitchell and Moyle (1983)), the mechanism by which redox change is coupled to proton translocation remains obscure. Wikström et al. (1981) presented arguments implicating cyt a and suggested a reciprocating site model for its involvement. Chan et al. (1979), on the other hand, interpreted the unusual spectroscopic, and hence, structural properties of Cu_a as an indication of unusual function and proposed a fairly detailed model demonstrating the plausibility of a Cu_a based pump. While Cu_a and cyt a appear to be associated with subunit II of the oxidase, recent biochemical work has implicated subunit III in proton translocation (Casey et al., 1980). The generality of its role is uncertain, however, owing to the occurrence of proton pump in the two subunit oxidase from Paracoccus denitrificans (Soloiz et al., 1982).

The unusual spectroscopic properties of cyt a, particularly its optical absorption red-shift relative to

low-spin heme a model compounds (Figure 32), have been interpreted in terms of the structure for its heme a chromophore shown in Figure 33, where -XH denotes a proton donating group associated with the polypeptide backbone (Callahan and Babcock, 1983). The results of this chapter demonstrate that the strength of the hydrogen bond between the formyl oxygen and the proton donor depends on the redox state of the cyt a iron. This redox-linked shift in hydrogen bond strength provides a channel by which electron transfer events at the metal can be coupled to protein-based proton translocation. Two different mechanisms for the coupling are discussed.

II. Hydrogen Bond Strength Correlations

A. Manifestations in Heme a Species

Figure 34 shows Soret excitation Raman spectra of oxidized and reduced beef heart cytochrome oxidase and of the reduced protein isolated from Thermus thermophilus (Fee et al., 1980) in the 1500-1700 cm^{-1} frequency region. Also included in the figure are Raman spectra of ferric and ferrous heme a $(NMeIm)_2$, a cyt a model compound in a nonhydrogen bonding solvent. In the proteins, the formyl vibration occurs at 1676 cm^{-1} for cyt a_3^{3+} and decreases to 1665 cm^{-1} for cyt a_3^{2+}. This behavior is typical of high-spin heme a model compounds in aprotic solvents and

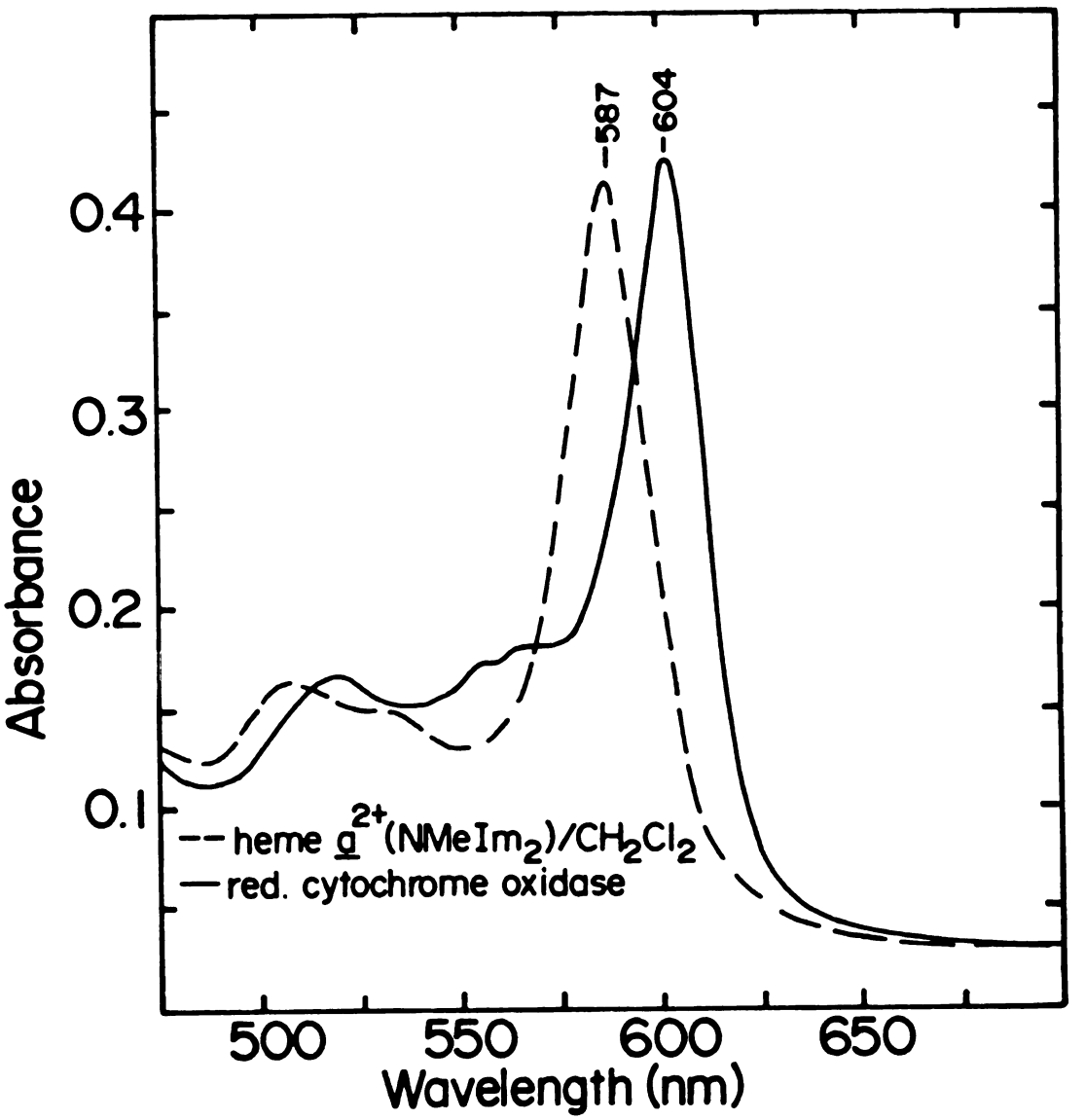

Figure 32. Visible region absorption spectra of reduced bis-imidazole heme a in CH_2Cl_2 and reduced cytochrome oxidase.

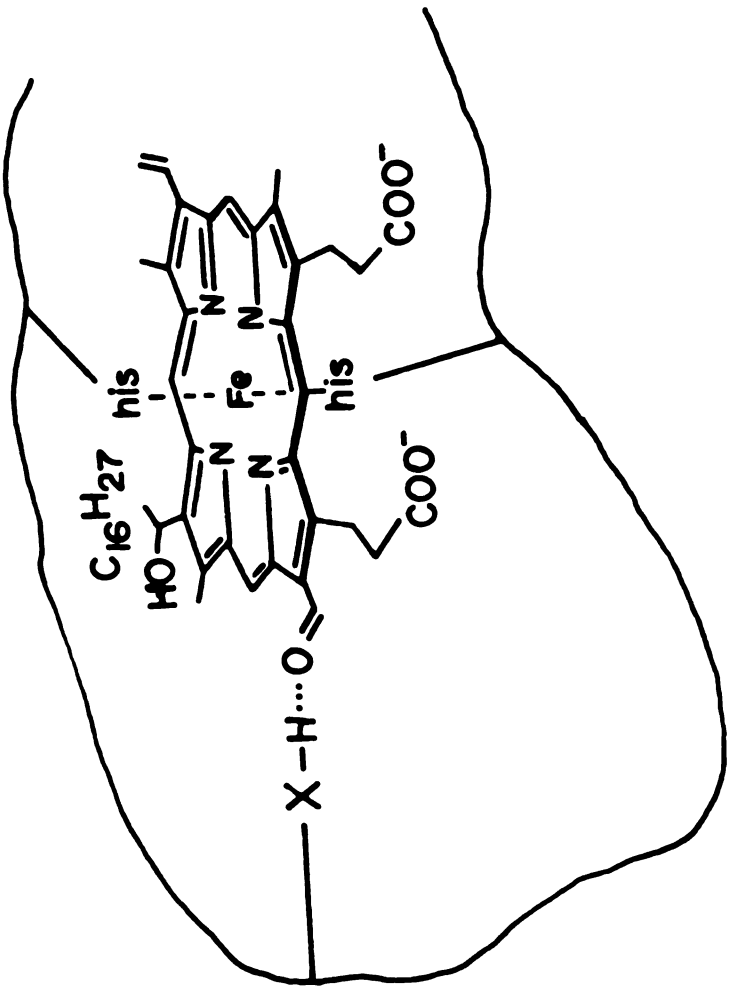

Figure 33. Postulated active site structure for cytochrome a in cytochrome oxidase. The heme a iron is six coordinate with histidines occupying the two axial ligation sites. The peripheral formyl group is involved in a hydrogen bond with a proton donor designated as X-H, which is associated with the polypeptide backbone.

Figure 34. High frequency Soret excitation Raman spectra of cytochrome oxidase and low-spin heme *a* model compounds. In (a) and (c), the beef heart enzyme, dissolved in 0.05 M Hepes, 0.5% lauryl maltoside, pH 7.4, was used. In (d) cytochrome oxidase (c_1aa_3) from *Thermus thermophilus* in the Hepes/maltoside buffer was used. In (b) and (e) the bis-(N-methyl imidazole) heme *a* complex was dissolved in methylene chloride. The carbonyl stretching frequency for cytochrome a_3 is indicated by ǂ in (a), (c) and (d).

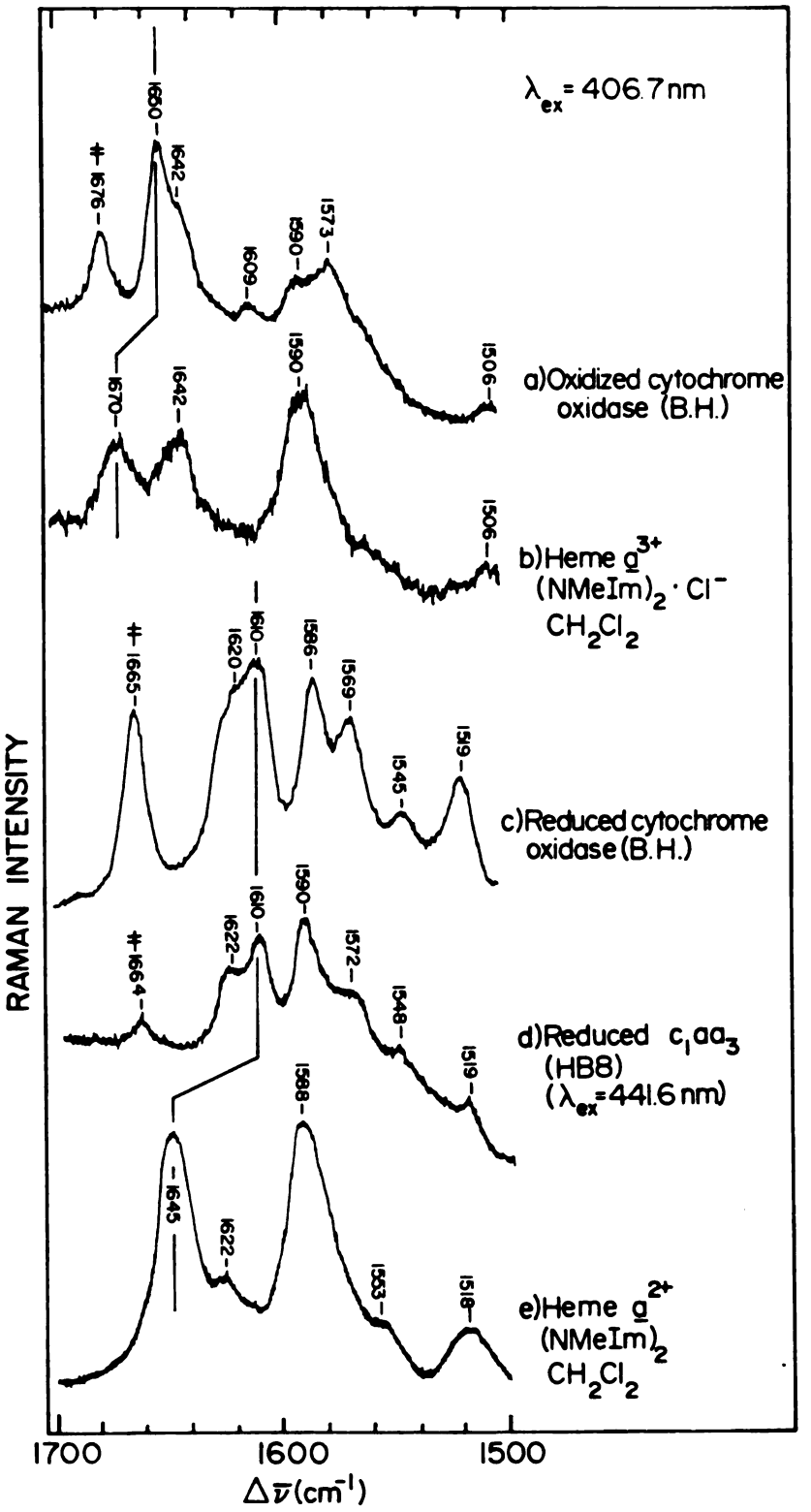
λex = 406.7nm
1676
1650
1642
1609
1590
1573
1506
a)Oxidized cytochrome oxidase (B.H.)
1670
1642
1590
1506
b)Heme a3+ (NMeIm)2 · Cl−
CH2Cl2
1665
1620
1640
1586
1569
1545
1519
c)Reduced cytochrome oxidase (B.H.)
1664
1622
1640
1590
1572
1548
1519
d)Reduced c1aa3 (HB8) (λex=441.6 nm)
1645
1622
1588
1553
1518
e)Heme a2+ (NMeIm)2 CH2Cl2
RAMAN INTENSITY
1700
1600
1500
Δν̄(cm−1)

Figure 34

indicates that the carbonyl group of $\underline{a}_3$ is isolated in a hydrophobic environment in both of its valence states (VanSteelandt-Frentrup et al., 1981; Babcock et al., 1981). The formyl vibrational frequencies for cyt a (Callahan and Babcock, 1983) and its model compounds are indicated by vertical lines in the figure. For both valence states, the in situ carbonyl shows a significant frequency decrease compared to its corresponding model compound. This decrease amounts to 20 cm^{-1} for oxidized cyt a and to 35 cm^{-1} for the reduced center. The Thermus protein shows an analogous decrease which, along with similar data for rat liver cytochrome oxidase (Babcock et al., 1981) indicates that the lower in situ frequency is not a peculiarity of the beef enzyme.

Shifts in carbonyl vibrational frequencies of this magnitude are commonly observed upon hydrogen bond formation (Murthy and Rao, 1968). Moreover, because the visible and Soret optical absorption bands of heme a are π-π^* transitions which involve the formyl as part of the system, an absorption red shift should accompany hydrogen bond formation. Both the magnitude of the formyl vibrational frequency decrease and of the absorption red-shift should increase as the strength of the hydrogen bond increases (Pimentel and McClellan, 1960). The proportionality between carbonyl frequency decrease and absorption red-shift appears to hold for cyt a in its two

valence states. For the ferric form, the α band absorption maximum is shifted by 10 nm (284 cm^{-1}) to 598 nm relative to its nonhydrogen bonded model and the carbonyl frequency decrease is 20 cm^{-1} (Table 8). For the ferrous form, the absorption red-shift relative to the nonhydrogen bonded model is greater, 17 nm (480 cm^{-1}) and likewise the vibrational frequency is decreased by 35 cm^{-1}.

To explore the coupling between the carbonyl vibrational frequency, the optical absorption red-shift and the hydrogen bond strength in cyt a in more detail, optical and Raman spectra for several low-spin heme a and copper porphyrin a model compounds have been recorded in different solvents and in the presence of various hydrogen donors. Copper porphyrin a was used to obtain spectroscopic parameters for the chromophore in the presence of more acidic donors. These cannot be used with heme a$(NMeIm)_2$ because they protonated N_e of the iron ligand, which results in the formation of the high-spin heme a complex. Deuterated rather than protonated phenol was used as a donor in order to avoid overlap of its vibrations with those of the porphyrin macrocycle in the high frequency region. Table 8 summarizes the results in terms of α band maximum, carbonyl frequency and hydrogen bond strength (see below) for the models and for cyt a. In Figure 35, the absorption red-shift is plotted as a function of both the carbonyl frequency decrease and the calculated hydrogen bond strength.

Table 8. Spectroscopic Characteristics of Hydrogen Bonded Heme a and Cu^{2+} Porphyrin a Species.

No.	Species	λ^{α}_{max} a) (nm)	$\Delta\bar{\nu}_{\alpha}$ b) (cm^{-1})	$\bar{\nu}_{C=O}$ c) (cm^{-1})	$\Delta\bar{\nu}_{C=O}$ d) (cm^{-1})	ΔH_{HB} e) ($\frac{kcal}{mole}$)
1	cytochrome a^{3+}	598	284	1650	20	3.0
2	heme $a^{3+}(NMeIm)_2$ in CH_2Cl_2	588	---	1670	--	---
3	Heme $a^{3+}(NMeIm)_2$ in CH_2Cl_2+phenol d_6	595	200	1652	18	2.7
4	heme $a^{3+}(NMeIm)_2$ in trichloroethanol	595	200	1654	16	2.4
5	heme $a^{3+}(NMeIm)_2$ in methanol	589	30	1666	4	0.6
6	cytochrome a^{2+}	604	480	1610	35	5.3
7	heme $a^{2+}(NMeIm)_2$ in CH_2Cl_2	587	---	1645	--	---
8	heme $a^{2+}(NMeIm)_2$ in H_2O	594	201	1633	12	1.8
9	heme $a^{2+}(NMeIm)_2$ in CH_2Cl_2+phenol d_6^2	598	313	1622	23	3.5
10	Cu^{2+} porphyrin a in CH_2Cl_2	596	---	1666	--	---

Table 8. Continued.

No.	Species	λ_{max}^{α} [a] (nm)	$\Delta\bar{\nu}_{\alpha}$ [b] (cm^{-1})	$\bar{\nu}_{C=O}$ [c] (cm^{-1})	$\Delta\bar{\nu}_{C=O}$ [d] (cm^{-1})	ΔH_{HB} [e] ($\frac{kcal}{mole}$)
11	Cu^{2+} porphyrin a in CH_2Cl_2+trifluoroacetic acid	613	465	1640	26	3.9
12	Cu^{2+} porphyrin a in trichloroethanol	606	277	1649	17	2.6
13	Cu^{2+} porphyrin a in CH_2Cl_2+p-chlorophenol	607	304	1642	24	3.6
14	Cu^{2+} porphyrin a in CH_2Cl_2+phenol d_6	606	277	1642	24	3.6

[a] α-band optical absorption maximum.

[b] Frequency difference in α-band optical absorption maxima for the indicated compound and the corresponding non-hydrogen bonded species.

[c] Formyl carbonyl stretching frequency.

[d] Frequency difference in carbonyl stretching frequencies for the indicated compound and the corresponding non-hydrogen bonded species.

[e] Hydrogen bond strength as calculated from Equation (6.1).

Figure 35. Absorption red-shift for cytochrome a, heme a or Cu porphyrin a species as a function of hydrogen bond enthalpy as calculated from Equation 6.1. The points are numbered according to the compounds listed in Table 1.

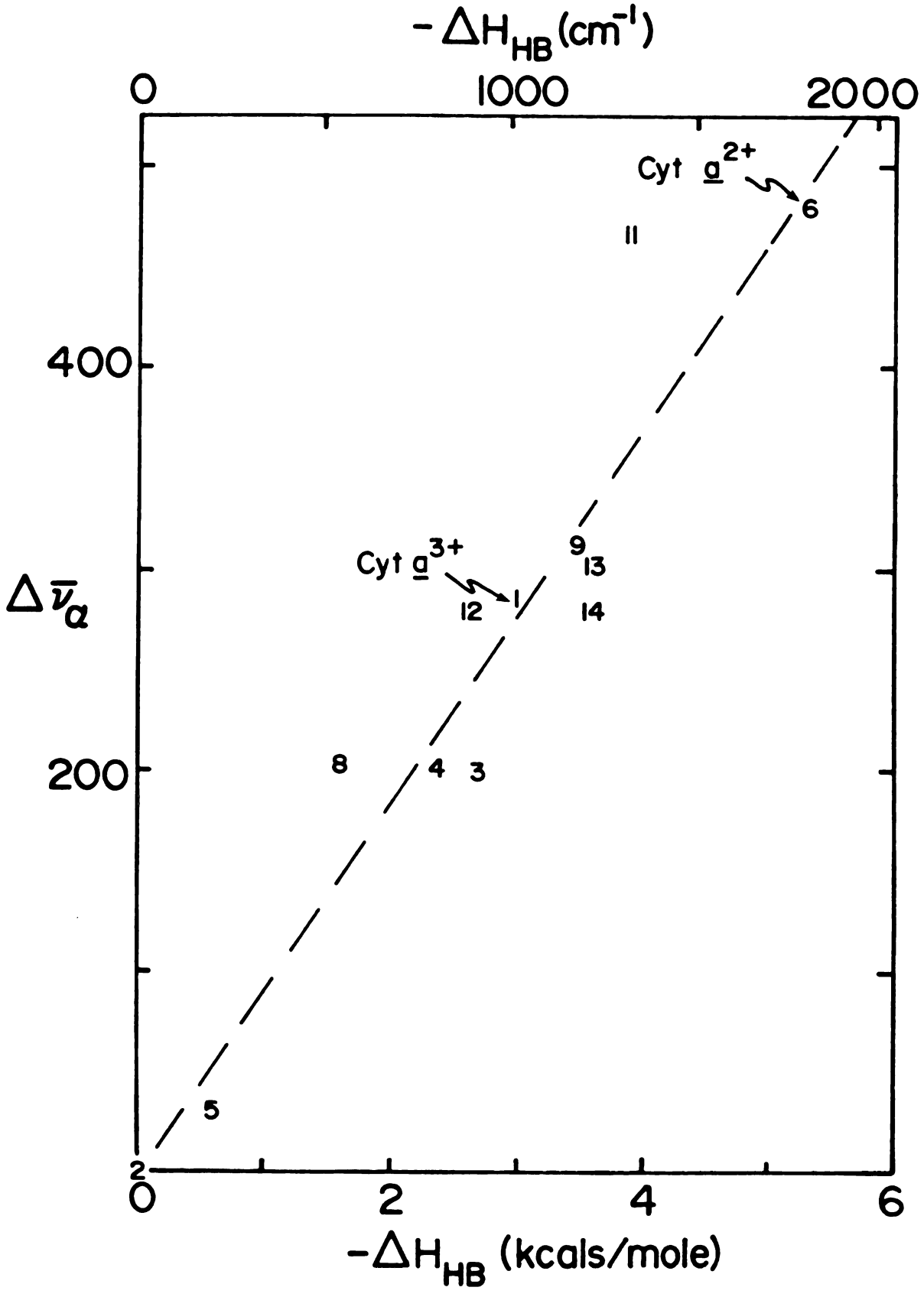
$-\Delta H_{HB}(cm^{-1})$
0
1000
2000
Cyt $\underline{a}^{2+}$
6
11
400
Cyt $\underline{a}^{3+}$
9
13
12
1
14
$\Delta\bar{\nu}_\alpha$
200
8
4
3
5
2
0
2
4
6
$-\Delta H_{HB}$ (kcals/mole)

Figure 35

The approximately linear relationship apparent in the figure is typically what one observes in correlating hydrogen bonding phenomena in a series of loosely related compounds (Arnett, et al., 1974).

B. Quantification of Hydrogen Bond Energies

From the formyl frequency shift observed upon hydrogen bond formation, an estimate of the strength of the hydrogen bond for the heme a species under consideration can be made. This relies upon a variation of the Badger Bauer rule, which has been widely applied to vibrational data obtained for the hydrogen donor involved in the bond (e.g., Pimentel and McClellan, 1960). The corresponding relationship for the acceptor is (Zadorozhnyi and Ischencko, 1965)

$$\frac{\Delta\bar{\nu}_{C=O}}{\bar{\nu}_{C=O}} = -K_{C=O}\Delta H_{HB} \qquad (6.1)$$

where ΔH_{HB} is the hydrogen bond enthalpy, $K_{C=O}$ is a proportionality constant, $\bar{\nu}_{C=O}$ is the vibrational frequency of the free (nonhydrogen bonded) acceptor. By using a series of aldehydes, ketones and carboxylic acids as acceptors and phenols or alcohols as donors, a value of $K_{C=O} = 4\ 10^{-3}$ mole/kcal has been estimated (Zadorozhnyi and Ischenko, 1965). Realizing that this value is likely to hold only roughly for heme a species, particularly for the diverse

class of donors in Table 8 (Arnett et al., 1974), it has been used to estimate ΔH_{HB} for the various complexes. These are given in Table 8 and are used in Figure 35 to obtain the correlation between hydrogen bond strength and absorption red-shift. When the hydrogen bond enthalpy is expressed in wavenumbers the slope of the least squares line drawn in the figure is 0.28. This value is within the range one expects for the proportionality between hydrogen bond strength and the π-π^* transition red-shift which results (Pimentel and McClellan, 1960).

From the data in Table 8 and Figure 35 it is apparent that both ferric and ferrous cyt a have optical, vibrational and hydrogen bond enthalpy characteristics which are consistent with the model compounds. An important conclusion follows from this observation because it indicates that the major protein-induced modification of the chromophore occurs by hydrogen bonding to the formyl group. Other perturbations, for example, shifts in the electrostatic potential at the heme (Warshel and Weiss, 1981) or point charge effects (Honig et al., 1979) may influence the optical spectrum as well but these effects appear to be small compared to the hydrogen bonding interaction. Moreover, the hydrogen-bonding effects are more pronounced for cyt a^{2+} than for cyt a^{3+}. Because the hydrogen bond strengthens upon reduction, the redox potential of cyt a is more positive than it would be in the absence of such an interaction. Modulation of the hydrogen bond strength

in situ for either oxidized or reduced cyt *a* may provide an explanation for the unusual redox properties of the heme *a* components of cytochrome oxidase (*e.g.*, Babcock *et al.*, 1978).

The chemical basis for the difference in hydrogen bond enthalpy for the two cyt *a* valence states is straightforward. Sheridan, Allen and their coworkers have investigated redox dependencies in hydrogen bond strength for both heme and FeS proteins (Valentine *et al.*, 1979; Sheridan *et al.*, 1981). In heme proteins, where they explored the iron ligand, histidine, as a proton donor, the ferric state is stabilized by hydrogen bond formation. In FeS proteins, where the metal ligand is a hydrogen acceptor, they noted stronger hydrogen bonds for the reduced cluster. The porphyrin *a* ligand to iron in cyt *a* resembles the FeS protein case in that it is a proton acceptor and we expect stronger hydrogen bonding in the ferrous state, *i.e.*, upon reduction of the iron the electron density on the carbonyl oxygen increases and it becomes a better proton acceptor. Cyt *a* behaves this way *in situ* and it is also observed when heme *a* model compounds are considered. For example, the hydrogen bond formed between phenol and low-spin heme *a* is stronger by $\sim$0.8 kcal/mole when the iron is in the ferrous, as opposed to the ferric, valence state (Table 8). The increased negative charge at the carbonyl oxygen in ferrous heme *a* is also apparent in that *a* 25 cm^{-1} decrease in

carbonyl stretching frequency, presumably due to population of the π^* antibonding orbital, is observed for ferrous heme a models compared to ferric heme a in the absence of hydrogen bonding effects (Figure 34).

Given the approximate nature of Equation (6.1), the calculated hydrogen bond strength change which occurs on redox cycling of cyt a is in the neighborhood of 2-2.5 kcal/mole (90-110 mV). This energy is comparable to the electrochemical proton gradient against which protons are translocated in mitochondria (estimated to lie between 160 and 230 mV with a best value of around 200 mV (Wikström et al., 1981), particularly if the hydrogen bond strength change is augmented by other redox-linked processes, e.g., a shift in electrostatic potential at the heme (Warshel and Weiss, 1981) or additional hydrogen bond contributions from the cyt a axial histidines (Valentine et al., 1979; Babcock et al., 1979). Alternatively, one could envision a situation in which both cyt a as discussed below, and Cu_a, as suggested by Chan et al (1979), operated as proton pumps in which the duty cycle for each would be one/half. Before discussing possible pump models for cyt a however, it is necessary to consider the relationship between the hydrogen bond enthalpy changes observed and the free energy actually made available for proton translocation. In the early literature on hydrogen bond formation, increases in hydrogen bond strength (decreases in ΔH_f^o)

for a series of hydrogen bonded structures appeared to be accompanied by decreases in ΔS_F^o so that the free energy change remained somewhat constant (Pimentel and McClellan, 1960). More recently, and arguing from a much larger data set, Arnett and coworkers (1974) concluded that such a generalization is not justified in that a hydrogen bond reaction series may be essentially isoentropic yet show large changes in ΔH_f^o. In these cases, the change in ΔH_f^o will be reflected in a change in ΔG_f^o. Such a situation is likely to occur in cyt a owing to the fact that the major contribution to the decrease in ΔS_f^o for a reaction series where it is observed is usually attributed to loss of translational entropy upon complexation. Because the proton donor to the cyt a formyl is most likely immobilized by its polypeptide environment, the translational entropy will be small regardless of the hydrogen bond strength. Thus we expect that changes in cyt a hydrogen bond enthalpy will be accompanied by a free energy change of a comparable magnitude and that this will be available for proton pumping.

III. H^+ Pump Models

From a variety of models in which the redox driven change in cyt a hydrogen bond strength could be used to translocate protons, two will be considered here. In the first, the free energy change at the formyl serves as a switch which produces a conformational change in a different

region of the protein which allows proton conduction. In the second, the proton hydrogen-bonded to the carbonyl is an integral component of a proton wire and is actually pumped during the redox cycle. Relevant to both of these models is the relationship between hydrogen bond strength and hydrogen bond geometry discussed by Valentine et al. (1979). The geometry is determined by two factors: the distance, r, between the heavy atoms involved in the hydrogen bond and the angular deviation of the bond, θ from linearity. With these definitions, the hydrogen bond strength is proportional to $\cos\theta/r$.

A. Conformational Change Model

In the first model, the reduction of cyt a leads to a decrease in either r or θ (or both). The change in local structure about the heme a chromophore is transmitted to the proton translocating section of the protein where a conformational change resulting in proton translocation occurs. Supporting this model is the observation that the major conformational change which occurs upon reduction of cytochrome oxidase is controlled by the redox state of cyt a (Cabral and Love, 1972). A second piece of potentially supporting evidence comes from the observation that dissociation of cytochrome oxidase subunit III abolishes the pH dependence in the midpoint potential of cyt a in the cyanide inhibited enzyme (Penttilä and Wikström, 1981).

The possible mechanics of proton conduction as related to a conformational change have been considered in detail by Nagle and Morowitz (1978). The mechanism by which the hydrogen bond geometry change at the heme a site is transmitted through the protein to the pumping section may bear some resemblance to that proposed by Perutz and Brunori (1982) for the control of the Root effect in fish hemoglobins.

B. Hydrogen Bond Chain Model

The second model represents a direct mechanism for proton translocation in that the formyl hydrogen bonded proton is pumped during the redox cycle. This kind of mechanism requires that covalent bonds involving hydrogen and the polypeptide heavy atom in the formyl hydrogen bond are made and broken during proton translocation. Because resonance Raman can provide vibrational information on only the chromophore moiety of a protein, we have no direct insight as to the identity of the proton donor to the cyt a carbonyl. However, we suspect that it is an -OH group from either an alcohol or a carboxylic acid side chain. An $-NH_2$ group is much less likely owing to the facility with which amines form Schiff base linkages with heme a (Ward et al., 1983) and -SH groups can be eliminated owing to the extremely weak hydrogen bonds they form (Perutz and Brunori, 1982).

With these considerations, the mechanism in Figure 36, which is similar in certain aspects to the switch model for bacteriorhodopsin proposed by Nagle and Mille (1981), can be postulated. In 36a, the stable form of ferric cyt a is shown where a fairly weak (3 kcal/mole) hydrogen bond exists between the peripheral C=O and the -OH donor. As indicated in the figure, the weak hydrogen bond assumes a nonlinear geometry ($\theta \neq 0^{o}$). Two proton-donating groups, R_r-H_d and R_l-H_b, are located in the immediate vicinity of the cyt a carbonyl. R_r-H_d is connected to the right-hand side of the membrane by an asymmetric hydrogen-bonded chain and R_l-H_b is similarly connected to the left side of the membrane (Nagle and Morowitz, 1978; Nagle and Mille, 1981). On the right hand side R_r-H_d is shown in the oxidized, resting form of the enzyme (Figure 36a) with H_d hydrogen-bonded to the oxygen of the donor group to cytochrome a. This interaction determines the configurational energy of the hydrogen bond chains, and in Figure 36a, the interaction, R-O$\cdots$$H_d$-$R_r$, holds the right hand side proton chain in its high energy conformation. The left hand side proton chain is in its low energy form. The concept of hydrogen bonded chains has been developed by Nagle and coworkers (Nagle and Morowitz, 1978; Nagle and Mille, 1981). Such a chain could conceivably span protein subunits so the involvement of Subunit III in cytochrome oxidase proton translocation may be accommodated by this model as well.

Figure 36. A possible mechanism for the redox-driven proton pump in cytochrome oxidase. The cytochrome <u>a</u> heme <u>a</u> moiety is indicated by Fe $\diagup$C = O; the iron valence is indicated. In (a), the stable oxidized form of the cyt <u>a</u> site is indicated. A hydrogen bonded chain in its higher energy configuration occurs to the right of the formyl group and is designated as H_d-R_r....; a hydrogen bonded chain in its lower energy configuration occurs to the left of the formyl and is designated as ...H_b-R_ℓ. Reduction is shown as a two step process which results in (c), the stable reduced form of the site. The arrows in (a) and (b) indicate the changes in structure which occur during steps 1 and 2, respectively. Reoxidation occurs by a two step process, with (d) as an intermediate, to regenerate the stable, oxidized cyt <u>a</u> configuration. The hydrogens involved in the pumping action are subscripted with letters a-d to identify their motions during the various steps.

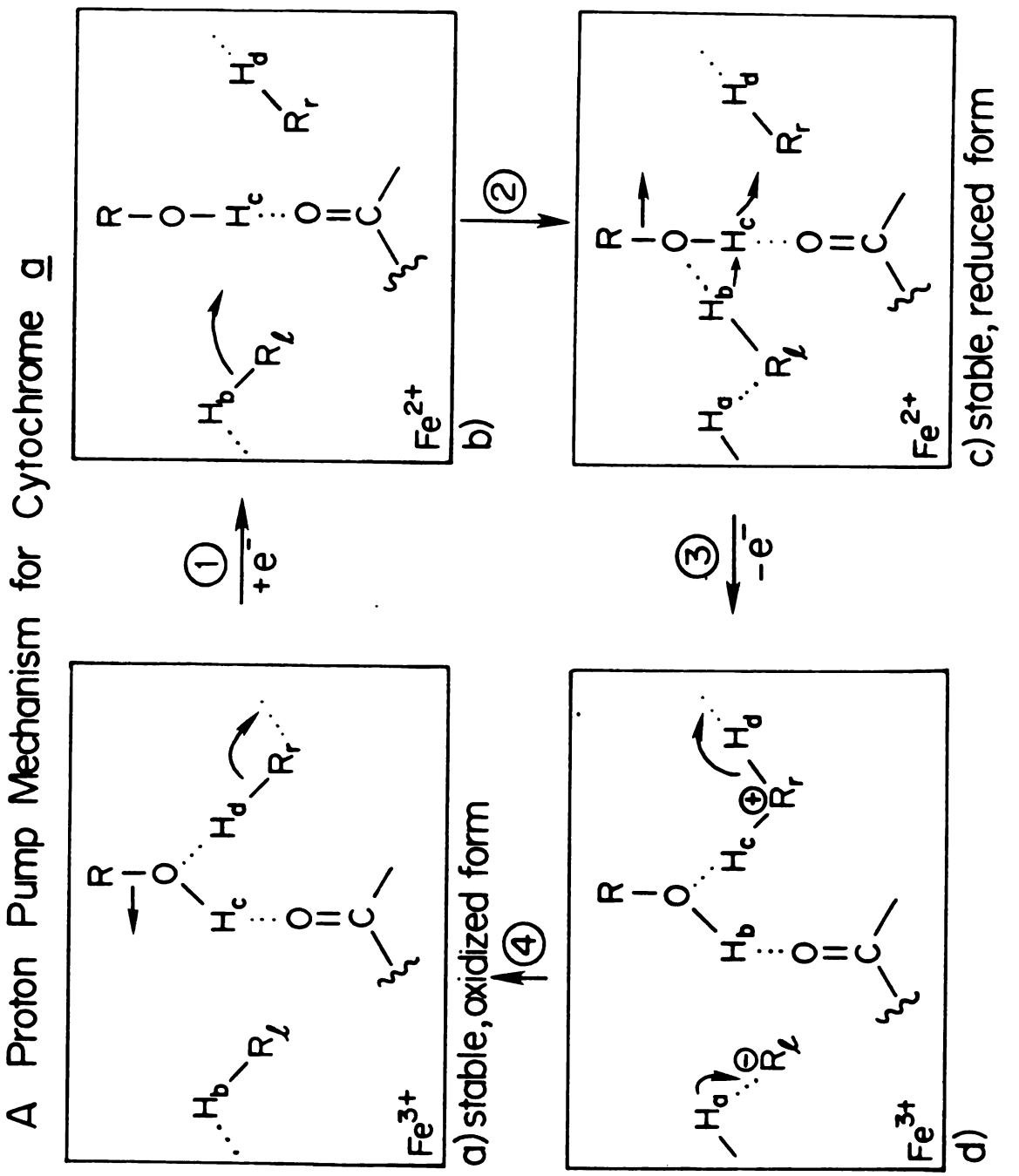
A Proton Pump Mechanism for Cytochrome a
a) stable, oxidized form
b)
c) stable, reduced form
d)
① +e⁻
② -e⁻
③
④
Fe3+
Fe2+

Figure 36

Proton pumping proceeds from left to right. Reduction of the iron results in a two step change in the hydrogen bond geometry and produces the stable reduced form of cyt a shown in Figure 36c. In the first step, process 1, reduction of the iron leads to greater electron density at the carbonyl oxygen. As a result, the C=O$\cdots$H$_c$-O hydrogen bond strengthens as it shifts to a more linear configuration The O$\cdots$H$_d$-R$_r$ hydrogen bond breaks and the right side of the chain relaxes to its lower energy configuration. Proton release on the right side may occur at this step, but it is not necessary. In the second step, the -OH$_c$ oxygen, which has become a stronger proton acceptor as a result of the strengthening of the OH$_c\cdots$O=C hydrogen bond (Huyskens, 1977), stabilizes the higher energy configuration in the left side chain as the R$_1$-H$_b\cdots$O hydrogen bond forms situations similar to this, i.e., ones in which an amino acid side chain acts as both a hydrogen donor and a hydrogen acceptor, do not appear to be unusual. Serine in fish hemoglobins (Perutz and Brunori, 1982) and tyrosine in HiPIP (Sheridan et al., 1981) provide two examples. Moreover, the two processes are correlated in that as the donor hydrogen bond strengthens the acceptor hydrogen bond will also strengthen (Huyskens, 1977). The result of reduction, then, produces the configuration shown in Figure 36c. Upon oxidation of cyt a the two step process shown in 3 and 4 returns the site to its resting oxidized conformation. In

step 3, the $OH_c \cdots O{=}C$ hydrogen bond weakens as the ROH_c group shifts to its relaxed configuration. As this occurs, the $H_c \cdots R_r$ bond forms and strengthens. The $H_b \cdots O$ hydrogen bond continues to strengthen as a result of the process and becomes covalent. The result is the state shown in Figure 36d. Although localized positive and negative charges are shown on R_r and R_l, respectively, they need not occur if the covalent bond breaking/bond making processes are closely coupled. In the final step in the process, 4, the R_l^- group picks up a proton from the left (H_a) to become neutral and returns to the resting low energy conformation. On the right, the $R_r^+H_2$ loses a proton to the right and is stabilized in the higher energy conformation by the $O \cdots H\text{-}R_r$ hydrogen bond.

The essential feature of the model of Figure 36 is the redox-linked switch from high energy configuration of the asymmetric hydrogen-bonded chain on the right and low energy configuration on the left to the opposite conformation, i.e., low energy on the right and high energy on the left. Relaxation of this state as oxidation occurs resets the system for a second cycle of proton translocation. One further point should be emphasized for this model. The 2-2.5 kcal/mole associated with cytochrome a hydrogen bond strength changes is not enough energy to make the proton pump significantly irreversible under steady state conditions in mitochondria. For this to occur, other redox coupled

events (e.g., those suggested above) must also contribute to the overall free energy required to make the pump thermodynamically feasible. The situation thus becomes analogous to Warshel and Weiss' (1981) view of hemoglobin where both chemical bond strength change (i.e., "strain") and electrostatic processes were proposed to contribute to the free energy difference between the R-state and the T-state. Within this context, the model of Figure 36 postulates the switching element and a source for part of the energy required to drive a proton pump in cytochrome oxidase.

CHAPTER 7

SUMMARY AND FUTURE WORK

I. Summary

Heme structures important for electron transfer and proton transfer in the enzyme cytochrome oxidase have been discussed. The lack of EPR signals from the $\underline{a}_3$ site of the protein, and the overlapping absorption properties of the two heme $\underline{a}$ chromophores have made cytochrome $\underline{a}_3$ almost inaccessible to spectroscopic probes. Although optical difference and MCD spectroscopies have provided some insight into the properties of cytochromes $\underline{a}_3$, resonance Raman spectroscopy has been shown to supply detailed structural information about this redox center. In addition to the structural information available with this technique, the frequency dependence of the resonance enhancement provides direct information about the electronic transitions of the chromophores.

In the resting enzyme, cytochrome $\underline{a}_3$ has been shown to be six coordinate and high-spin. The identity of the sixth ligand is not known, but μ-oxo bridge (Blumberg and Peisach, 1979) and sulfur bridge (Powers et al., 1981)

structures have been proposed. The oxygenated enzyme, a late intermediate in oxygen reduction, displays very little absorption intensity in the Soret region and a Raman spectrum similar in band frequencies to the resting form. These properties may be a reflection of an intermediate spin (S=3/2) state of cyt $\underline{a}_3$ in the oxygenated enzyme (Shaw *et al.*, 1978; Woodruff *et al.*, 1982) although the appropriate heme *a* model compounds have not been fully investigated. In all liganded or native forms of the enzyme studied, the formyl of cytochrome $\underline{a}_3$ is observed to be in a hydrophobic environment. The apolar nature of the $\underline{a}_3$ site may be important for the ready solubility of molecular oxygen and for fine-tuning the redox potential of this site.

The alkaline pH dependence of the enzyme reported in Chapter 5 shows spectral shifts induced in the $\underline{a}_3$ site at pH 9.0. Similar studies at acidic pH levels allow the specification of pH 6.5 - 8.5 as the pH range for the enzyme in its native spectral and hence structural, form.

The red-shifted cytochrome *a* absorption spectrum and anomalous C=O stretching frequency have been interpreted as arising from a hydrogen bonding interaction between a nearby amino acid (possibly tyrosine) and the peripheral aldehyde of the cytochrome *a* ring. The linear relationship that exists between α band red-shift and the downshift in C=O stretching frequency allows the quantification of the hydrogen bond strengths found *in vivo*. The hydrogen bond strengths differ between ferrous and ferric cyt *a* by

2 - 2.5 kcal/mole. This strengthening of the hydrogen bond upon reduction of the enzyme may be used to drive redox-linked events such as proton pumping. Two models, one a conformational change model and the other which involves hydrogen bond chains, have been presented.

II. Future Work

This work has focussed on the high frequency region (>1000 cm^{-1}) of the resonance Raman spectra of cytochrome oxidase and its derivatives. The low frequency region of the spectrum still needs to be understood. Mostly bending vibrations and out-of-plane bending modes and stretching frequencies are expected in the 100-1000 cm^{-1} region. Woodruff *et al.* (1980) have proposed that several low frequency vibrations of oxidized cytochrome oxidase are due to Cu_{a_3} since their band positions are similar to those observed in type 1 copper-protein Raman spectra. Their arguments that these vibrations do not correspond to cytochrome a_3 vibrations are not valid, but some of the low frequency vibrations may reflect the cyt a_3 - Cu_{a_3} interaction. Excitation frequencies at the maximum or slightly to the red of the cyt a_3 electronic transitions are needed for selective enhancement of the a_3 low frequency vibrations. The cyt a_3 - Cu_{a_3} exchange coupling can be eliminated or modified by generating a form of the enzyme with cyt a_3 oxidized

and Cu_{a_3} reduced. This can be done by chemical oxidation (e.g., ferricyanide or porphyrexide) of the reduced enzyme or by formation of the 1/4 reduced enzyme (Brudvig et al., 1980). Cytochrome a_3 out-of-plane vibrations would be expected to shift as the structure around Cu_{a_3} is changed. Experimentally, this requires an anaerobic flow system to keep the enzyme in its modified form and to avoid photoreduction of cytochrome a.

A more direct probe of the cyt a_3 - Cu_{a_3} site involves excitation into the 655 nm absorption band of the oxidized enzyme. This band is present in the optical spectrum when the exchange coupling between the two metal centers is strong. Vibrations of both the heme and copper centers would be expected to be enhanced if this electronic transition were a copper based charge transfer band. Because of the low extinction of the band ($\sim$3 mM^{-1} cm^{-1}), this experiment requires high concentrations, low laser powers (λ_{ex} = 647.1 nm, Kr^+ laser) and a flowing sample arrangement. (Preliminary attempts have not yielded any results in two different laboratories).

To study the reaction intermediates of cytochrome oxidase, in addition to the low-temperature triple trapping method of Chance et al., (1975) Raman experiments on energized cytochrome oxidase vesicles could be performed. Wikström (1980) has shown that forms of the enzyme with spectra similar to the low temperature intermediates are generated

in ATP energized cytochrome oxidase vesicles. He attributes this to partial reverse electron flow through the enzyme, and, if this interpretation is correct then changes in structure at the catalytic site could be monitored. ATP has also been shown to red-shift the absorption spectrum of cytochrome a in mitochondria (Erecińska et al., 1972), so if the hydrogen bonded carbonyl of cytochrome a is involved in the H^+-pumping mechanism of the enzyme, shifts in the 1610 cm^{-1}/1650 cm^{-1} bands would be expected. As stated before, when dealing with the oxidized form of cytochrome a laser excitation induces photoreduction of this heme center. Procedures that can be utilized to minimize the problem are: 1) use of flowing sample arrangement, 2) removal of the putative flavin contaminant by using cytochrome c affinity chromatography (Thompson and Ferguson-Miller, 1983) or 3) the use of low temperatures combined with visible excitation (Bocian et al., 1978).

The role of cytochrome a in the H^+-pumping function of the enzyme needs to be more firmly established. The pH dependent midpoint potential of cytochrome a is one of the major arguments for the involvement of this center in the H^+-pumping mechanism. Cytochrome a displays a -20 mV/pH unit redox potential dependence (Artzatbonov et al., 1978; Carithers and Palmer, 1981) which is quite different from the -60 mV/pH unit dependence expected if one H^+/e- were taken up in the reduction reaction. A -20 mV/pH unit

potential dependence can be explained if the pK_a of the protonated group in the oxidized form differs by only 1-2 pK units from the reduced form. The protonatable groups are probably amino acid residues on the surface of the protein that have redox-linked pK_a's similar to the Bohr effect in hemoglobin. The identity of these amino acids and their function for proton translocationhas yet to be established.

As stated in Chapter 1, DCCD binding to subunit III or removal of subunit III blocks proton translocation (Wikström et al., 1983). Resonance Raman experiments that monitor the structure of cyt a, in particular its formyl stretching vibration, in the DCCD bound or subunit III-less forms of the enzyme might depict an inactive hydrogen bonded structure. Preliminary experiments of this type (i.e., DCCD bound cytochrome oxidase) reveal small shifts in the carbonyl stretching frequency of the oxidized and reduced enzyme. These shifts are not fully understood and should be investigated further.

Small but reproducible shifts in the C=O stretching frequency of cytochrome a^{2+} are also observed when the deuterium is substituted for hydrogen in the aqueous solvent (D_2O/H_2O). D_2O incorporation was used to investigate whether the hydrogen involved in the hydrogen bond to the peripheral aldehyde was exchangeable. Because deuterium bonds generally are weaker than hydrogen bonds (McDougall

and Long, 1962) a change in ν(C=O) is expected if deuterium is incorporated. There is a specific effect on only the 1610 - 1620 cm^{-1} region (predominantly cyt a) of the reduced enzyme in D_2O. Because the shifts observed are rather small, Raman difference spectroscopy (Shelnutt et al., 1979) or high resolution conventional RRS must be used. If the shifts observed are a reflection of deuterium substitution for hydrogen in the cytochrome a formyl group hydrogen bond, this can help interpret similar shifts observed in DCCD binding to the H_2O solubilized enzyme.

The study of bacterial oxidases, because of the simpler subunit structure, may provide insight into the energy transduction mechanism of this enzyme. The resonance Raman spectral differences of mitochondrial cytochrome oxidase, and of the two subunit oxidases from Paracoccus denitrificans and Rhodopsuedomonas Sphaeroides which pump protons with a ratio of $2H^+/e-$, (Wikström et al., 1983), $\sim$0.6 $H^+/e-$ (Solioz et al., 1982) and zero $H^+/e-$ (Gennis, et al., 1982), respectively, may reveal the structures necessary for proton pumping. The special feature of bacterial proteins is that modified amino acids can be added to the growth medium and therefore small polypeptide changes can be made. If hydrogen bond chains are important in the proton pumping mechanism, the elimination or variation of certain acidic or basic amino acids could inhibit this function of the enzyme.

Several spectroscopic questions remain outstanding concerning cytochrome oxidase and its heme a chromophores. The split Soret band observed for cyt a at low temperatures (77 K) (Nicholls and Chance, 1974) may be caused by the additional electron withdrawing capacity of the hydrogen bonded formyl group relative to the unperturbed formyl. The extent of splitting of the Soret maxima for a series of chlorins has been shown to be related to the electron-withdrawing strength of the peripheral substituents (Ward, 1983). Low temperature optical spectra of hydrogen bonded heme a model compounds can be recorded in order to test this hypothesis for heme a species.

Although heme a has a vinyl group at position 4 of the porphyrin macrocycle, no vibration has been assigned to the C=C stretch. In protoheme containing species this vibration is observed at $\sim$1620 cm^{-1}. For heme a either the vinyl group is not coupled to the π system of the ring or it is coupled with other normal modes of the ring and therefore not a group frequency. A similar observation has been made for the vinyl group of chlorophyll a (Lutz *et al.*, 1982) and the explanation given was that the vinyl group lies out of the plane of the ring.

The use of dye lasers with visible excitation of the heme a chromophores allows the acquisition of data for excitation profiles. If any charge transfer bands or transitions due to cyt a_3 are present under the strong

cyt a absorption in this region, vibrations that follow a different frequency dependence than those of cytochrome a will be observed. This could supply out-of-plane axial ligand vibrational information or cytochrome a_3 specific information. Excitation profiles also contain information about the electronic states of the species monitored. The symmetry of the ring and the degree of splitting of the x, y degenerate transition moments are possible pieces of information available.

With tunability in both the visible and Soret regions, with elimination of the photoreduction problem and with high resolution data acquisition, resonance Raman spectroscopy, in conjunction with other spectroscopic techniques (optical, MCD and EPR) will continue to be a useful probe of the chromophores involved in the catalytic function of cytochrome oxidase.

REFERENCES

REFERENCES

Abe, M., Kitagawa, T. and Kyogoku, Y. (1978) J. Chem. Phys. 69, 4526-4534.

Adar, F. (1975) Arch. Biochem. Biophys. 170, 644-650.

Adar, F. and Erecińska, M. (1979) Biochem. 18, 1825-1829.

Adar, F. and Yonetani, T. (1978) Biochim. Biophys. Acta 502, 80-86.

Alben, J. O., Moh, P. P. Fiamingo, F. G., and Attschuld, R. A. (1981) Proc. Nat'l. Acad. Sci. USA 78, 234-237.

Antalis, T. M. and Palmer, G. (1982) J. Biol. Chem. 257, 6194-6206.

Artzatbanov, V. Y., Konstantinov, A. A., and Skulachev, V. P. (1978) FEBS Lett. 87, 180-185.

Arnett, E. M., Mitchell, E. J. and Murty, T. S. S. R. (1974) J. Am. Chem. Soc. 96, 3875-3891.

Asher, S. A. (1981) in Methods in Enzymology, Vol. 76, Academic Press, New York, pp. 371-413.

Aton, B., Doukas, A. G., Callender, R. H., Becher, B., Ebrey, T. G. (1977) Biochem. 16, 2995-2999.

Azzi, A. (1980) Biochim. Biophys. Acta 594, 231-252.

Babcock, G. T. and Chang, C. K. (1979) FEBS Lett. 97, 358-362.

Babcock, G. T. and Salmeen, I. (1979) Biochem. 18, 2493-2498.

Babcock, G. T., Vickery, L. E. and Palmer, G. (1976) J. Biol. Chem. 251, 7907-7919.

Babcock, G. T., Vickery, L. E. and Palmer, G. (1978) J. Biol. Chem. 253, 2400-2411.

Babcock, G. T., Ondrias, M. R., Gobeli, D. A., Van Steelandt, J. and Leroi, G. E. (1979) FEBS Lett. 108, 147-151.

Babcock, G. T., Van Steelandt, J., Palmer, G., Vickery, L. E., and Salmeen, I. (1979) in Cytochrome Oxidase (King, T. E. et al., eds) Elsevier/North Holland Biomedical Press, pp. 105-115.

Babcock, G. T., Callahan, P. M., Ondrias, M. R. and Salmeen, I. (1981) Biochem. 20, 959-966.

Baum, J. C. and McClure, D. S. (1979) J. Am. Chem. Soc. 101, 2340-2343.

Beinert, H. and Shaw, R. W. (1977) Biochim. Biophys. Acta 504, 187-199.

Bickar, D., Bonventura, J. and Bonaventura, C. (1982) Biochem. 21, 2661-2666.

Bisson, R., Jacobs, B. and Capaldi, R. (1980) Biochem. 19, 4173-4178.

Blair, D. F., Bocian, D. F., Babcock, G. T. and Chan, S. I. (1982) Biochem. 21, 6928-6935.

Blokzijl-Homan, M. F. J. and Van Gelder, B. F. (1971) Biochim. Biophys. Acta 234, 493-498.

Blumberg, W. E. and Peisach, J. (1979) in Cytochrome Oxidase (King, T. E. et al., eds), Elsevier/North-Holland Biomedical Press, pp. 153-159.

Bocian, D. F., Lemley, A. T., Petersen, N. O., Brudvig, G. W. and Chan, S. I. (1979) Biochem. 18, 4396-4402.

Brudvig, G. W., Stevens, T. H., and Chan, S. I. (1980) Biochem. 19, 5275-5285.

Brudvig, G. W., Stevens, T. H., Morse, R. H. and Chan, S. I. (1981) Biochem. 20, 3912-3921.

Cabral, F. and Love, B. (1972) Biochim. Biophys. Acta 238, 181-186.

Cabral, F. and Love, B. (1972) Biochim. Biophys. Acta 283, 181-184.

Callahan, P. M. and Babcock, G. T. (1981) Biochem. 20, 952-958.

Callahan, P. M. and Babcock, G. T. (1983) Biochem. 22, 452-461.

Capaldi, R. A. (1982) Biochem. Biophys. Acta 694, 291-306.

Carithers, R. P., and Palmer, G. (1981) J. Biol. Chem. 256, 7967-7976.

Carter, K. A., Tsai, A. and Palmer, G. (1981) FEBS Lett. 132, 243-246.

Casey, R. P. and Azzi, A. (1983) FEBS Lett. 154, 237-242.

Casey, R. P., Thelen, M. and Azzi, A. (1980) J. Biol. Chem. 255, 3994-4000.

Caughey, W. S., Smythe, G. A., O'Keeffe, D. H., Maskasky, J. E. and Smith, M. L. (1975) J. Biol. Chem. 250, 7602-7622.

Chan, S. I., Bocian, D. F., Brudvig, G. W., Morse, R. H., Stevens, T. H. (1978) in Frontiers of Biological Energetics, (Dutton, P. L., et al. eds) Vol. 2, Academic Press, New York, pp. 883-888.

Chan, S. I., Bocian, D. F., Brudvig, G. W., Morse, R. H. and Stevens, T. H. (1979) Developments in Biochemistry 5, Cytochrome Oxidase, (King, T. E., Orii, Y., Chance, B. and Okunuki, K., eds) Elsevier/North Holland, Amsterdam, pp. 177-188.

Champion, P. M. and Albrecht, A. C. (1979) J. Chem. Phys. 71, 1110-1121.

Chance, B. and Williams, G. R. (1955) J. Biol. Chem. 217, 409-427.

Chance, B. and Williams, G. R. (1956) Adv. Enzymology 17, 65-134.

Chance, B., Saronio, C. and Leigh, J. S. (1975) J. Biol. Chem. 250, 9226-9237.

Choi, S., Spiro, T. G., Langry, K. C., Smith, K. N., Budd, D. L. and LaMar, G. N. (1982), J. Am. Chem. Soc. 104, 4345-4351.

Clark, R. J. H. and Stewart, B. (1979) Structure and Bonding B6, 1-80.

Clore, G. M. and Chance, B. (1978) Biochem. J. 173, 811-820.

Clore, G. M., Andreasson, L.-E., Karlsson, B., Asa, R. and Malmstrom, B. G. (1980) Biochem. J. 185, 139-154.

Collins, D. M., Countryman, R. and Hoard, J. L. (1972) J. Am. Chem. Soc. 94, 2066-2072.

Criddle, R. S. and Bock, R. M. (1959) Biochim. Biophys. Res. Comm. 1, 138-142.

Davis, R. C., Ditson, S. L., Fentiman, A. F. and Pearlstein, R. M. (1981) J. Amer. Chem. Soc. 103, 6823-6826.

Dockter, M. E., Steinemann, A. and Schatz, G. (1978) J. Biol. Chem. 253, 311-317.

Dolphin, D. H., Sams, J. R. and Tsin, T. G. (1977) Inorg. Chem. 16, 711-717.

Eccles, J. and Honig, B. (1982) Biophys. J. 37, 228a.

Erecińska, M. and Wilson, D. F. (1978) Arch. Biochem. Biophys. 151, 304-315.

Erecińska, M., Wilson, D. F., Sata, N. and Nicholls, P. (1972) Arch. Biochem. Biophys. 151, 188-193.

Fee, J. A. Choc, M. G., Findling, K. L., Lorence, R., and Yoshida, T. (1980) Proc. Nat'l. Acad. Sci, USA 77, 147-151.

Felton, R. H. and Yu, N.-T. (1978) in The Porphyrins (Dolphin, D., ed), Vol. 3, Part A. Academic Press, New York, pp. 347-393.

Ferguson-Miller, S. (1983), personal communication.

Frey, T. G., Chan, S. H. P. and Shatz, G. (1978) J. Biol. Chem. 253, 4389-4395.

Friedman, J. M. and Hochstrasser, R. M. (1973) Chem. Phys. 1, 457-467.

Friedman, J. M., Rousseau, D. L. and Adar, F. (1977) Proc. Nat'l. Acad. Sci. USA 74,2607-2711.

Fuhrop, J. H. and Smith, K. M. (eds), in Laboratory Methods in Porphyrin and Metalloporphyrin Research (1975), Elsevier/North Holland, Amsterdam, p. 42.

Gennis, R. B., Casey, R. P., Azzi, A. and Ludwig, B. (1982) Eur. J. Biochem. 125, 189-195.

Georgevich, G., Darley-Usmar, V. M., Malatesta, F., and Capaldi, R. A. (1983) Biochem., in press.

Gouterman, M. (1959) J. Chem. Phys. 30, 1139-1161.

Gouterman, M. (1961) J. Mol. Spec. 6, 138-163.

Haddad, M. S. and Hendrickson, D. N. (1978) Inorg. Chem. 17, 2622-2630.

Halaka, F. G. (1981) Ph.D. Thesis, Michigan State University.

Halaka, F. G., Babcock, G. T. and Dye, J. L. (1981) J. Biol. Chem. 256, 1084-1087.

Halaka, F. G., Barnes, Z. K., Babcock, G. T. and Dye, J. L. (1982) J. Biol. Chem., submitted.

Hartzell, C. R. and Beinert, H. (1974) Biochim. Biophys. Acta 368, 318-338.

Hartzell, C. R., Hansen, R. E. and Beinert, H. (1973) Proc. Nat'l. Acad. Sci. USA 70, 2477-2481.

Heitler, W. (1954) in The Quantum Theory of Radiation, 3rd edition, Oxford University Press (Clarendon), New York.

Henderson, R., Capaldi, R. A. and Leigh, J. S. (1977) J. Mol. Biol. 112, 631-648.

Hinkle, P. and Mitchell, P. (1970) J. Bioenerg. 1, 45-60.

Hinkle, P. C., Kim, J. J. and Racker, E. (1972) J. Biol. Chem. 247, 1338-1339.

Honig, B., Dinur, U., Nakanishi, K., Balogh-Nair, V., Gawinowicz, M. A., Arnaboldi, M. and Motto, M. G. (1979) J. Am. Chem. Soc. 101, 7084-7086.

Hori, H. and Kitagawa, T. (1980) J. Am. Chem. Soc. 102, 3608-3613.

Huong, P. V. and Pommier, J. C. (1977) C. R. Acad. Sci. Ser C. 286, 519.

Huyskens, P. L. (1977) J. Am. Chem. Soc. 99, 2578-2582.

Keilin, D. (1966) in The History of Cell Respiration and Cytochromes, (prepared by J. Keilin), Cambridge University Press, Cambridge.

Kitagawa, T., Ozaki, Y. and Kyogoku, Y. (1978) in Advances in Biophysics (Kotani, M., ed), Vol. 11, University Park Press, Baltimore, MD, pp. 153-196.

Kolks, G., Frihart, C. R., Rabinowitz, H. N. and Lippard, S. J. (1976) J. Am. Chem. Soc. 98, 5720-5721.

Kumar, C., Nagui, A., Chance, B., Ching, Y., Powers, L. and Hartzell, C. R. (1981) Biochem. J. 41, 409a.

Landrum, J. T., Reed, C. A., Hatano, K. and Scheidt, W. R. (1978) J. Am. Chem. Soc. 100, 3232-3233.

Lemberg, R. (1962) Nature (London) 193, 373-374.

Lemberg, R. (1964) Proc. Roy Soc. B159, 429-435.

Lemberg, M. R. (1969) Phys. Rev. 49, 48-121.

Lemberg, R. and Barrett, J. (1973) in Cytochrome, Academic Press, New York.

Lemberg, R. and Pilger, T. B. G. (1964) Proc. Roy Soc. London, Ser. B. 159, 436-448.

Lemberg, R., Bloomfield, B., Caiger, P. and Lockwood, W. (1955) Australian J. Exptl. Biol. 33, 435-444.

Lehninger, A. L., Ul Hassan, M., and Sudduth, H. C. (1954) J. Biol. Chem. 210, 911-922.

Longuet-Higgins, H., Rector, C. W. and Platt, J. R. (1950) J. Chem. Phys. 18, 1174-1181.

Ludwig, B. (1980) Biochim. Biophys. Acta 594, 177-189.

Lutz, M., Hoff, A. J. and Brehamet, L. (1982) Biochim. Biophys. Acta 679, 331-341.

Maley, G. F. and Lardy, H. A. (1954) J. Biol. Chem. 210, 903-909.

Malmström, B. G. (1979) Biochim. Biophys. Acta 549, 281-303.

Maltempo, M. M. (1976) Biochim. Biophys. Acta 434, 513-518.

Marcus, M. A., Lemley, A. T. and Lewis, A. (1979) J. Raman Spec. 8, 22-25.

Maroney, P. M. and Hinkle, P. (1983) J. Biol. Chem., in press.

Mashiko, T., Kastberm, M. E., Spartalian, K., Scheidt, R. W. and Reed, C. A. (1978) J. Am. Chem. Soc. 100, 6354-6355.

Mathies, R., Freedman, T. B. and Stryer, L. (1977) J. Mol. Biol. 109, 367-372.

Mauzerzall, D. (1965) Biochem. 4, 1801-1810.

McClain, M. W. and Harris, R. A. (1977) in Excited States (Lin, E. C., ed), Academic Press, New York, pp. 1-56.

McDougall, A. O. and Long, F.A.J. (1962) Chem. Soc. 66, 429-433.

Mitchell, P. (1961) Nature 191, 144-148.

Mitchell, P. and Moyle, J. (1983) FEBS Lett. 151, 167-178.

Moffitt, W. (1954) J. Chem. Phys. 22, 320-333.

Murthy, A. S. N. and Rao, C. N. R. (1968) Appl. Spec. Rev. 2, 69-191.

Nafie, L. A., Pezolet, M. and Peticolas, W. L. (1973) Chem. Phys. Letts. 20, 563-568.

Nagai, K., Kitagawa, T. and Morimoto, H. (1980) J. Mol. Biol. 136, 271-289.

Nagle, J. F. and Mille, M. (1981) J. Chem. Phys. 74, 1367-1372.

Nagle, J. F. and Morowitz, H. J. (1978) Proc. Nat'l. Acad. Sci. USA 75, 298-302.

Nicholls, P. (1976) Biochim. Biophys. Acta 430, 13-29.

Nicholls, P. and Chance, B. (1974) in Molecular Mechanisms of Oxygen Activation (Hayaishi, O., ed), Academic Press, New York, pp. 479-534.

Nicholls, D. and Locke, R. (1981) in Chemiosmotic Proton Circuits in Biological Membranes (Skulachev, V. P. and Hinkle, P. C., eds), Addison-Wesley, Reading, MA.

Nozawa, T., Orii, Y., Kaito, A., Yamamoto, T. and Hatano, M. (1979) in Developments in Biochem. Vol. 5, Cytochrome Oxidase (King, T. E., Orii, Y., Chance, B. and Okunuki, K., eds), Elsevier, Amsterdam, pp. 117-128.

Ohnishi, T., Blum, H., Leigh Jr., J. S. and Salerno, T. C. (1979) in Membrane Bioenergetics (Lee, C. P. et al., eds), Addison-Wesley, Reading, MA, pp. 21-30.

Ohnishi, T., LoBrutto, R., Salerno, J. C., Bruckner, R. C. and Frey, T. G. (1983) J. Biol. Chem. 247, 14821-14825.

O'Keeffe, D. H., Barlow, C. H., Smythe, G. A., Fuchsman, W. H., Moss, T. H., Lilienthal, H. R. and Caughey, W. S. (1975) Bioinorg. Chem. 5, 125-147.

Ondrias, M. R. and Babcock, G. T. (1980) Biochem. Biophys. Res. Commun. 93, 29-35.

Orii, Y. and King, T. E. (1976) J. Biol. Chem. 251, 7487-7493.

Palmer, G., Babcock, G. T. and Vickery, L. E. (1976) Proc. Nat'l. Acad. Sci. USA 73, 2206-2210.

Peisach, J. (1978) in Frontiers of Biological Energetics (Dutton, P. L. et al., eds) Vol. 2, Academic Press, New York, pp. 873-881.

Pentillä, T. (1983) Eur. J. Biochem., in press.

Pentillä, T. and Wikstrom, M. (1981) in Vectorial Reactions in Electron and Ion Transport in Mitochondria and Bacteria (Palmieri, F. et al., eds), Elsevier/North Holland, Amsterdam, pp. 71-80.

Perrin, M. H., Gouterman, M. and Perrin, C. L. (1969), J. Chem. Phys. 50, 4137-4150.

Person, P. and Zipper, H. (1964) Biochim. Biophys. Acta 92, 605-607.

Perutz, M. F. and Brunori, M. (1982) Nature 299, 421-426.

Petty, R. H., Welch, B. R., Wilson, L. J., Bottomley, L. A. and Kadish, K. M. (1980) J. Am. Chem. Soc. 102, 611-620.

Pimentel, G. C. and McClellan, A. L. (1960) in The Hydrogen Bond, W. H. Freeman and Company, San Francisco, pp. 157-164.

Platt, J. R. (1956) in Radiation Biology (Hollander, A., ed) Vol. III, Chapter 2, McGraw-Hill, New York.

Powers, L., Chance, B., Ching, Y. and Angiolillo, P. (1981) Biophys. J. 34, 465-498.

Prochaska, L. J., Bisson, R., Capaldi, R. A., Steffens, G. C. M., and Buse, G. (1981) Biochim. Biophys. Acta 637, 360-373.

Reed, C. A. and Landrum, J. T. (1979) FEBS Lett. 106, 265-267.

Reinhammer, B., Malkin, R., Jensen, P., Karlsson, B., Andréasson, L.-E., Asa, R., Vänngård, T. and Malmström, B. G. (1980) J. Biol. Chem. 255, 5000-5003.

Remba, R. D., Champion, P. M., Fitchen, D. B., Chiang, R. and Hager, L. P. (1979) Biochem. 18, 2280-2290.

Reynafarje, B., Alexandre, A., Davies, P. and Lehninger, A. L. (1982) Proc. Nat'l. Acad. Sci. USA 79, 7218-7222.

Rosevear, P., Van Aken, T., Baxter, J. and Ferguson-Miller, S. (1980) Biochem. 19, 4108-4115.

Rousseau, D. L., Friedman, J. M. and Williams, P. F. (1978) in Topics in Current Physics, Vol. 11, Chapter 6, Springer, New York, pp. 202-251.

Saari, H., Pentillä, T. and Wikström, M. (1980) Biomembranes 12, 325-338.

Salmeen, I., Rimai, L., Gill, D., Yamamoto, T., Palmer, G., Hartzell, C. R. and Beinert, T. H. (1973) Biochem. Biophys. Res. Commun. 52, 1100-1107.

Salmeen, I., Rimai, L. and Babcock, G. T. (1978) Biochem. 17, 800-806.

Saraste, M., Penttilä, T. and Wikström, M. (1981) Eur. J. Biochem. 115, 261-268.

Scholler, D. M. and Hoffman, B. M. (1979) J. Am. Chem. Soc. 101, 1655-1662.

Scott, R. A. and Gray, H. B. (1980) J. Amer. Chem. Soc. 102, 3219-3224.

Sebald, W., Machleidt, W. and Wachter, E. (1980) Proc. Nat'l. Acad. Sci. USA 77, 785-789.

Seiter, C. H. A. (1978) in Frontiers of Biological Energetics (Dutton, P. L., Leigh, Jr., J. S. and Scarpa, A., eds) Academic Press, New York, pp.798-804.

Seiter, C. H. A. and Angelos, S. G. (1980) Proc. Nat'l. Acad. Sci. USA 77, 1806-1808.

Shaw, R. W., Hansen, R. E. and Beinert, H. (1978) J. Biol. Chem. 253, 6637-6640.

Shaw, R. W., Hansen, R. E. and Beinert, H. (1979) Biochim. Biophys. Acta 548, 386-396.

Shelnutt, J. A. (1980) J. Chem. Phys. 72, 3948-3958.

Shelnutt, J. A. (1981) J. Am. Chem. Soc. 103, 4275-4277.

Shelnutt, J. A. (1981) J. Chem. Phys. 74, 6644-6657.

Shelnutt, J. A., O'Shea, D. C., Yu, N.-T., Cheung, L. D. and Felton, R. H. (1976) J. Chem. Phys. 64, 1156-1165.

Shelnutt, J. A., Cheung, L. D., Chang, R. C. C., Yu, N.-T. and Felton, R. H. (1977) J. Chem. Phys. 66, 3387-3398.

Shelnutt, J. A., Rousseau, D. L., Dethmers, J. K. and Margoliash, E. (1979) Proc. Nat'l. Acad. Sci. USA 76, 3865-3869.

Sheridan, R. P., Allen, L. C. and Carter Jr., C. W. (1981) J. Biol. Chem. 256, 5052-5057.

Sheves, M., Nakanishi, K. and Honig. B. (1979) J. Amer. Soc. 101, 7086-7088.

Sievers, G., Österlund, K. and Ellfolk, N. (1979) Biochim. Biophys. Acta 581, 1-14.

Simpson, W. T. (1949) J. Chem. Phys. 17, 1218-1221.

Smith, D. W. and Williams, R. J. P. (1970) in Structure and Bonding, Vol. 17, Springer-Verlag, Berlin, pp. 1-45.

Solioz, M., Carafoli, E. and Ludwig, B. (1982) J. Biol. Chem. 257, 1579-1582.

Sone, N. and Yanagita, Y. (1982) Biochim. Biophys. Acta 682, 216-226.

Spaulding, L. D., Chang, C. C., Yu, N.-T., and Felton, R. H. (1975) J. Am. Chem. Soc. 97, 2517-2525.

Spiro, T. G. (1974) Accts. Chem. Res. 7, 339-345.

Spiro, T. G., Stong, J. D. and Stein, P. (1979) J. Am. Chem. Soc. 101, 2648-2655.

Steffens, G. J. and Buse, G. (1979) Hoppe-Seyler's Z. Physiol. Chem. 360, 613-619.

Stevens, T. H., Martin, C. T., Wang, H., Brudvig, G. W., Scholes, C. P., and Chan, S. I. (1982) J. Biol. Chem. 275, 12106-12113.

Stevens, T. H., Brudvig, G. W., Bocian, D. F. and Chan, S. I. (1979) Proc. Nat'l. Acad. Sci. USA 76, 3320-3324.

Sutherland, J. C., Vickery, L. E. and Klein, M. P. (1974) Rev. Sci. Instrum. 45, 1089-1094.

Takemori, S. and King, T. E. (1965) J. Biol. Chem. 240, 504-513.

Thompson, D. and Ferguson-Miller, S. (1983) Biochem., in press.

Tsubaki, M., Nagai, K. and Kitagawa, T. (1980) Biochem. 19, 379-385.

Tweedle, M. F., Wilson, L. J., García-Iñiguez, L., Babcock, G. T. and Palmer, G. (1978) J. Biol. Chem. 253, 8065-8071.

Tzagoloff, A. (1982) in Mitochondria, Plenum Publishing Corp., New York.

Valentine, J. S., Sheridan, R. P., Allen, L. C. and Kahn, P. C. (1979) Proc. Nat'l. Acad. Sci. USA 76, 1009-1013.

Vanderkooi, J. M., Landesberg, R., Hayden, G. W. and Owen, C. S. (1977) Eur. J. Biochem. 81, 339-347.

Vanneste, W. H. (1966) Biochem. 5, 838-848.

Van Gelder, B. F. and Beinert, H. (1969) Biochim. Biophys. Acta 189, 1-24.

Van Steelandt-Frentrup, J., Salmeen, I. and Babcock, G. T. (1981) J. Am. Chem. Soc. 103, 5981-5982.

Ward, B., in preparation.

Ward, B., Callahan, P. M., Young, R., Babcock, G. T. and Chang, C. K. (1983) J. Am. Chem. Soc. 105, 634-636.

Warshel, A. and Weiss, R. M. (1981) J. Am. Chem. Soc. 103, 446-451.

Weiss, C. (1972) J. Mol. Spec. 44, 37-80.

Wever, R., Van Ark, G. and Van Gelder, B. F. (1977) FEBS Lett. 84, 388-390.

Wikstrom, M. K. F. (1977) Nature (London) 266, 271-273.

Wikström, M. (1981) Proc. Nat'l Acad. Sci. USA 78, 4051-4054.

Wikström, M. and Krab, K. (1979) Biochim. Biophys. Acta 549, 177-222.

Wikström, M. K. F., Harmon, H. J., Ingledew, W. J. and Chance, B. (1976) FEBS Lett. 65, 259.

Wikström, M., Krab, K. and Saraste, M. (1981) in Cytochrome Oxidase - A Synthesis, Academic Press, London.

Wikström, M., Krab, K. and Saraste, M. (1981) Ann. Rev. Biochem. 50, 623-655.

Wikström, M., Saraste, M. and Penttilä, T., (1983) personal communication.

Wilson, D. F., Lindsay, J. G. and Brocklehurst, E. S. (1972) Biochim. Biophys. Acta 256, 277-286.

Wilson, M. T., Lalla-Maharajh, W., Darley-Usmar, V., Bonaventura, J., Bonaventura, C. and Brunori, M. (1980) J. Biol. Chem. 255, 2722-2728.

Winter, D. B., Bruynickx, W. J., Foulke, F. G., Grinich, N. P. and Mason, H. S. (1980) J. Biol. Chem. 255, 11408-11414.

Woodruff, W. H., Dallinger, R. F., Antalis, T. M. and Palmer, G. (1981) Biochem. 20, 1332-1338.

Woodruff, W. H., Kessler, R. J., Ferris, N. S., Dallinger, R. F., Carter, K. R., Antalis, T. M. and Palmer, G. (1982) in "Electrochemical and Spectrochemical Studies of Biological Redox Components" (Kadish, K. M., ed), Advances in Chemistry Series 201, American Chemical Society pp. 625-659.

Yamamoto, T., Palmer, G., Gill, D., Salmeen, I. and Rimai, L. (1973) J. Biol. Chem. 248, 5211-5213.

Yamanaka, T., Kamita, Y. and Kukumori, Y. (1981) J. Biochem. (Tokyo) 89, 265-273.

Zadorozhnyi, B. A. and Ischenko, I. K. (1965) Opt. Spectry. 19, 306-308.

Zerner,M., Gouterman, M. and Kobayashi, H. (1966) Theoret. Chim. Acta (Berlin) 6, 363-400.

Zobrist, M. and LaMar, G. N. (1978) J. Am. Chem. Soc. 100, 1944-1946.